AD_____

Award Number: DAMD17-03-1-0019

TITLE: Incorporating Model Parameter Uncertainty into Prostate IMRT Treatment Planning

PRINCIPAL INVESTIGATOR: David Y. Yang, Ph.D.

CONTRACTING ORGANIZATION: Stanford University
Stanford, California 94305-5401

REPORT DATE: April 2005

TYPE OF REPORT: Annual Summary

PREPARED FOR: U.S. Army Medical Research and Materiel Command
Fort Detrick, Maryland 21702-5012

REPORT DOCUMENTATION PAGE

Form Approved
OMB No. 074-0188

1. AGENCY USE ONLY (Leave blank)	2. REPORT DATE	3. REPORT TYPE AND DATES COVERED
	April 2005	Annual Summary (1 Apr 2003 - 31 Mar 2005)

4. TITLE AND SUBTITLE
Incorporating Model Parameter Uncertainty into Prostate IMRT Treatment Planning

5. FUNDING NUMBERS
DAMD17-03-1-0019

6. AUTHOR(S)
David Y. Yang, Ph.D.

7. PERFORMING ORGANIZATION NAME(S) AND ADDRESS(ES)
Stanford University
Stanford, California 94305-5401

E-Mail: yong@reyes.stanford.edu

8. PERFORMING ORGANIZATION REPORT NUMBER

9. SPONSORING / MONITORING AGENCY NAME(S) AND ADDRESS(ES)
U.S. Army Medical Research and Materiel Command
Fort Detrick, Maryland 21702-5012

10. SPONSORING / MONITORING AGENCY REPORT NUMBER

11. SUPPLEMENTARY NOTES

12a. DISTRIBUTION / AVAILABILITY STATEMENT
Approved for Public Release; Distribution Unlimited

12b. DISTRIBUTION CODE

13. ABSTRACT (Maximum 200 Words)

IMRT has become one of the main tools for prostate cancer treatment. Current IMRT inverse planning is mainly performed using dose-based objective functions, which oversimplify the problem and ignore the useful biological properties of target and normal tissue. Although different biological model-based objective functions have been investigated in IMRT optimization, the parameters involved in the biological models are very coarse. The objective of this investigation is to establish a framework to consider model parameter uncertainties in prostate IMRT optimization. In order to implement this, a mathematical frameset was first established based on the estimation theory and statistical analysis. Biological model parameter uncertainties and clinical end point data were then incorporated into inverse treatment planning process and a clinically practicable inverse planning framework was established. 30 prostate cancer cases were studied using this technique. The results demonstrated that the proposed technique is capable of greatly improving the sensitive structure sparing without losses of target dose coverage and homogeneity. In addition, by including the model parameters uncertainties, we also implemented an algorithm to optimize the time-dose-fractionation for prostate cancer treatment. This investigation sheds important insight into the complex plan optimization and dose-time-fractionation problems and is valuable for improving prostate cancer patient care.

14. SUBJECT TERMS
Inverse planning, dose optimization, biological models, IMRT

15. NUMBER OF PAGES
113

16. PRICE CODE

17. SECURITY CLASSIFICATION OF REPORT	18. SECURITY CLASSIFICATION OF THIS PAGE	19. SECURITY CLASSIFICATION OF ABSTRACT	20. LIMITATION OF ABSTRACT
Unclassified	Unclassified	Unclassified	Unlimited

Table of Contents

I. INRTODCUCTION

The postdoctoral fellowship grant was awarded to the principal investigator (PI) for the period of April 1, 2003—March 31, 2005. The purpose of this investigation is to introduce a framework for including model parameter uncertainties into prostate Intensity Modulation Radiation Therapy (IMRT) dose optimization so that biological model-based objective function can be used with improved confidence level. The specific aims of the proposal are: (1) to establish a mathematical formalism to incorporate model parameter uncertainty into IMRT optimization; (2) to identify the clinically relevant biological model parameter variance range; and (3) to study the prostate cancer treatment planning including the model uncertainty information. Under the generous support from the U.S. Army Medical Research and Materiel Command (AMRMC), the PI has contributed significantly to the radiation treatment of prostate cancer. Several conference abstracts and refereed papers have been resulted from the support. The fellowship also allowed the PI to obtain research training in prostate cancer while accomplishing the proposed projects. The preliminary data and research opportunity gained under the support of this grant has enabled the PI to obtain offers of an assistant professor in the Department of Radiation Oncology at a few prestigious universities.

II. RESEARCH AND ACCOMPLISHMENTS

Adenocarcinoma of the prostate is the most common malignancy in men in the western countries. Options for active management of organ-confined prostate cancer include radical prostatectomy and definitive radiotherapy with either external beams or interstitial brachytherapy. Intensity Modulated Radiation Therapy (IMRT) is quickly replacing conventional techniques for the treatment of prostate cancer. Most IMRT optimization systems at present use dose and/or dose volume-based objective functions[1], which guide the IMRT planning by imposing a penalty according to the difference between the computed and prescribed doses. A well-known drawback of the dose-based inverse planning is that the nonlinear dose response of tumor or normal structures is not fully considered. A number of mathematical models have been developed over the years to better describe the biological effect of radiation and considerable works have also been done to use these biological models to construct more meaningful objective functions for therapeutic dose optimization[2]. Generally speaking, radiobiological formalism involves the use of model parameters that are of considerable uncertainty[3-6]. For instance, the radiosensitivity of Webb's TCP model varies from 0.157 Gy^{-1} to 0.090 Gy^{-1} when model parameters were fit to 103 patients' data[3]. In order to improve the dose distribution and the outcome of prostate cancer radiotherapy, we implemented a mathematical formalism to include all types of model parameter uncertainties to the dose optimization in the first part of this project. Based on this result, in second and third parts of work, we developed a biological optimization framework and incorporated the model parameter uncertainties into IMRT optimization based on the clinical outcome knowledge. We also implemented an algorithm to optimize the time-dose-fractionation for the radiation treatment of prostate cancer with inclusion of the biological model parameter uncertainties.

An important issue in inverse treatment planning is how to formalize the clinical goals to objectively evaluate the figures of merit of different IMRT plans. Over the last two decades, attempts have been made by many researchers to capture the main feature(s) of the dose volume effects. A power law model represents one of the successful techniques in dealing with the dose-volume effects of sensitive structures[7]. In this model an equivalent dose uniformly irradiating the whole organ, D_{eq}, can be used to represent the situation in which a fractional partial volume, v, is irradiated to a dose, D, by a simple power law model: $D_{eq}=v^{1/n}D$. A remarkable characteristic of this model is that, although only a single organ-specific parameter, n, is used, clinical and biological data

has shown that this power law holds well at low complication levels[7, 8]. Based on this relation, Mohan et al[9] introduced the concept of effective dose to represent a non-uniform dose distribution in a sensitive structure. Kutcher and Burman[10] applied the same power model independently to each volume element of the histogram and introduced the concept of effective volume to reduce the DVH of an inhomogeneous dose distribution in a sensitive structure to a uniform dose distribution. Following their study, in this project we define the effective volume $(\Delta V_{eff})_i$ for a voxel i with volume ΔV and dose $D_c(i)$ as follows

$$(\Delta V_{eff})_i = \Delta V (D_c(i)/D_{ref})^{1/n} \qquad (1)$$

and extend this concept to handle the voxels in the tumor target, where n is an organ-dependent parameter and D_{ref} is the reference dose. For a sensitive structure, n is a small positive number ($0<n<1$) and the value of parameter n reflects the architecture (serial or parallel) of the sensitive structure. For a target, n should be assigned with a small negative value ($-1<n<0$).

The objective function, f, expressed as a function of the effective volume in the voxel domain for an organ should take the form of

$$f = f(\{(\Delta V_{eff})_i\}), \qquad (2)$$

A more general form of inverse planning objective function can be written as a hybrid of the dose-volume based and the dose-based functions. In this situation, the overall objective function of the system takes the form of

$$F = \sum_{\tau=1}^{t_\tau} r_\tau \frac{1}{N_\tau} \sum_{i=1}^{N_\tau} \{1+\eta_1^t [D_c(i)/D_{\tau,ref}]^{1/n_\tau}\} \left| D_c(i) - D_0^T(i) \right|^{k_\tau}$$
$$+ \sum_{\sigma=1}^{s_\sigma} r_\sigma \frac{1}{N_\sigma} \sum_{i=1}^{N_\sigma} \{1+\eta_1^s [D_c(i)/D_{\sigma,ref}]^{1/n_\sigma}\} D_c(i)^{k_\sigma}, \qquad (3)$$

where t_τ and s_σ are the numbers of targets and sensitive structures, $D_0^T(i)$ is the prescription dose in target voxel i, subscripts τ and σ represent target τ and sensitive structure σ, N_τ, N_σ, r_τ, r_σ n_τ, n_σ, $D_{\tau,ref}$, $D_{\sigma,ref}$, k_τ, and k_σ represent the total numbers of voxels, structure specific importance factors, n parameters, reference doses, power of dosimetric deviation from the specified criteria for target τ and sensitive structure σ, respectively. The factor $\left| D_c(i) - D_0^T(i) \right|^{k_\tau}$ for target or $D_c(i)^{k_\sigma}$ for a sensitive structure represents the contribution from dosimetric deviation from the ideal situation. If the k_τ and k_σ are set to zero, the objective function becomes purely dose-volume driven. In particular,

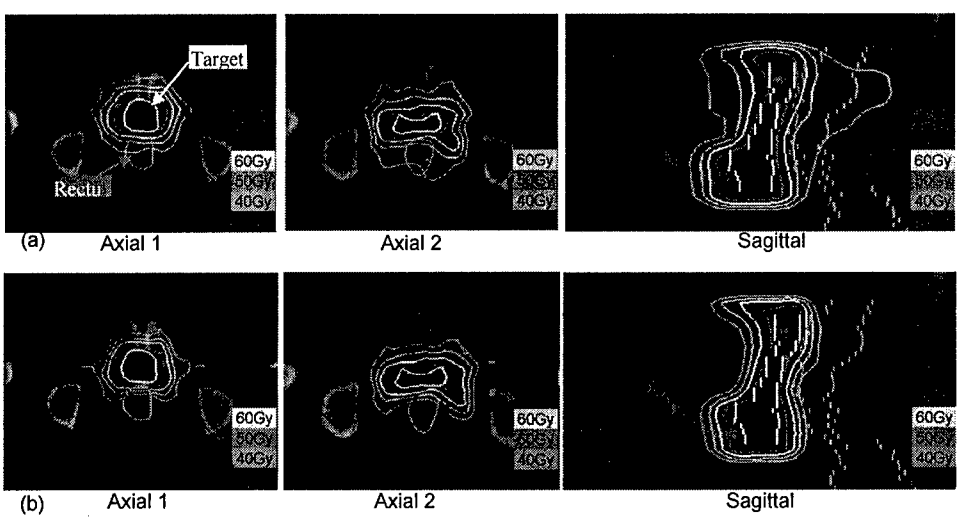

Fig. 1. Comparison of the isodose distributions of the two prostate IMRT plans: (a) the conventional dose-based approach; (b) the newly proposed approach. The results on two transverse slices and a sagittal slice are shown.

if we set k_σ to zero and k_τ to a non-zero value, the objective function for a target becomes a hybrid of dose-volume and dose based, whereas the objective functions for critical structures remain to be purely dose-volume based. On the other hand, when all the n parameters in Eq. (4) are set to be $+\infty$, no dose-volume effects are considered and Eq. (4) is reduced to the conventional dose-based objective function.

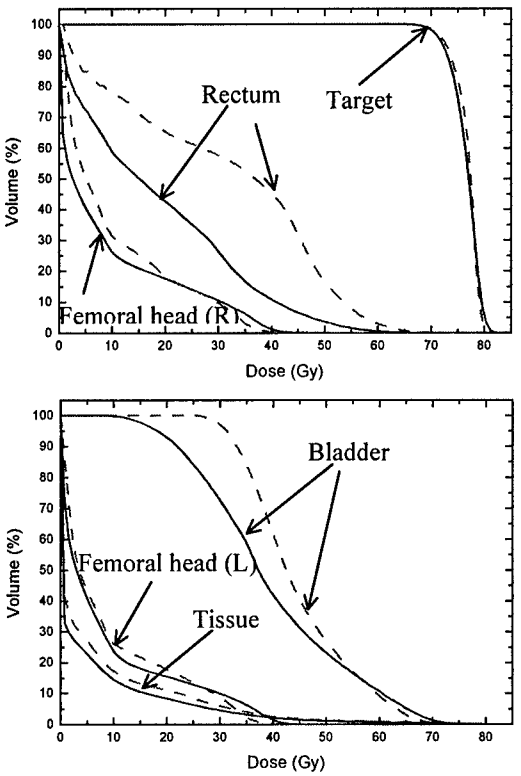

Fig. 2. Comparison of Dose Volume Histograms (DVHs) of the prostate IMRT plans obtained using the proposed approach (solid curves) and the conventional dose-based approach (dash lines).

The proposed optimization algorithm is used to study 30 prostate cancer cases and the results were compared with that of the conventional dose based IMRT optimization technique. Figures 1 and 2 are the results of the two IMRT plans obtained using the proposed and conventional techniques for a typical prostate case. Figure 1 compares the isodose distributions in two transverse slices and a sagittal slice for the two plans. The DVHs of the target and sensitive structures are plotted in figure 2, in which the solid and dashed lines represent the DVHs obtained using the new and conventional approaches, respectively. It is found that, for comparable target coverage, the new inverse planning technique greatly improves the critical structure sparing, especially the rectum sparing. Furthermore, it is intriguing that the non-sensitive structure normal tissue also receives fewer doses in comparison with that of the dose-based optimization. Our results suggest that the improvement in the critical structure sparing is achieved not at the cost of higher target dose inhomogeneity, which is commonly seen in IMRT plan optimization. The calculated NTCPs of rectum, bladder and femoral heads for both IMRT plans are listed in table I. According to the table, it is seen that the NTCPs of the sensitive structures are improved significantly. For the rectum, for example, the NTCP is reduced from 0.45% to 0.03%.

Table I Comparison of the normal tissue complication probabilities (NTCP) for the two IMRT plans for the prostate case

NTCP (%)	The dose-based IMRT plan	The proposed IMRT plan
Bladder	0.017	0.00030
Rectum	0.45	0.029
Femoral head (R)	0.000076	0.0000038
Femoral head (L)	0.000032	0.000015

We also implemented a method for optimizing the treatment protocols for prostate cancer with the biological model parameter uncertainties included. The study starts from an extended LQ model with inclusion of the "4-R's"[11, 12]. The optimum dose-time-fractionation is then formulated as a problem of searching for the highest tumor biologically effective dose (BED) while keeping the normal tissue BED constant. A salient feature of the technique is that various influencing radiobiology parameters, such as the redistribution and reoxygenation, are incorporated naturally

during the optimization process. The optimized tumor BED as a function of the overall treatment time for different potential doubling time, T_{pd} (15, 30 and 40 days), is shown in figure 3. It is shown that the overall treatment time should be larger than a minimum value to maximize the tumor BED when the resensitization effect is considered and the minimum overall time slightly depends on the potential double time T_{pd}.

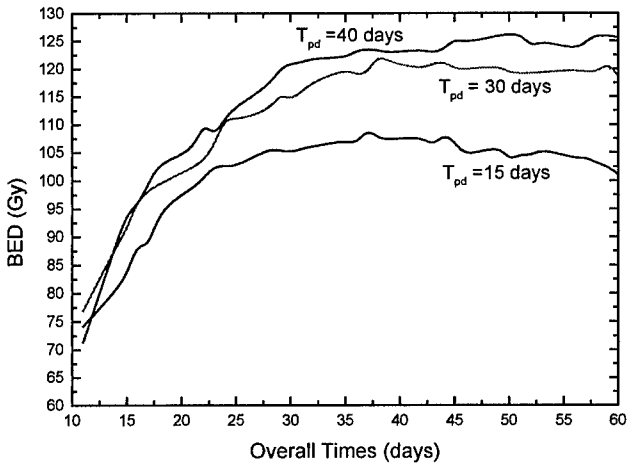

Figure 3. The optimized tumor BED as a function of the overall treatment time when T_{pd} =15, 30, 40 days.

The optimum fractional dose distributions with the maximum fractional dose constraints set to 3 Gy and 5 Gy are shown in figure 4. In figures 4a and 4b, the α/β ratio for tumor is 1.5 Gy and the overall time is 43 days. In figures 4c and 4d, the α/β ratio for tumor is 3.0 Gy and the overall time is 38 days. It is interesting to observe that many fractional doses become zero and a hypofractionation scheme with the size of the maximum fractional dose constraints is more favorable. The non-zero fractionations are almost equally spaced over the entire treatment time and the optimum number of fractionation is determined mainly by the maximum fractional dose constraint. For example, the number of optimum fractionation is 20 and 9, respectively, for the maximum fractional dose constraint of 3 and 5 Gy. Our results indicate that hypofractionation remains to be the optimum treatment scheme even when the α/β ratio for tumor is the same as that of the late responding tissue (both are 3.0 Gy).

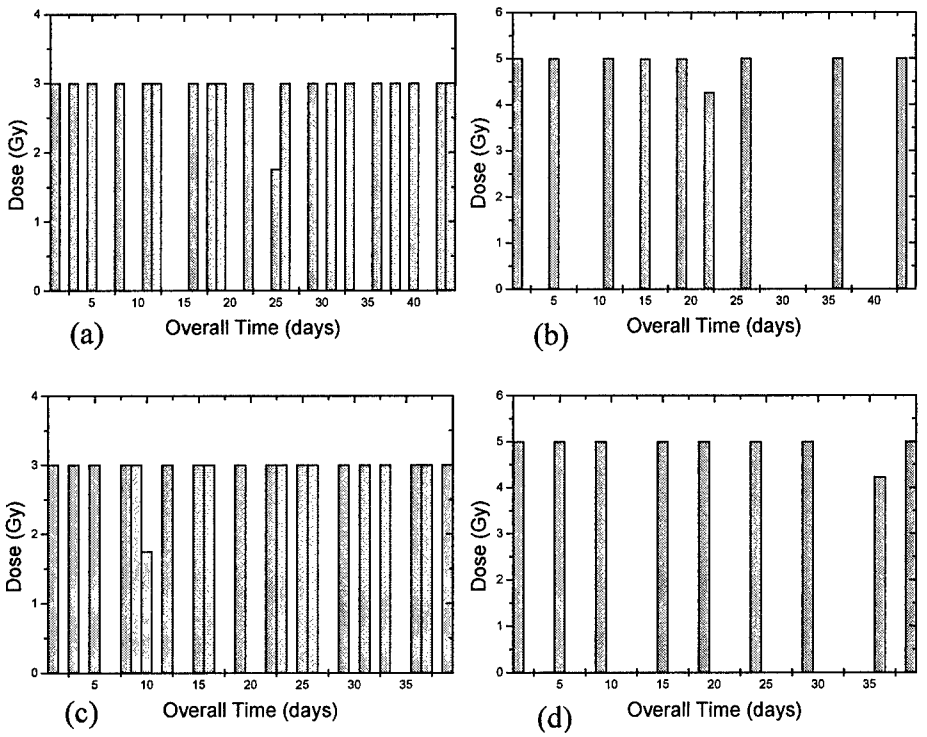

Figure 4. The optimum fractionation doses with τ_S = 2 days for slowly proliferating tumors. (a) α/β = 1.5 Gy, the maximum fractional dose constraint is 3 Gy and the overall treatment time is 43 days; (b) α/β = 1.5 Gy, the maximum fractional dose constraint is 5 Gy and the overall treatment time is 43 days; (c) α/β = 3 Gy, the maximum fractional dose constraint is 3 Gy and the overall treatment time is 38 days; and (d) α/β = 3 Gy, the maximum fractional dose constraint is 5 Gy and the overall treatment time is 38 days.

III. KEY RESEARCH ACCOMPLISHMENTS

- Developed a series of mathematical formulae to incorporate model parameter uncertainty into IMRT optimization.
- Verified the new method in the prostate cancer case and better dose coverage/sparing can be obtained with appropriate parameters.
- Developed a clinical knowledge-based IMRT inverse treatment planning with the obtained model parameters and studied 30 prostate cancer cases using the proposed inverse planning framework.
- Implemented an algorithm to optimize the time-dose-fractionation for the radiation treatment of prostate cancer with inclusion of the biological model parameter uncertainties.

IV. REPORTABLE OUTCOMES

The following is a list of publications resulted from the grant support. Copies of the publication materials are enclosed with this report.

Refereed publication:

1. Yang Y. and Xing L. Optimization of radiotherapy dose-time-fractionation with consideration of tumor specific biology. International Journal of Radiation Oncology Biology and Physics, (submitted), 2005.
2. Yang Y and Xing L. Towards Biologically Conformal Radiation Therapy (BCRT): Selective IMRT Dose Escalation Under the Guidance of Spatial Biology Distribution. Medical physics, (Accepted), 2005.
3. Yang Y. and Xing L. Clinical knowledge-based inverse treatment planning. Physics in Medicine and Biology 49: 5101-5117(2004).
4. Lian J. and Xing L. Incorporating Model Parameter Uncertainty into Inverse Treatment Planning, Medical Physics 31: 2711-2720 (2004).
5. Lian J., Cotrutz C. and Xing L. Therapeutic treatment plan optimization with probability density-based dose prescription. Medical Physics 30: 655-666 (2003).

Published Abstracts:

1. Yang Y. and Xing L. Inverse Treatment Planning with Adaptively Determined Voxel-Dependent Importance Factor, 46th annual Meeting of AAPM, Pittsburgh, July 2004.
2. Yang Y. and Xing L. Clinical knowledge-based inverse treatment planning. In: the 46th American Society for Therapeutic Radiation and Oncology (ASTRO) meeting, Atlanta, 2004.
3. Tan C., Yang Y., Boyer A. and Xing L. Enhancing the efficacy of radiation therapy by incorporating spatial distribution of heterogeneous biology. In: the 46th American Society for Therapeutic Radiation and Oncology (ASTRO) meeting, Atlanta, 2004.
4. Lian J., Spielman D., Cotrutz C., Hunjan S., Adalsteinsson E., King C., Luxton G., Kim D., Daniel B. and Xing L. Including metabolic uncertainty into proton MR spectroscopic imaging (MRSI)-guided inverse treatment planning. In: the 45th American Association of Physicists in Medicine (AAPM) Meeting, San Diego, 2003
5. Lian J. and Xing L. Biological Model Based IMRT Optimization with Inclusion of Parameter Uncertainty. In: the 14th International Conference on the Use of Computers in Radiation Therapy (ICCR), Seoul, Korea, 2004

New Employment:
With the help of this grant and associated publications, the previous PI (Jun Lian) has obtained an assistant professor position in the Department of Radiation Oncology at the University of North Carolina at Chapel Hill. The Current PI (Yong Yang) has obtained offers of assistant professor in the department of radiation oncology at several prestigious universities (written offers from UCSF and University of Pittsburgh, and verbal offer from UCLA). He is in the process of choosing one of them to start his academic research career. He plans to continue his research in prostate cancer to contribute to better prostate patient care.

V. CONCLUSIONS

Inverse planning is an important step in IMRT and its performance crucially determines the quality of IMRT treatment plans. In this work, a technique for incorporating biological model parameter uncertainties into inverse treatment planning has been developed. By including model parameter uncertainties, we provide a mechanism for incorporating clinical end point data into inverse treatment planning process and established a clinically practicable inverse planning framework. The new formalism sheds important insight into the problem of therapeutic plan optimization. The results of 30 prostate cancer cases demonstrated that the proposed technique is capable of greatly improving the sensitive structure sparing with comparable target dose coverage and homogeneity. In addition, through accounting for the known uncertainties in the model parameters, we implemented an algorithm to optimize the time-dose-fractionation for the radiation treatment of prostate cancer. The investigation sheds useful insight into the complex dose-time-fractionation problem in prostate cancer radiation therapy and is valuable for drafting the optimum clinical trials for prostate cancer radiotherapy and for interpreting clinical outcome data.

References

1. Deasy J O, Niemierko A, Herbert D, Yan D, Jackson A, Ten Haken R K, Langer M, and Sapareto S. Methodological issues in radiation dose-volume outcome analyses: summary of a joint AAPM/NIH workshop *Med Phys* 29, 2109-27 (2002).
2. Brahme A. Individualizing cancer treatment: biological optimization models in treatment planning and delivery. *Int J Radiat Oncol Biol Phys* 49 327-37 (2001).
3. Levegrun S, Jackson A, Zelefsky M J, Skwarchuk M W, Venkatraman E S, Schlegel W, Fuks Z, Leibel S A, and Ling C C. Fitting tumor control probability models to biopsy outcome after three-imensional conformal radiation therapy of prostate cancer: pitfalls in deducing radiobiologic parameters for tumors from clinical data. Int J Radiat Oncol Biol Phys. 51, 1064-80 (2001).
4. Fenwick J D. Predicting the radiation control probability of heterogeneous tumour ensembles: data analysis and parameter estimation using a closed-form expression. Phys Med Biol. 43, 2159-78 (1998).
5. Xing L, Li J G, Pugachev A, Le Q T, and Boyer A L. Estimation theory and model parameter selection for therapeutic treatment plan optimization. *Medical Physics* 26, 2348-58 (1999).
6. Niemierko A. Reporting and analyzing dose distributions: a concept of equivalent uniform dose *Medical Physics* 24, 103-10 (1997).
7. Lyman J T and Wolbarst A B. Optimization of radiation therapy, III: A method of assessing complication probabilities from dose-volume histograms. *International Journal of Radiation Oncology, Biology, Physics*. 13, 103-9 (1987).
8. Starkschall G, Pollack A, and Stevens C W. Treatment planning using a dose-volume feasibility search algorithm. *Int J Radiat Oncol Biol Phys* **49** 1419-27 (2001).

9. Mohan R, Mageras G S, Baldwin B, Brewster L J, Kutcher G J, Leibel S, Burman C M, Ling C C, and Fuks Z. Clinically relevant optimization of 3-D conformal treatments. *Medical Physics* **19** 933-44 (1992).
10. Kutcher G J and Burman C. Calculation of complication probability factors for non-uniform normal tissue irradiation: the effective volume method. *International Journal of Radiation Oncology, Biology, Physics* **16** 1623-30 (1989).
11. Brenner D J, Hlatky L R, Hahnfeldt P J, Hall E J, Sachs R K. A convenient extension of the linear-quadratic model to include redistribution and reoxygenation. Int J Radiat Oncol Biol Phys 32: 379-390 (1995).
12. Withers HR. Biologic basis for altered fractionation schemes. Cancer 55: 2086-2095 (1985).

Appendix. Copies of manuscripts (see attachment)

Optimization of Radiotherapy Dose-Time-Fractionation with Consideration of Tumor Specific Biology

Yong Yang, Ph.D. and Lei Xing[a)], Ph.D.

Department of Radiation Oncology, Stanford University School of Medicine,

Stanford, CA 94305-5847

Short title: Optimization of Radiotherapy Dose-Time-Fractionation Scheme

[a)] Author to whom correspondence should be addressed:

Department of Radiation Oncology
Stanford University School of Medicine,
Clinical Cancer Center
875 Blake Wilbur Drive, Rm CC-G204
Stanford, CA 94305-5847
Telephone: (650) 498-7896
Fax: (650) 498-4015
Email: lei@reyes.stanford.edu

Submitted to: *International Journal of Radiation Oncology, Biology, Physics*

Abstract

Purpose: To explore the influence of the "four Rs" of radiobiology on external beam radiotherapy for fast and slowly proliferating tumors and develop an optimization framework for tumor-biology specific dose-time-fractionation scheme.

Materials and Methods: The LQR model proposed by Brenner et al (IJROBP, 32(2), 1995) is used to describe radiation response of tumor, in which the time dependence of sublethal damage repair is included and redistribution and reoxygenation effects are described using a term of resensitization with an average resensitization time. The optimum radiotherapeutic strategy is defined as the treatment scheme that maximizes tumor biologically effective dose (BED) while keeping normal tissue BED constant. Simulated annealing optimization technique is used to search for the optimal radiotherapeutic strategies. The influence of different model parameters on total dose, overall treatment time, fraction size and intervals is also studied.

Results: For fast proliferating tumors the optimum overall time is similar to the assumed T_k, the time from the beginning of treatment to the starting of accelerated proliferation, and almost independent of interval patterns. Significant increase in tumor control can be achieved using accelerated schemes for the tumors with doubling time smaller than 3 days, but little is gained for those with doubling time greater than 5 days. It is also found that the incomplete repair of normal tissues between two consecutive fractions in standard fractionation has almost no influence on the fractional doses, even for the hyperfractionation with an interval time of 8h. When the resensitization effect is included, the fractional doses at the beginning and end of each irradiated week become obviously higher than others in the optimum scheme and the hyperfractionation scheme has little advantage over the standard or hypofractionation one. For slowly proliferating tumors, provided that the α/β ratio of the tumor is comparable to that of the normal tissues, a hypofractionation is more favorable. The overall treatment time should be larger than a minimum, which is predominantly determined by the resensitization time.

Conclusion: The "four Rs" of radiobiology play an important role in the design of radiation therapy treatment protocol. To maximize the efficacy of radiation therapy, the properties of the different types of tissues as characterized by the "four Rs" should be exploited and incorporated into the patient treatment through the optimization of dose-time-fractionation. The proposed technique provides a useful tool to systematically optimize radiotherapy for fast and slow proliferating tumors. The study sheds important insight into the complex problem of dose-time-fractionation and suggests that tumor site-specific optimization has great potential to improve therapeutic outcome.

Key word: Optimization, linear-quadratic model, fractionation, biological model, radiobiology, TCP, NTCP.

INTRODUCTION

Generally, there are three main directions to improve radiotherapy: 1) improving physical dose distributions(1-6); 2) optimizing radiotherapy dose-time-fractionation scheme(7-10); and 3) modifying radiation response in tumor (radiosensitizers)(11, 12) and/or normal tissues (radioprotectors)(13, 14) using chemical agents. With clinical implementation of new radiotherapy techniques, such as intensity-modulated radiotherapy (IMRT)(1-5), it is now possible to achieve optimal physical dose distributions on a patient specific basis. On the other hand, the application of radiobiology studies in clinical practice is still at a primitive stage and a forward comparison of tumor control probability (TCP) and normal tissue complication probability (NTCP) is often employed in the design of patient treatment protocol. To facilitate the design of optimum patient treatment protocols and fully exploit the potential of radiobiology research carried out over the years, it is highly desirable to develop a technique for inverse optimization of dose-time-fractionation (15-20). This will not only allow us to better understand the influence of various biological parameters on radiation therapy treatment of cancer, but also provide a practical tool to obtain the optimal total dose, overall treatment time, fraction sizes and intervals for each disease site.

It is well known that the radiation response of a tissue can be characterized by the "four Rs"(21) of radiobiology: repair of sublethal damage, repopulation, redistribution and reoxygenation. Different approaches have been used to model the radiation response, but the most commonly accepted one is the linear-quadratic (LQ) model(7, 22). The original LQ model describes the mechanism of cell killing and captures the characteristics of sublethal damage repair. The model has been extended to include time effect and the influence of the "four Rs"(23, 24). Current standard fractionation and hyperfractionation schemes exploit the difference in the repair capability to sublethal damage between early-responding tissue and late-responding tissue while various accelerated schemes are motivated by the attempt to reduce the tumor repopulation effect. A recent research(9) has taken the difference in repair rate of sublethal damage of early-responding and late-responding tissues into account in designing brachytherapy protocols. The result suggested that larger doses should be given at the beginning and end

of treatment for accelerated treatment regimens. For external beam radiotherapy, however, little systematic study has been done to exploit the temporal processes of the repair, repopulation and resensitization (redistribution and reoxygenation) and their influence on the optimum treatment strategy for different types of tumors.

In this work, we describe a method for optimizing the treatment protocols for fast proliferating tumors (e.g., head and neck cancer) and slowly proliferating tumors (e.g., prostate cancer). The study starts from an extended LQ model with inclusion of the "4-R's". The optimum dose-time-fractionation is then formulated as a problem of searching for the highest tumor biologically effective dose (BED) while keeping the normal tissue BED constant. A salient feature of the technique is that various influencing radiobiology parameters, such as the redistribution and reoxygenation, are incorporated naturally during the optimization process. The general reference drawn from this study is that tumor and normal tissue biology plays a significant role in the success of radiotherapy and a truly individualized treatment is highly desirable to maximize the efficacy of radiation therapy.

METHODS AND MATERIALS

The LQR model for fractionation scheme

The LQR model proposed by Brenner et al(24) is used in this study to describe radiation response of tumor. In this model the time dependence of sublethal damage repair is included and the redistribution and reoxygenation effects are cast in a term of resensitization with an average resensitization time. The surviving fraction S of tumor cells irradiated with an arbitrary fractionation scheme can be expressed as

$$S = \exp[\, -\alpha D - \beta G(\tau_R) D^2 + (\frac{1}{2}\sigma^2) G(\tau_S) D^2 + H(T_{tot}, T_k)(T_{tot} - T_k)/T_{pd}\,], \quad (1)$$

where α and β are linear quadratic constants characterizing the intrinsic radiosensitivity, σ^2 is variance of Gaussian distribution of α, τ_R is repair time, τ_S is average resensitization time, D is total dose, T_{tot} is overall treatment time, T_{pd} is average potential doubling time, and T_k is "kick-off" time of accelerated proliferation, representing the time

from the beginning of treatment to the starting of accelerated proliferation. $H(x,x_0)$ denotes the Heaviside function and is defined as

$$H(x,x_0)=\begin{cases}0, & if \quad 0\le x<x_0\\ 1, & if \quad x\ge x_0\end{cases}. \qquad (2)$$

$G(\tau)$ is the generalized Lea-Catcheside function defined by

$$G(\tau)=(\frac{2}{D^2})\int_0^{T_{tot}} duR(u)\int_0^{u} dwR(w)\exp[-(u-w)/\tau], \qquad (3)$$

where R(t) is the dose rate function. For an arbitrary fractionation scheme with fractional dose distribution $\{d_1\ldots, d_i,\ldots\}$, and fractional intervals $\{\Delta t_1\ldots, \Delta t_i,\ldots\}$ (d_i represents the ith fractional dose and Δt_i represents the time interval between fractions i and $i+1$). Assuming that the delivery time for each fraction is ignorable, we can rewrite equation (1) using equation (3) as follows

$$S=\exp\{\sum_{i=1}^{I}[-\alpha d_i-\beta G_i(\tau_r)d_i^2+\frac{1}{2}\sigma^2 G_i(\tau_s)d_i^2]+H(T_{tot},T_k)(T_{tot}-T_k)/T_{pd}\}, \quad (4)$$

where I is total fraction number. Here $G_i(\tau)$ is calculated for each fraction with following form:

$$G_i(\tau)=1+\frac{2}{d_i}\sum_{j=1}^{i-1} d_j\prod_{k=j}^{i-1}\exp(-\Delta t_k/\tau). \quad (5)$$

For normal tissues, we only consider the cell killing and incomplete repair of sublethal damage, i.e., only the first two terms in equation (4) are included.

Optimization formulation

The goal here is to maximize tumor BED while keeping normal tissue BED constant. BED is calculated using the cell survival S given by equation (4) according to (17, 22):

$$BED = -\frac{1}{\alpha}\ln(S). \qquad (6)$$

TCP and NTCP are calculated using (19, 25)

$$TCP \ or \ NTCP=\exp(-N_0S)=\exp[-N_0\exp(-\alpha BED)], \qquad (7)$$

where N_0 is the total number of tumor or normal tissue cells. To proceed, it is convenient to use the BED of the standard scheme (70Gy, 2Gy/f, 1f/d, 5f/w) as a reference because

its properties are well understood and extensive clinical data for the scheme has been accumulated. Mathematically, the dose-time-fractionation optimization can be found by minimizing the objective function

$$F = BED_{t0} / BED_t, \qquad (8)$$

under the constraints

$$BED_{nl} = BED_{nl0}, \qquad (9)$$

and

$$BED_{ne} \leq BED_{ne0}, \qquad (10)$$

where BED_t, BED_{nl}, and BED_{ne} are the *BED*s of the target, late-responding normal tissue and early-responding tissue for the optimal scheme, respectively, and BED_{t0}, BED_{nl0}, and BED_{ne0} represent the same for the standard scheme.

Theoretically, the interval time between two consecutive fractions can be treated as one of the system variables and optimized by computer. With clinical practicality in mind, we only study two patterns of intervals: five fractions per week (interval=1 day) with weekend break (standard fractionation) and 10 fractions per week (interval between two fractions in the same day is 8 h) with the overnight and weekend breaks (hyperfractionation). The overall time is from 2 weeks to 8 weeks with an increment of 1 day. For each overall treatment time, our optimization program will then search for the optimal fractional doses that maximize the tumor BED with constant normal tissue BED.

By introducing Lagrange multipliers, λ_l and λ_e, the optimization problem with constraints(26, 27) specified in equations (9) and (10) can be expressed as

$$F = BED_{t0} / BED_t + \lambda_l (BED_{nl} - BED_{nl0}) + \lambda_e H(BED_{ne}, BED_{ne0})(BED_{ne} - BED_{ne0}), \qquad (11)$$

where $H(x,x_0)$ is the Heaviside function defined in equation (2). A simulated annealing optimization technique(28, 29) is used to optimize the objective function (11) with the fractional doses as the optimization variables. For each given interval pattern, the optimal overall treatment time is found by comparing the optimal tumor BEDs obtained for all possible overall treatment times.

Estimation of Radiobiologic Parameters

Before optimizing the dose-time-fractionation, it is important to determine the values or the variation ranges of the model parameters for the studied tumor sites. Seven independent parameters for each tumor site and three parameters for each normal tissue are needed, which are α, α/β ratio, T_k, T_{pd}, τ_R, τ_S, and $\frac{1}{2}\sigma^2$ for tumor and α, α/β ratio, and τ_R for normal tissue. In this study α is set to be 0.315/Gy for both late-responding and early–responding normal tissues. α/β ratio and repair time τ_R are chosen to be 3 Gy, 4 h and 10 Gy, 0.5 h for the late-responding and early–responding tissues, respectively(10, 22, 30). For fast proliferating tumors, the estimated doubling time, T_{pd}, is around 3 days as indicated by recent studies(31, 32) and the commonly accepted α is 0.35/Gy with α/β ratio = 10 Gy(10, 22). T_k for head and neck (HN) tumors as revealed by some studies is in the range of 21 to 35 days(33), and the repair time of the tumor cell τ_R is around 0.5 h(9, 30). The resensitization process includes both the redistribution and reoxygenation effects. It is estimated that the resensitization time τ_S is comparable to the cell cycle time or reoxygenation characteristic time, i.e., hours to days. In this work we assume τ_S to be in the range of 0.5-3 days for fast proliferating tumors(24). $\frac{1}{2}\sigma^2$ represents the amplitude for the resensitization and is assumed to be 0.02. In addition, in order to convert the resultant BED to TCP we assume that the total number of tumor cells $N_0 = 10^8$.

For slowly proliferating tumors, such as prostate tumor, α is assumed to be 0.10/Gy and α/β ratio in the range of 1.0~4.0 Gy, as suggested by several recent studies(19, 34, 35). The estimated doubling time during radiotherapy is around 40 days, with a range from 16 to 61 days(36). Because there is no T_k data available for slowly proliferating tumors, in this work we study the extreme situation, i.e., $T_k = 0$. The results should be extendable to situations with nonzero T_k values. The repair time of prostate tumor cells is 1.9 h, suggested by Fowler et al(35). A recent study(37) showed that there might be no full redistribution of cells around the cell cycle between radiation fractions spaced by 1 day. Thus, we assume τ_S to be in the range of 1-3 days. We choose $\frac{1}{2}\sigma^2$ =

$\frac{1}{3}\beta$ for slowly proliferating tumors. Table 1 summarizes the values of model parameters used in this work for the fast and slow proliferating tumors.

RESULTS

Fast proliferating tumors

Overall treatment time

Figures 1a and 1b show the optimized tumor BED as a function of the overall treatment time for three different T_k's (21, 28 and 35 days) for the two studied interval patterns (standard fractionation and hyperfractionation). Other parameters used to obtain the data are listed in Table 1. It is found that there exists an optimum overall treatment time with which the maximum tumor BED is achieved for each T_k. The optimum overall time is similar to the assumed T_k and almost independent of interval patterns. For the standard fractionation, for example, TCP increases by about 60% for a treatment with the optimum overall time as compared with the conventional 7-week overall time if T_k=28 days.

Figures 2a and 2b show the BED as a function of the overall treatment time for a few different T_{pd} values (2, 3, 4 and 5 days) for the two studied interval patterns. In both cases, the influence of T_{pd} is more pronounced when T_{pd} is small. When T_{pd} is larger than 5 days, shortening the overall time results in almost no increase in tumor BED. For example, the difference in TCPs between the treatment schemes with the optimum overall time and the conventional 7-week overall time is only about 3% when T_{pd}=5 days for the standard fractionation.

In figures 3a and 3b we show the results for τ_S =0.5, 1, 2, to 3 days for the two interval patterns. While the BED is sensitive to the variation of τ_S, the optimum overall time is not.

Total dose

The optimized total dose versus the over time for a few T_k's is shown in figure 4 for the two interval patterns. As expected, the total dose increases with the overall time. Generally, the fractional dose increases with the reduction of overall time. In order to keep normal tissue complications (mainly late complications) constant, the total dose must be decreased. Figure 4 also suggests that the hyperfractionation require a higher total dose than the standard fractionation for the same overall time. In addition, it is seen that the optimized total dose is independent of T_k for both types of fractionation regimes.

Fractional doses

Figures 5 and 6 show the optimum fractional doses obtained for two examples: one for the standard fractionation with overall time of 40 days and total fraction number of 29 and the other for the hyperfractionation with overall time of 46 days and total fraction number of 68. In figures 5a and 6a we plot the results with τ_R =0 h for both tumor and normal tissues and τ_S =0 h for tumor. These parameter values represent the situation that the sublethal damage repair for both tumor and normal tissues and the resensitization of tumor cells are completed immediately after irradiation. In this situation, it is found that a uniform fractional dose is more favorable. The result is intuitively conceivable because evenly distributed fractional doses maximize the repair of the late-responding tissue, leading to the maximum tumor BED with a given normal tissue damage. The influence of different normal tissue repair time on the optimum fractional doses with fixed τ_S =0 h and τ_R =0.5 h for tumor is shown in figures 5b-c and 6b-c. For the standard fractionation, when late tissue repair time τ_R is set to be 4 h, the optimum fractional doses remain uniform. This is because the sublethal damage repair of normal tissue is almost completed during the interval between two consecutive fractions (24 h). When τ_R of normal tissue increases from 4 h to 12 h, higher fractional doses at the beginning and end of each week become preferable. The ratio of the averaged "spike" dose with the averaged dose of remaining fractions is 1.4. For the hyperfractionation, the dose "spikes" occur even if the normal tissue repair time τ_R is 4 h. The ratio in this case is 1.1. The effect becomes more pronounced as τ_R is increased to 8 h and the ratio becomes 1.4.

Figures 5d and 6d illustrate the results for the average tumor resensitization time τ_S =24 h with τ_R = 0.5 h for tumor and 4 h for the late-responding tissue. Similar to the situation discussed above, the optimal fractional doses at the beginning and end of each week are higher when the resensitization effect is included. The ratios of the averaged "spike" dose with the averaged dose of remaining fractions are 1.2 and 1.3 for the standard fractionation and hyperfractionation, respectively.

Interval patterns

A comparison of the tumor BED of the standard fractionation and hyperfractionation for the same late tissue complication as a function of overall treatment time is plotted in figure 7. The influences of different normal tissue repair time (τ_R) and tumor average resensitization time (τ_S) are also illustrated. In figure 7a we ignore the resensitization effect and assume that the sublethal damage repair is completed immediately after irradiation (i.e., $\frac{1}{2}\sigma^2$, τ_S and τ_R for tumor and normal tissues are all set to be zero). The results show that, in this situation, the BED for the hyperfractionation is higher than that for the standard fractionation. Figures 7b and 7c show the results with the incomplete repair considered but the resensitization effect ignored. The tumor repair time is set to 0.5 h and the late tissue repair time 4 h and 8 h in figures 7b and 7c, respectively. It is found that, although the hyperfractionation is better than the standard fractionation, the BED difference between the two fractionation regimes decrease as the late tissue repair time increases. Figure 7d shows the results with the resensitization effect included. The average resensitization time for tumor is 24 h with τ_R = 0.5 h for tumor and 4 h for the late tissue. As seen from the data, the BEDs for the two regimes are very close in this situation.

Slowly proliferating tumors

When the α/β ratio for tumor is lower than that for the surrounding normal tissues, our formulae suggest that a single fractionation irradiation is the optimum scheme if the resensitization effect is ignored. Clinically, however, a single fractionation irradiation

may result in disastrous acute sequelae and consequential late effect. Because there is currently no good way to model the acute sequelae and consequential late effects, in this work we simply restrict the fractional dose to within a given value to consider these effects.

Overall treatment time

The optimized tumor BED as a function of the overall treatment time for different T_{pd} (15, 30 and 40 days) is shown in figure 8a. The maximum fractional dose is constrained to 5 Gy in this calculation. Other parameters used to obtain these data are listed in Table 1. Different from fast proliferating tumors, we found that the overall treatment time should be larger than a minimum value to maximize the tumor BED when the resensitization effect is considered. The optimum BED increases gradually with the overall time before this minimum overall time and after it the BED almost keeps constant. It is also shown that the minimum overall time slightly depends on the potential double time T_{pd}. The larger the T_{pd}, the larger the minimum overall time is. For example, the minimum overall time is about 5-6 weeks for T_{pd} = 40 days, but about 3-4 weeks when T_{pd} = 15 days. In addition, the curve for T_{pd} = 15 days shows that the tumor BED slightly decreases after about 6 weeks due to the influence of tumor cell proliferation. However, the decrease disappears if T_k takes 28 days rather than 0(data not shown). Figure 8b gives the results for different τ_S (1, 2 and 3 days) with T_{pd} = 40 days. It is seen that the minimum overall time is significantly dependent on τ_S: the larger the τ_S, the larger the minimum overall time. The minimum overall time is about 3 weeks for τ_S = 1 day, 6 weeks for τ_S = 2 days and larger than 9 weeks for τ_S = 3 days. This conclusion implies that longer overall treatment time is preferred for the slow proliferating tumors (e.g, tumors with more hypoxic cells).

The data in the above are obtained with maximum fractional dose constraint of 5 Gy. The calculation can be easily extended to other constraint values and similar conclusions can be reached.

Total dose

Figure 9a shows the optimized total dose as a function of the overall treatment time when the maximum fractional dose is 3, 4, 5 and 6 Gy, respectively. The parameters used to obtain these curves are listed in Table 1. Unlike the case of fast proliferating tumors, in this circumstance, total dose does not change with the overall treatment time because the optimum total fractionation number is purely determined by the given maximum fractional dose constraint. Furthermore, as shown in figure 9b, total dose increases with the decrease of maximum fractional dose constraints.

Fractionation scheme

The optimum fractional dose distributions with the maximum fractional dose constraints set to 3 Gy and 5 Gy are shown in figure 10. In figures 10a and 10b, the α/β ratio for tumor is 1.5 Gy and the overall time is 43 days. In figures 10c and 10d, the α/β ratio for tumor is 3.0 Gy and the overall time is 38 days. It is interesting to observe that many fractional doses become zero and a hypofractionation scheme with the size of the maximum fractional dose constraints is more favorable. The non-zero fractionations are almost equally spaced over the entire treatment time and the optimum number of fractionation is determined mainly by the maximum fractional dose constraint. For example, the number of optimum fractionation is 20 and 9, respectively, for the maximum fractional dose constraint of 3 and 5 Gy. Our results also indicate that hypofractionation remains to be the optimum treatment scheme even when the α/β ratio for tumor is the same as that of the late responding tissue (both are 3.0 Gy).

The change of the optimized tumor BED with the total dose with tumor α/β=1.5 and 3 Gy and τ_S=1 days are shown in figure 11a. The overall treatment time is 46 days for all calculations shown in figure 11a. It is found that the tumor BED decreases with the increase of total dose and a hypofractionation schemes yields a higher tumor BED even if the tumor α/β ratio is the same as that of the late responding tissue. Figure 11b shows the influence of different τ_S (1, 2, and 3 days) on the BED. For the same maximum fractional dose constraint, the optimized tumor BED decreases with the increase of resensitization time τ_S. The smaller the fractional dose, the larger the influence of resensitization time τ_S is. Unlike the fast proliferating tumors, the fractional dose and interval time do not

change with τ_S as shown in figures 11c and d, in which the τ_S is set to 1 day and 3 days, respectively.

DISCUSSIONS

Several clinical and experimental studies suggest that the estimated doubling time for HN tumors is as short as 2-3 days(31, 32) and the accelerated tumor growth is similar for all HN tumor sites and stages. In this situation, our calculation indicates that there exists an optimum overall treatment time that maximizes tumor control while keeping the normal tissue complication constant. We found that the optimum overall time is close to the assumed T_k and almost independent of fractionation patterns and tumor resensitization time, which is similar to that proposed by Fowler(10). However, when the doubling time is larger than 5 days, it is found that the tumor control improves little by shortening the overall treatment time, suggesting that the gain of accelerated schemes is extremely sensitive to the tumor proliferation rate. The conclusion appears to be consistent with the results of randomized prospectively controlled clinical trials for HN tumors by the European Cooperative Radiotherapy Group (ECRG) (38). When compared with the standard fractionation scheme, the ECRG data show that the accelerated scheme substantially increases the local control rate for tumors with T_{pd}< 4 days, whereas for tumors with T_{pd}> 4 days, there is no detectable difference between the two fractionation schemes. Therefore, in order to truly benefit from accelerated fractionation, it is essential to select patients with fast-proliferating tumors.

The repair time is typically less than 1 h for tumor and around 4 h for slow repair component of normal tissues, as suggested by a number of clinical and laboratory-based animal studies(9, 30, 39). As shown in this work, this difference in the repair rate has almost no influence on the fractional doses for the standard fractionation. For hyperfractionation with two consecutive fractions spaced by 8 h, the difference results in slightly higher fractional doses at the beginning and end of each week. This result is in accordance with the dose "spikes" effect mentioned by Brenner et al(9) for brachytherapy treatment with an overall treatment time of 120 h. The dose "spikes" effect becomes

larger with the lengthening of repair time for normal tissues as illustrated in this study. The underlying biology of this effect is that normal tissue cells can get better repaired during the longer rest of weekends. Interestingly, including of the resensitization effect leads to similar results as shown in figures 5d and 6d. We attribute this feature to the increased tumor cell killing caused by the sufficient resensitization during the weekends. Furthermore, this work indicates that the studied hyperfractionation scheme leads to better tumor control as compared to the standard fractionation scheme even when the incomplete repair is included. However, when the resensitization effect (τ_S=1 day) is considered, the advantage of the hyperfractionation becomes less obvious as shown in figure 7d, suggesting that the standard fractionation or a hypofractionation scheme may be more suitable for hypoxic tumors.

For slowly proliferating tumors, the typical doubling time is about 40 days and the α/β ratio is in the range of 1 to 4 Gy. Animal studies and clinical observations support that the α/β value for late rectal damage is greater than 4 Gy(40). Under this circumstance, it is obvious that hypofractionation is the optimum choice. Our work also suggests that a hypofractionation scheme is preferable even if α/β ratios for both tumors and late rectal tissues are close, e.g., all equal to 3.0 Gy.

Different from fast proliferating tumors, there is no biological advantage to shorten the overall treatment time for tumors with slow proliferation rate. Furthermore, if the resensitization effect is considered, there exists a minimum overall treatment time below which the tumor control starts to decrease. The main reason responsible for this phenomenon is that enough interval time between two consecutive fractions is required to sufficiently sensitize the tumor cells. Our study suggests that current overall treatment time (6-7 weeks) should be kept for the hypofractionation scheme. This will enhance the tumor control and reduce the risk of acute sequelae and consequential late effect that is not easily modeled by currently available radiobiology theory. In addition, as shown in figures 11a and b, although a larger fractional dose results in a higher tumor control, the enhancement becomes insignificant when the fractional dose is greater than 5-6 Gy when α/β ratios for the tumor and later rectal tissue are comparable or when the resensitization time is large (e.g., τ_S=3 days). Therefore, a fractional dose of 5-6 Gy seems to be suitable for prostate hypofractionation treatment. We note that the risk involved in this kind of

treatment is relatively low. The experience of 22 years in London with 232 prostate cancer patients treated with a 6×6 Gy scheme in 3 weeks has indicated comparable local response and minimal late morbidity when compared with the standard fractionation scheme(41).

Finally, it should be recognized that the LQR model used in this investigation is far from satisfactory in modeling the responses of tumors and normal tissues and there is also considerable uncertainty in the currently available model parameters. Notably, using a single resensitization time for both redistribution and reoxygenation effects in LQR model should be improved in the future so that the tumor response can be more properly described. In order to yield clinically meaningful results, more sophisticated radiobiology model and more accurate parameters are needed. In addition, theory that better describes the acute reactions and consequential late effect should also be in place.

CONCLUSIONS

In this work we have described a general framework for dose-time-fractionation optimization and explored the influences of the "four Rs" of radiobiology on radiation therapy for fast and slowly proliferating tumors. Different dose-time-fractionation schemes are evaluated in reference to the standard fractionation and the role of various biological parameters in the design of a treatment protocol is elaborated. Our study indicates that it is clinically significant to design radiation therapy treatment based on the specific biological properties of the tumor and normal tissues. The investigation sheds useful insight into the complex dose-time-fractionation problem in radiation therapy and is valuable for drafting the optimum clinical trials for different tumor sites and for interpreting clinical outcome data.

ACKENOLECKMENT

This research is supported in part by Department of Defense (DAMD17-03-1-0019) and the National Cancer Institute (5 R01 CA98523-01).

Table 1 Model parameters used in our study

Parameters	Fast Proliferating Tumors	Slowly Proliferating Tumors
LQ constant for tumor, α	0.35/Gy	0.10/Gy
α/β ratio for tumor	10Gy	1.5Gy
"Kick-off" time for tumor, T_k	28 days	0 days
Doubling time for tumor, T_{pd}	3 days	40 days
Resensitization time for tumor, τ_S	1 days	2 days
Repair time for tumor, $\tau_{R,\,tumor}$	0.5 h	1.9 h
Variance of Gaussian distribution of α, $\frac{1}{2}\sigma^2$	0.02	$\frac{1}{3}\beta$
LQ constant for late-responding normal tissue, α	0.315/Gy	0.315/Gy
α/β ratio for late-responding normal tissue	3 Gy	3 Gy
Repair time for late-responding normal tissue, τ_{R,L_tissur}	4 h	4 h
LQ constant for early-responding normal tissue, α	0.315/Gy	0.315/Gy
α/β ratio for early-responding normal tissue	10 Gy	10 Gy
Repair time for early-responding normal tissue, $\tau_{R,E\text{-}tissue}$	0.5 h	0.5 h

Legends

Figure 1. The optimized tumor BED as a function of overall treatment time when T_k =21, 28 and 35 days. (a) Results for standard fractionation (1f/d, 5 f/w); and (b) Results for hyperfractionation (2f/d, 10 f/w).

Figure. 2. Influence of doubling time T_{pd} (2, 3, 4 and 5 days) on the optimum overall treatment time. (a) Results for standard fractionation (1f/d, 5 f/w); and (b) Results for hyperfractionation (2f/d, 10 f/w).

Figure 3. Influences of average resensitization time τ_S (0.5, 1, 2, and 3 days) on the optimum overall treatment time. Parameters used to obtain this curves are listed in table 1. (a) Results for standard fractionation (1f/d, 5 f/w); (b) Results for a hyperfractionation pattern (2f/d, 10 f/w).

Figure 4. The optimized total dose as a function of overall treatment time when T_k = 21, 28 and 35 days.

Figure 5. The optimum fractional doses for four different sets of τ_R and τ_S for the standard fractionation. The overall treatment time is 40 days and the total fraction number is 29.

Figure 6. The optimum fractionation dose for four different sets of τ_R and τ_S for the hyperfractionation. The overall treatment time is 46 days and total fraction number is 68.

Figure 7. A comparison of the tumor BEDs under the same normal tissue BED constraints for the standard fractionation and hyperfractionation schemes.

Figure 8. The optimized tumor BED as a function of the overall treatment time when T_{pd} =15, 30, 40 days (a) and τ_S = 1, 2, 3 days (b). The maximum fractional dose is restricted to 5 Gy.

Figure 9. (a) The optimized total doses as a function of overall treatment time for different maximum fractional dose constraints (3, 4, 5 and 6 Gy). (b) The optimized total doses as a function of the overall fractionation number.

Figure 10. The optimum fractionation doses with τ_S = 2 days for slowly proliferating tumors. (a) α/β = 1.5 Gy, the maximum fractional dose constraint is 3 Gy and the overall treatment time is 43 days; (b) α/β = 1.5 Gy, the maximum fractional dose constraint is 5 Gy and the overall treatment time is 43 days; (c) α/β = 3 Gy, the maximum fractional dose constraint is 3 Gy and the overall treatment time is 38 days; and (d) α/β = 3 Gy, the maximum fractional dose constraint is 5 Gy and the overall treatment time is 38 days.

Figure 11. (a) The optimized tumor BED as a function of total dose for different α/β ratios and τ_S. (b) The optimized tumor BED as a function of total doses for different τ_S; (c) and (d) The optimum fractional doses for τ_S = 1 and 3 days. In all calculation the overall time is set as 46 days.

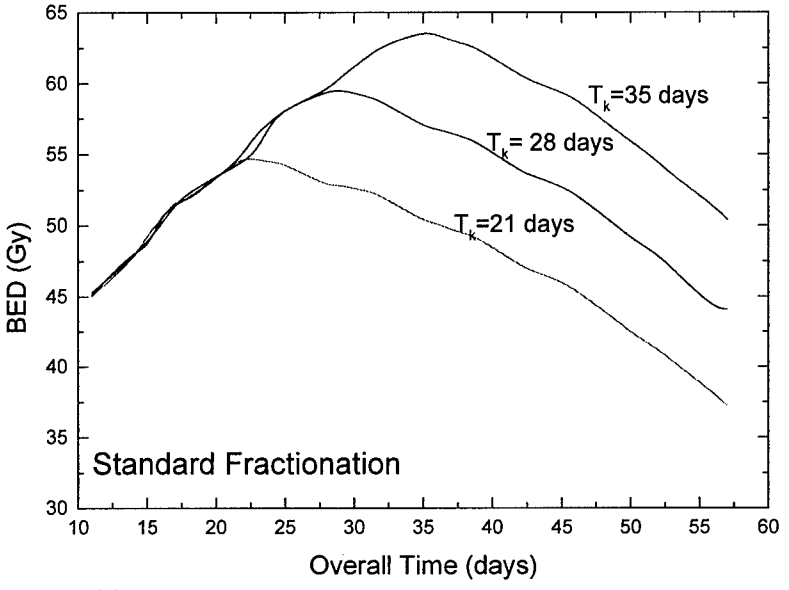
65
60
55
50
45
40
35
30
BED (Gy)
T_k=35 days
T_k= 28 days
T_k=21 days
Standard Fractionation
10
15
20
25
30
35
40
45
50
55
60
Overall Time (days)

(a)

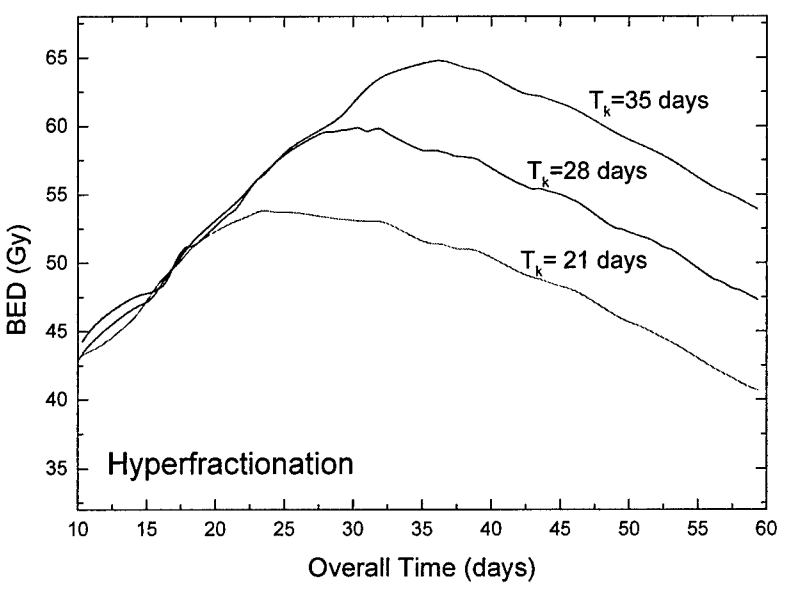
65
60
55
50
45
40
35
BED (Gy)
T_k=35 days
T_k=28 days
T_k= 21 days
Hyperfractionation
10
15
20
25
30
35
40
45
50
55
60
Overall Time (days)

(b)

Figure 1

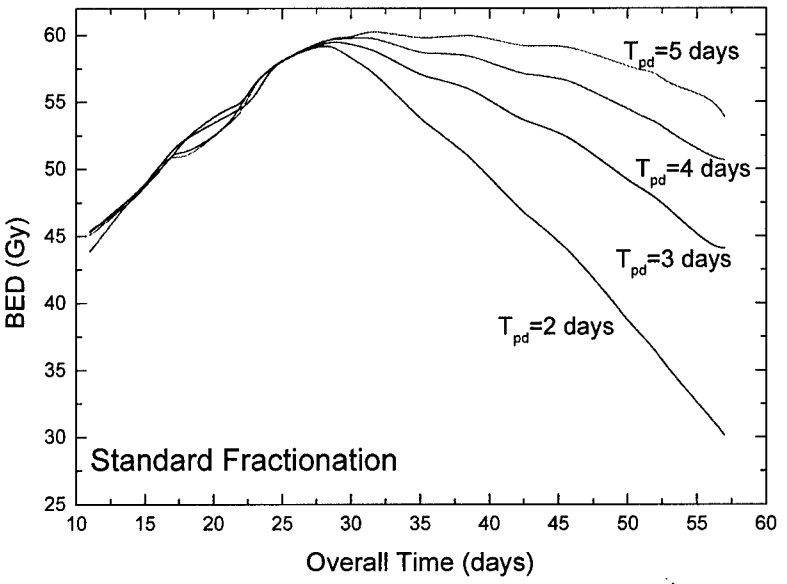
BED (Gy)
Overall Time (days)
T_{pd}=5 days
T_{pd}=4 days
T_{pd}=3 days
T_{pd}=2 days
Standard Fractionation

(a)

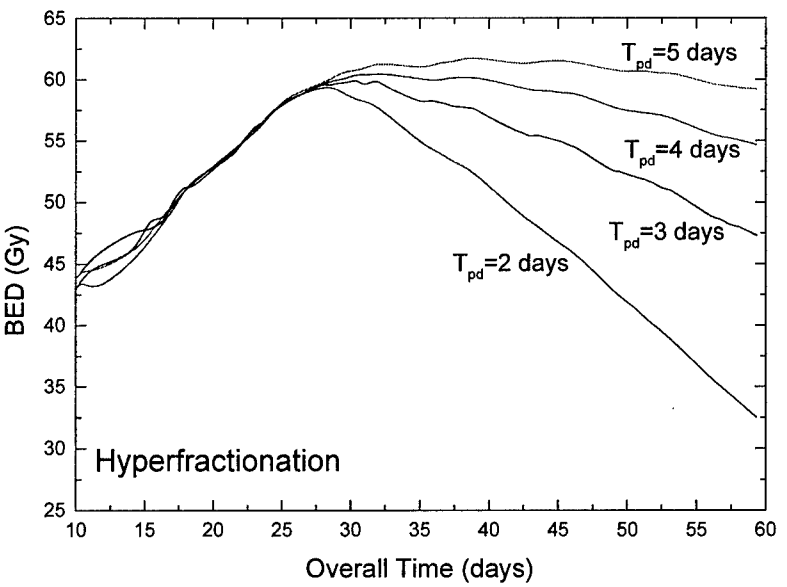
BED (Gy)
Overall Time (days)
T_{pd}=5 days
T_{pd}=4 days
T_{pd}=3 days
T_{pd}=2 days
Hyperfractionation

(b)

Figure 2

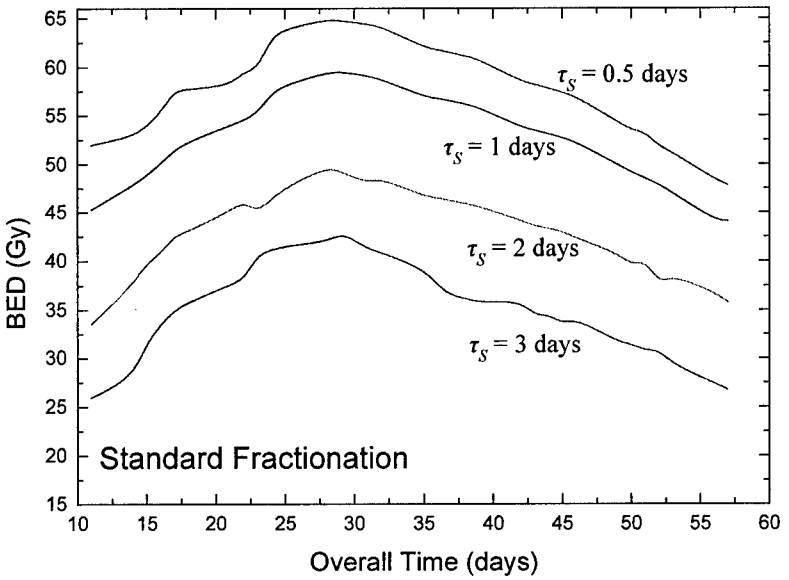
BED (Gy)
Overall Time (days)
τ_S = 0.5 days
τ_S = 1 days
τ_S = 2 days
τ_S = 3 days
Standard Fractionation

(a)

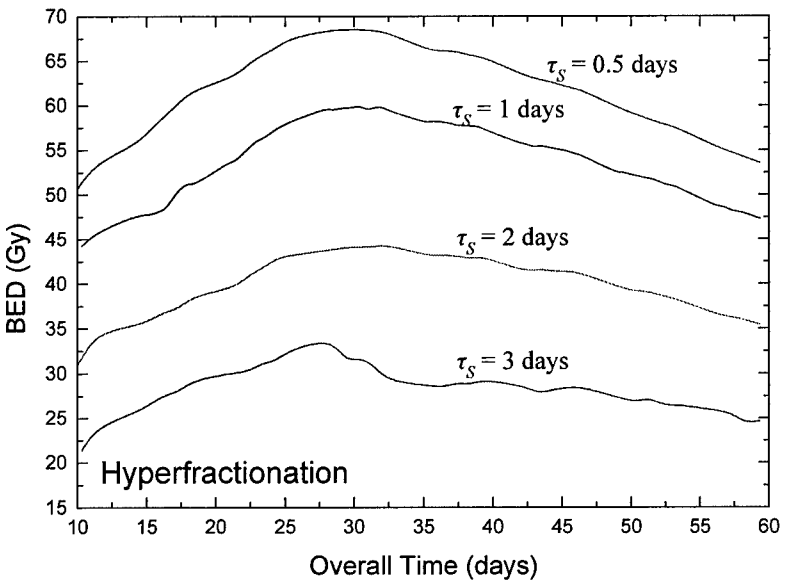
BED (Gy)
Overall Time (days)
τ_S = 0.5 days
τ_S = 1 days
τ_S = 2 days
τ_S = 3 days
Hyperfractionation

(b)

Figure 3

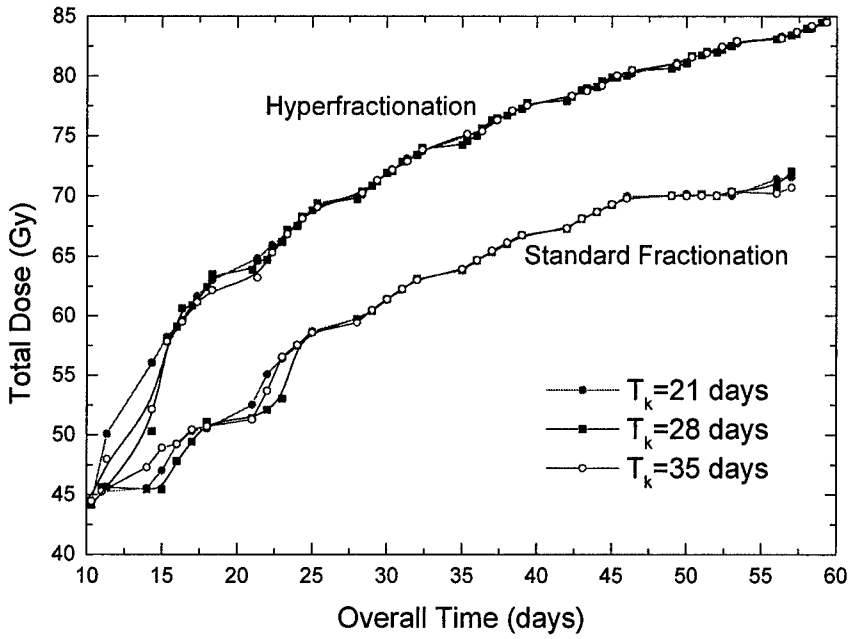
Hyperfractionation
Standard Fractionation
T_k=21 days
T_k=28 days
T_k=35 days
Total Dose (Gy)
Overall Time (days)
85
80
75
70
65
60
55
50
45
40
10
15
20
25
30
35
40
45
50
55
60

Figure 4

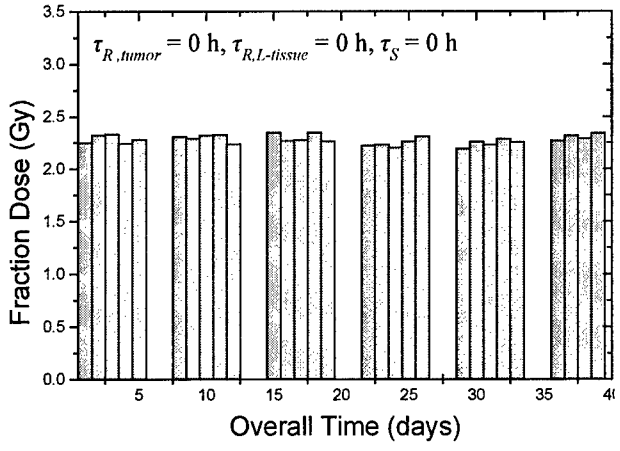

(a)

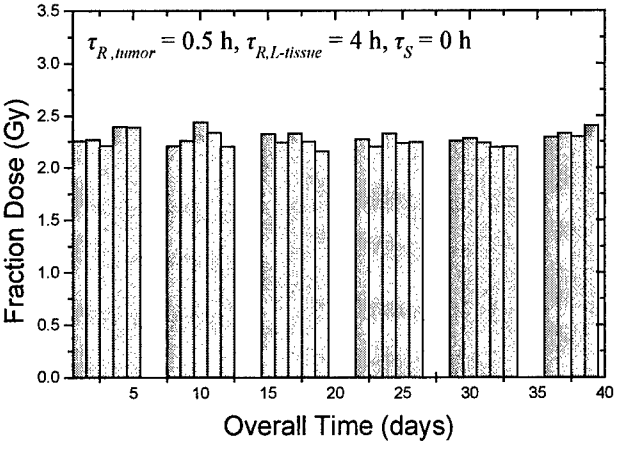

(b)

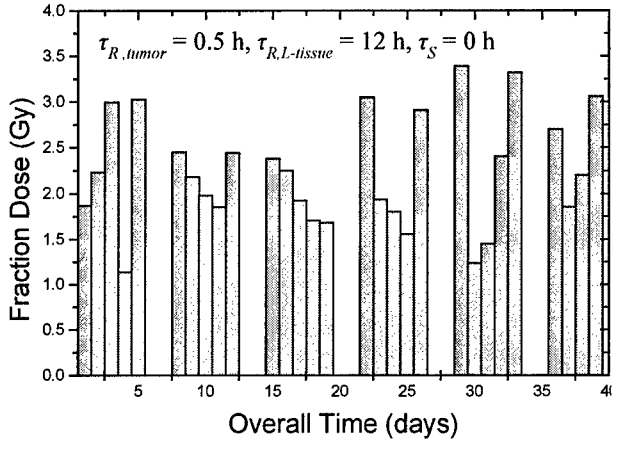

(c)

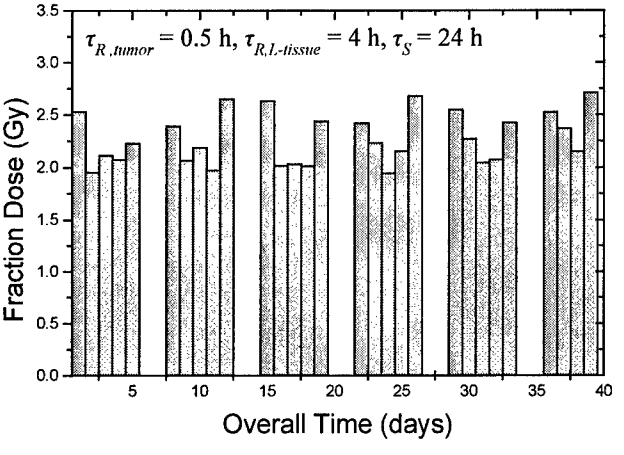

(d)

Figure 5

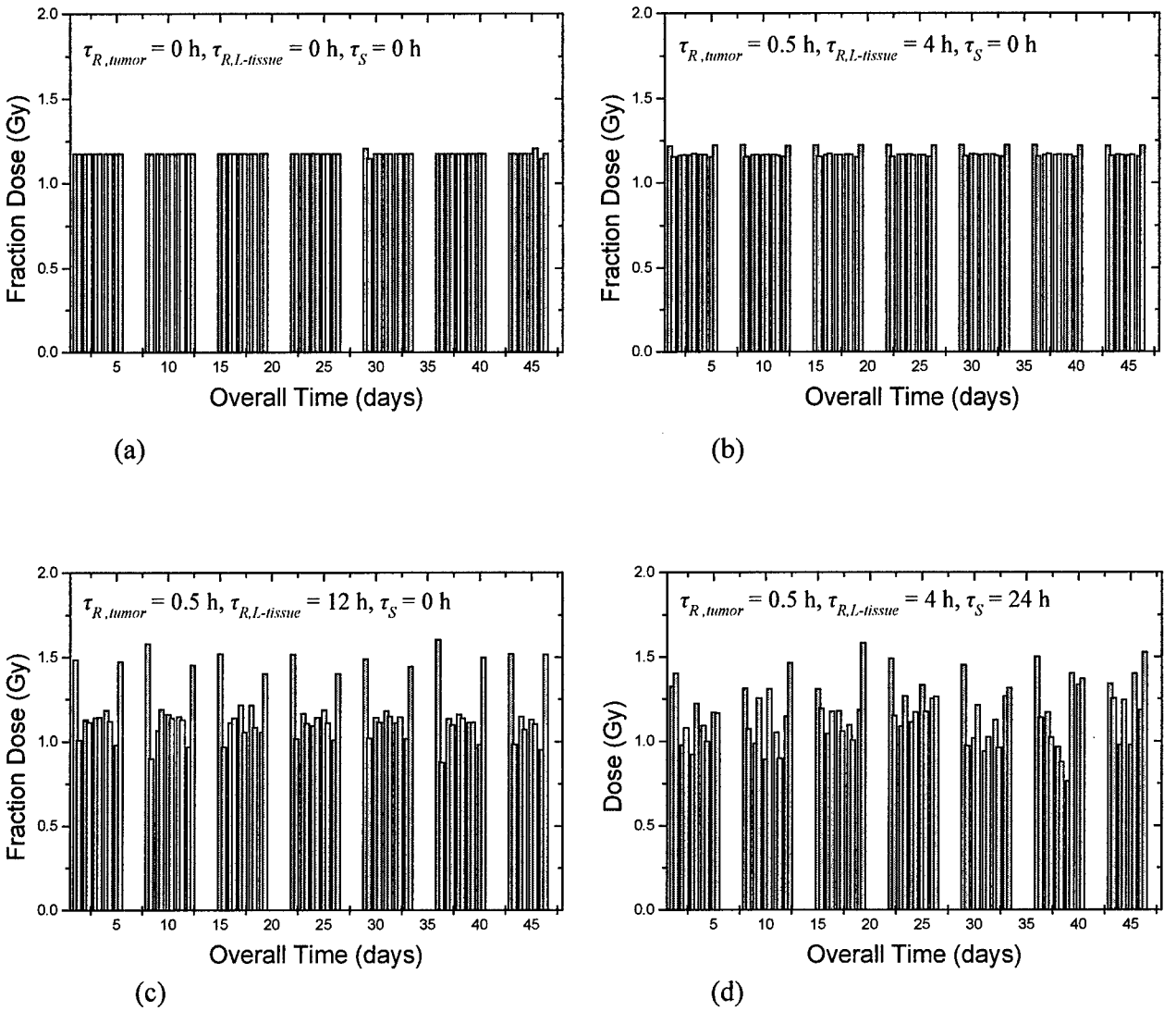
$\tau_{R,tumor}$ = 0 h, $\tau_{R,L\text{-}tissue}$ = 0 h, τ_S = 0 h
Fraction Dose (Gy)
Overall Time (days)
(a)
$\tau_{R,tumor}$ = 0.5 h, $\tau_{R,L\text{-}tissue}$ = 4 h, τ_S = 0 h
Fraction Dose (Gy)
Overall Time (days)
(b)
$\tau_{R,tumor}$ = 0.5 h, $\tau_{R,L\text{-}tissue}$ = 12 h, τ_S = 0 h
Fraction Dose (Gy)
Overall Time (days)
(c)
$\tau_{R,tumor}$ = 0.5 h, $\tau_{R,L\text{-}tissue}$ = 4 h, τ_S = 24 h
Dose (Gy)
Overall Time (days)
(d)

Figure 6

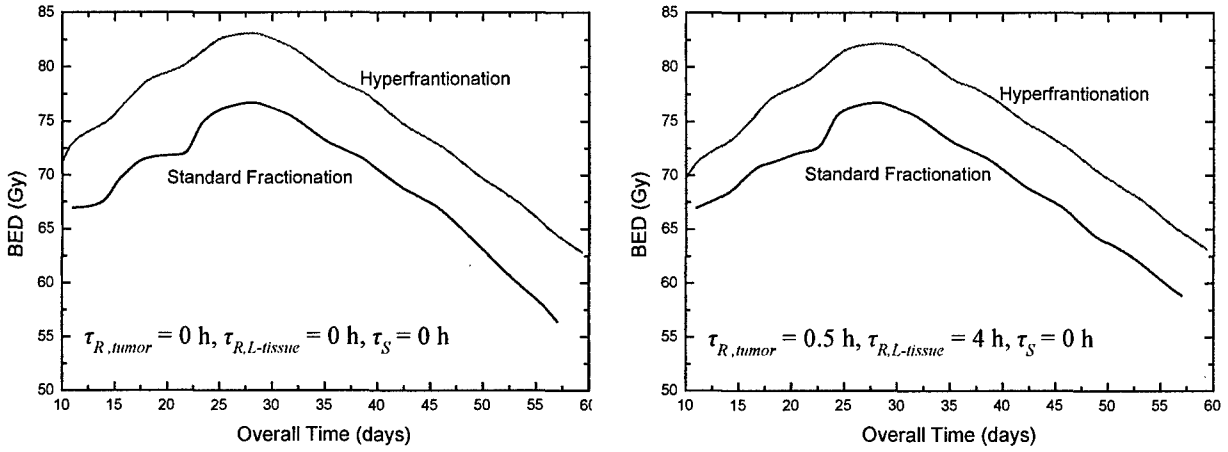

(a)

(b)

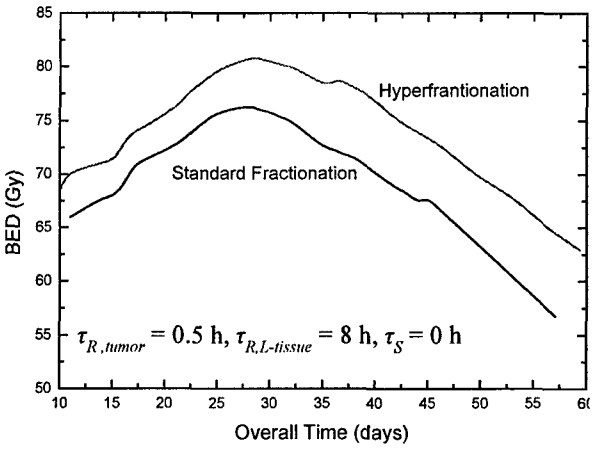

(c)

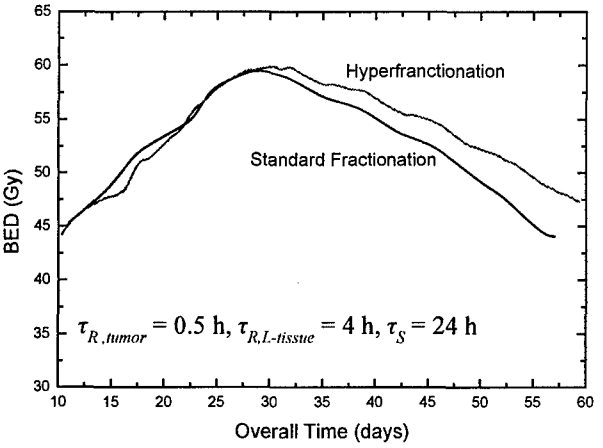

(d)

Figure 7

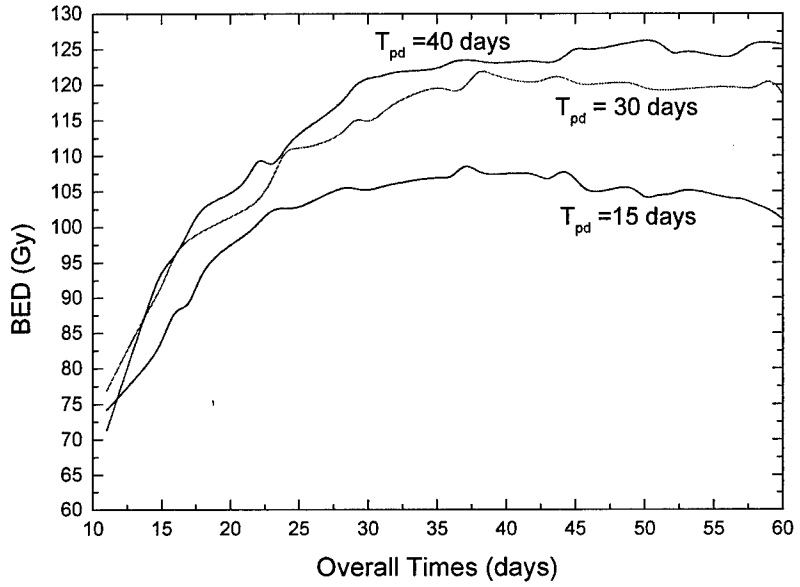
T_{pd} =40 days
T_{pd} = 30 days
T_{pd} =15 days
BED (Gy)
Overall Times (days)

(a)

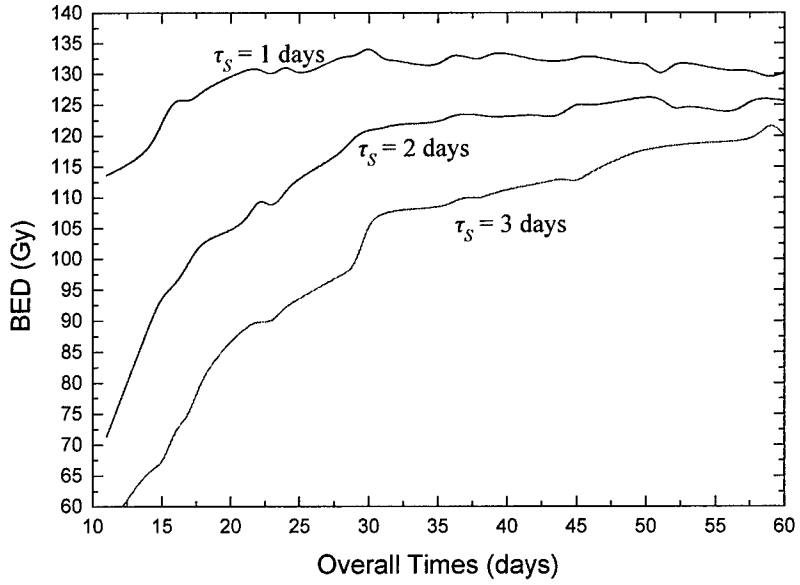
τ_S = 1 days
τ_S = 2 days
τ_S = 3 days
BED (Gy)
Overall Times (days)

(b)

Figure 8

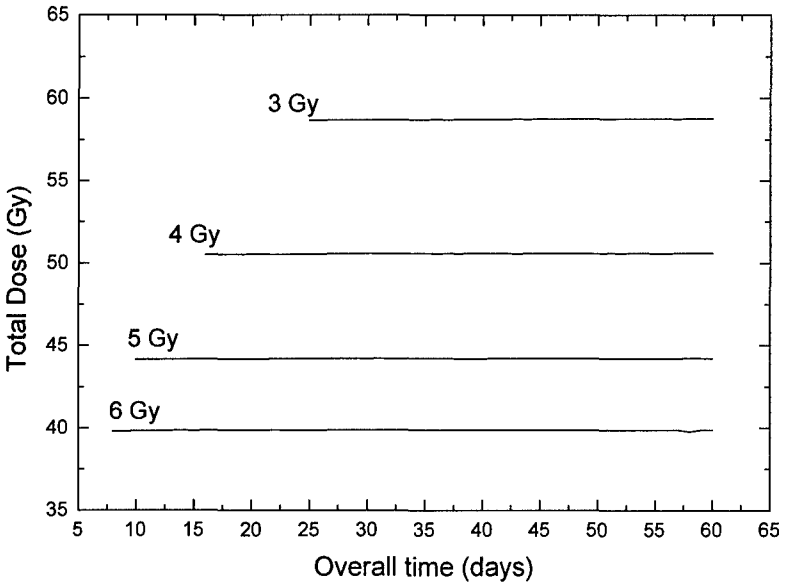
Total Dose (Gy)
Overall time (days)
3 Gy
4 Gy
5 Gy
6 Gy
65
60
55
50
45
40
35
5
10
15
20
25
30
35
40
45
50
55
60
65

(a)

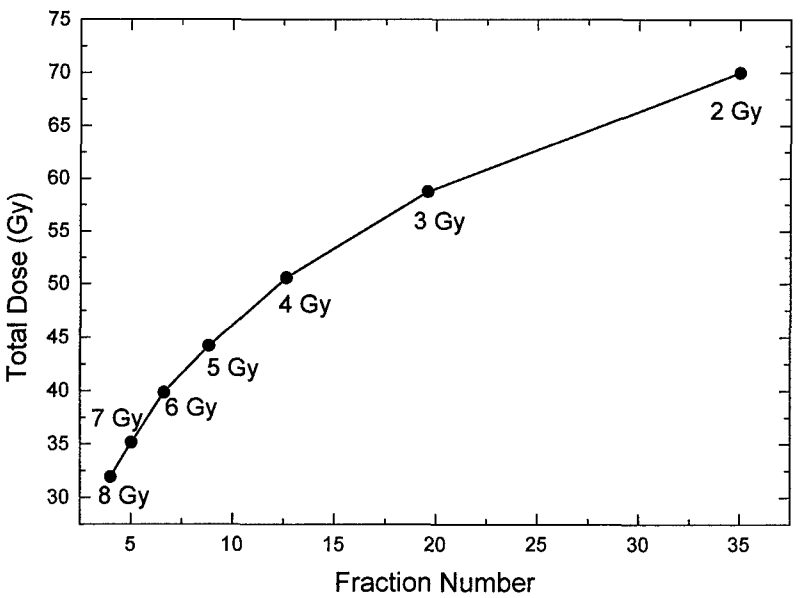
Total Dose (Gy)
Fraction Number
2 Gy
3 Gy
4 Gy
5 Gy
6 Gy
7 Gy
8 Gy
75
70
65
60
55
50
45
40
35
30
5
10
15
20
25
30
35

(b)

Figure 9

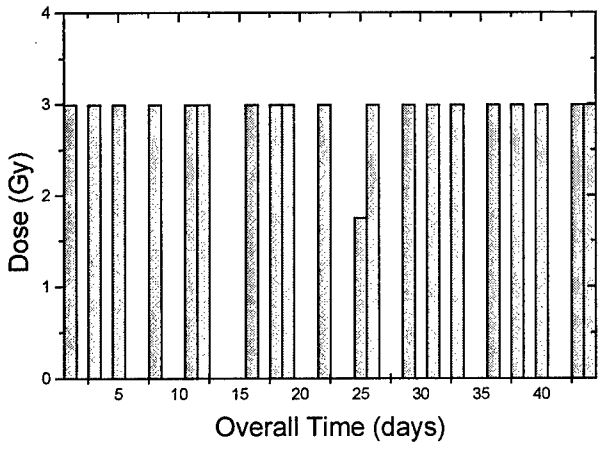

(a)

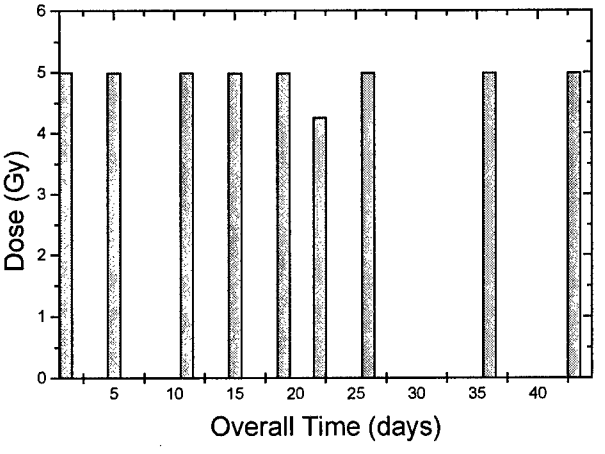

(b)

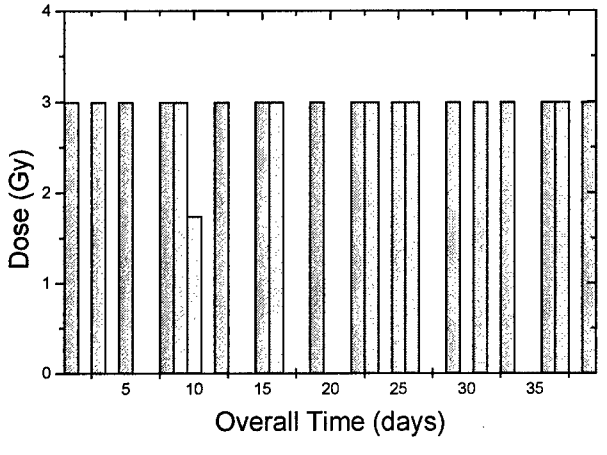

(c)

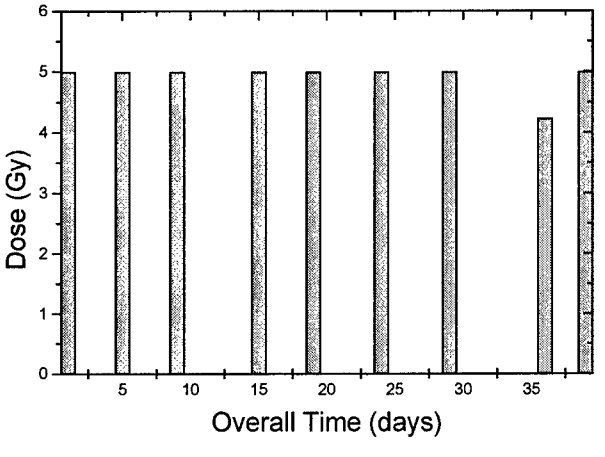

(d)

Figure 10

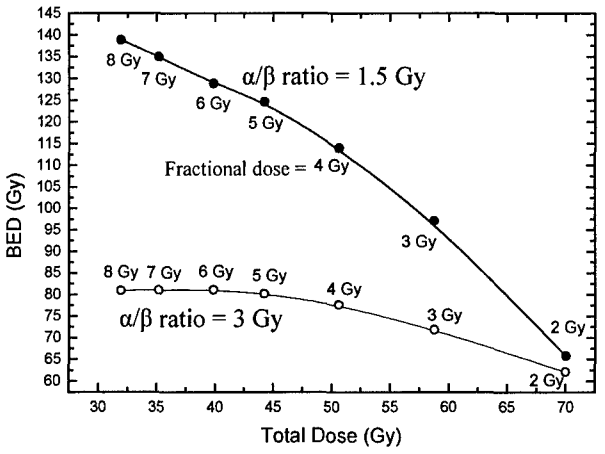

(a)

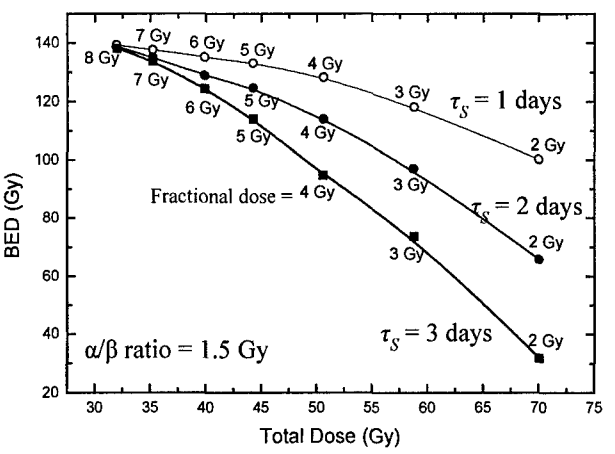

(b)

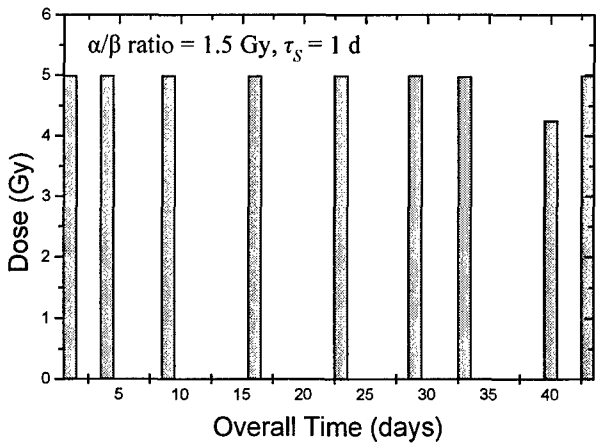

(c)

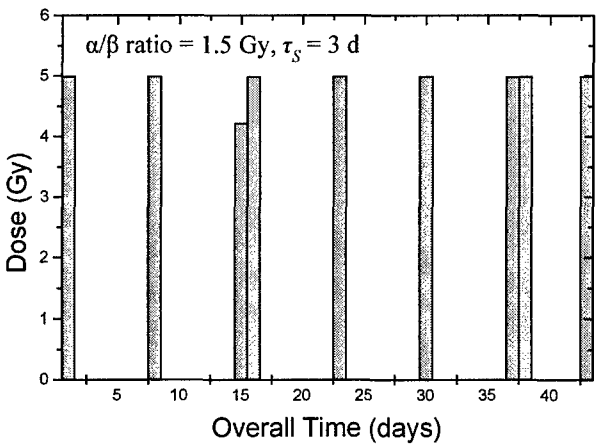

(d)

Figure 11

Reference:

1. Brahme A. Individualizing cancer treatment: biological optimization models in treatment planning and delivery. Int J Radiat Oncol Biol Phys 2001; 49: 327-337.

2. Burman C, Chui CS, Kutcher G, Leibel S, Zelefsky M, LoSasso T, Spirou S, Wu Q, Yang J, Stein J, et al. Planning, delivery, and quality assurance of intensity-modulated radiotherapy using dynamic multileaf collimator: a strategy for large-scale implementation for the treatment of carcinoma of the prostate. International Journal of Radiation Oncology, Biology, Physics 1997; 39: 863-873.

3. Eisbruch A. Intensity-modulated radiotherapy of head-and-neck cancer: encouraging early results. Int J Radiat Oncol Biol Phys 2002; 53: 1-3.

4. Mackie TR, Smith AR. Intensity-modulated conformal radiation therapy and 3-dimensional treatment planning will significantly reduce the need for therapeutic approaches with particles such as protons. Medical Physics 1999; 26: 1185-1187.

5. Yang Y, Xing L. Clinical knowledge-based inverse treatment planning. Phys Med Biol 2004; 49: 5101-5117.

6. Rosenman JG, Halle JS, Socinski MA, Deschesne K, Moore DT, Johnson H, Fraser R, Morris DE. High-dose conformal radiotherapy for treatment of stage IIIA/IIIB non-small-cell lung cancer: technical issues and results of a phase I/II trial. Int J Radiat Oncol Biol Phys 2002; 54: 348-356.

7. Thames HD HJ. Fractionation in radiotherapy. London: Taylor & Francis, 1987.

8. Withers HR. Biologic basis for altered fractionation schemes. Cancer 1985; 55: 2086-2095.

9. Brenner DJ, Hall EJ, Huang Y, Sachs RK. Optimizing the time course of brachytherapy and other accelerated radiotherapeutic protocols. Int J Radiat Oncol Biol Phys 1994; 29: 893-901.

10. Fowler JF. Biological factors influencing optimum fractionation in radiation therapy. Acta Oncol 2001; 40: 712-717.

11. Young SD, Hill RP. Effects of reoxygenation on cells from hypoxic regions of solid tumors: analysis of transplanted murine tumors for evidence of DNA overreplication. Cancer Res 1990; 50: 5031-5038.

12. Lee DJ, Cosmatos D, Marcial VA, Fu KK, Rotman M, Cooper JS, Ortiz HG, Beitler JJ, Abrams RA, Curran WJ, et al. Results of an RTOG phase III trial (RTOG 85-27) comparing radiotherapy plus etanidazole with radiotherapy alone for locally advanced head and neck carcinomas. Int J Radiat Oncol Biol Phys 1995; 32: 567-576.

13. Peters GJ, van der Wilt CL, Gyergyay F, van Laar JA, Treskes M, van der Vijgh WJ, Pinedo HM. Protection by WR-2721 of the toxicity induced by the combination of cisplatin and 5-fluorouracil. Int J Radiat Oncol Biol Phys 1992; 22: 785-789.

14. Weiss JF, Kumar KS, Walden TL, Neta R, Landauer MR, Clark EP. Advances in radioprotection through the use of combined agent regimens. Int J Radiat Biol 1990; 57: 709-722.

15. Thames HD, Jr., Withers HR, Peters LJ, Fletcher GH. Changes in early and late radiation responses with altered dose fractionation: implications for dose-survival relationships. Int J Radiat Oncol Biol Phys 1982; 8: 219-226.

16. Cooper JS. Will altered fraction schemes alter the future? Int J Radiat Oncol Biol Phys 1990; 19: 1621-1622.

17. Jones B, Dale RG, Finst P, Khaksar SJ. Biological equivalent dose assessment of the consequences of hypofractionated radiotherapy. Int J Radiat Oncol Biol Phys 2000; 47: 1379-1384.

18. Mohan R, Wu Q, Manning M, Schmidt-Ullrich R. Radiobiological considerations in the design of fractionation strategies for intensity-modulated radiation therapy of head and neck cancers. Int J Radiat Oncol Biol Phys 2000; 46: 619-630.

19. King CR, DiPetrillo TA, Wazer DE. Optimal radiotherapy for prostate cancer: predictions for conventional external beam, IMRT, and brachytherapy from radiobiologic models. Int J Radiat Oncol Biol Phys 2000; 46: 165-172.

20. Fowler JF, Tome WA, Fenwick JD, Mehta MP. A challenge to traditional radiation oncology. Int J Radiat Oncol Biol Phys 2004; 60: 1241-1256.

21. Withers HR. Biological basis of radiation therapy for cancer. Lancet 1992; 339: 156-159.

22. Fowler JF. The linear-quadratic formula and progress in fractionated radiotherapy. Br J Radiol 1989; 62: 679-694.

23. Hahnfeldt P, Hlatky L. Resensitization due to redistribution of cells in the phases of the cell cycle during arbitrary radiation protocols. Radiat Res 1996; 145: 134-143.

24. Brenner DJ, Hlatky LR, Hahnfeldt PJ, Hall EJ, Sachs RK. A convenient extension of the linear-quadratic model to include redistribution and reoxygenation. Int J Radiat Oncol Biol Phys 1995; 32: 379-390.

25. Brenner DJ. Dose, volume, and tumor-control predictions in radiotherapy. Int J Radiat Oncol Biol Phys 1993; 26: 171-179.

26. Crooks SM, Xing L. Application of constrained least-squares techniques to IMRT treatment planning. Int J Radiat Oncol Biol Phys 2002; 54: 1217-1224.

27. Starkschall G. A constrained least-squares optimization method for external beam radiation therapy treatment planning. Medical Physics 1984; 11: 659-665.

28. Webb S. Optimisation of conformal radiotherapy dose distributions by simulated annealing. Phys Med Biol 1989; 34: 1349-1370.

29. Pugachev A, Li JG, Boyer AL, Hancock SL, Le QT, Donaldson SS, Xing L. Role of beam orientation optimization in intensity-modulated radiation therapy. International Journal of Radiation Oncology, Biology, Physics 2001; 50: 551-560.

30. Turesson I, Thames HD. Repair capacity and kinetics of human skin during fractionated radiotherapy: erythema, desquamation, and telangiectasia after 3 and 5 year's follow-up. Radiother Oncol 1989; 15: 169-188.

31. Wilson GD, Dische S, Saunders MI. Studies with bromodeoxyuridine in head and neck cancer and accelerated radiotherapy. Radiother Oncol 1995; 36: 189-197.

32. Fowler JF, Chappell R. Non-small cell lung tumors repopulate rapidly during radiation therapy. Int J Radiat Oncol Biol Phys 2000; 46: 516-517.

33. Roberts SA, Hendry JH. Time factors in larynx tumor radiotherapy: lag times and intertumor heterogeneity in clinical datasets from four centers. Int J Radiat Oncol Biol Phys 1999; 45: 1247-1257.

34. Brenner DJ, Martinez AA, Edmundson GK, Mitchell C, Thames HD, Armour EP. Direct evidence that prostate tumors show high sensitivity to fractionation (low

alpha/beta ratio), similar to late-responding normal tissue. Int J Radiat Oncol Biol Phys 2002; 52: 6-13.

35. Fowler JF, Ritter MA, Chappell RJ, Brenner DJ. What hypofractionated protocols should be tested for prostate cancer? Int J Radiat Oncol Biol Phys 2003; 56: 1093-1104.

36. Haustermans KM, Hofland I, Van Poppel H, Oyen R, Van de Voorde W, Begg AC, Fowler JF. Cell kinetic measurements in prostate cancer. Int J Radiat Oncol Biol Phys 1997; 37: 1067-1070.

37. Scott SL, Gumerlock PH, Beckett L, Li Y, Goldberg Z. Survival and cell cycle kinetics of human prostate cancer cell lines after single- and multifraction exposures to ionizing radiation. Int J Radiat Oncol Biol Phys 2004; 59: 219-227.

38. Begg AC, Hofland I, Van Glabbeke M, Bartelink H, C. HJ. Predictive value of potential doubling time for radiotherapy of head and neck tumor patients: Results from the European Cooperative Trial 22851. Semin Radiat Oncol 1992; 2: 22-25.

39. Cox JD, Pajak TF, Marcial VA, Coia L, Mohiuddin M, Fu KK, Selim H, Rubin P, Ortiz H. ASTRO plenary: interfraction interval is a major determinant of late effects, with hyperfractionated radiation therapy of carcinomas of upper respiratory and digestive tracts: results from Radiation Therapy Oncology Group protocol 8313. Int J Radiat Oncol Biol Phys 1991; 20: 1191-1195.

40. Brenner DJ. Fractionation and late rectal toxicity. Int J Radiat Oncol Biol Phys 2004; 60: 1013-1015.

41. Lloyd-Davies RW, Collins CD, Swan AV. Carcinoma of prostate treated by radical external beam radiotherapy using hypofractionation. Twenty-two years' experience (1962-1984). Urology 1990; 36: 107-111.

Towards Biologically Conformal Radiation Therapy (BCRT): Selective IMRT Dose Escalation Under the Guidance of Spatial Biology Distribution

Yong Yang and Lei Xing[a)]

Department of Radiation Oncology, Stanford University School of Medicine,

Stanford, CA 94305-5847

Short title: IMRT Dose Escalation

[a)] Author to whom correspondence should be addressed:

Department of Radiation Oncology
Stanford University School of Medicine,
Clinical Cancer Center
875 Blake Wilbur Drive, Rm CC-G204
Stanford, CA 94305-5847
Telephone: (650) 498-7896
Fax: (650) 498-4015
Email: lei@reyes.stanford.edu

Submitted to: *Medical Physics*

Abstract

It is well known that the spatial biology distribution (e.g., clonogen density, radiosensitivity, tumor proliferation rate, functional importance) in most tumors and sensitive structures is heterogeneous. Recent progress in biological imaging is making the mapping of this distribution increasingly possible. The purpose of this work is to establish a theoretical framework to quantitatively incorporate the spatial biology data into IMRT inverse planning. In order to implement this, we first derive a general formula for determining the desired dose to each tumor voxel for a known biology distribution of the tumor based on a linear-quadratic (LQ) model. The desired target dose distribution is then used as the prescription for inverse planning. An objective function with the voxel-dependent prescription is constructed with incorporation of the nonuniform dose prescription. The functional unit density distribution in a sensitive structure is also considered phenomenologically when constructing the objective function. Two cases with different hypothetical biology distributions are used to illustrate the new inverse planning formalism. For comparison, treatments with a few uniform dose prescriptions and a simultaneous integrated boost are also planned. The biological indices, TCP and NTCP, are calculated for both types of plans and the superiority of the proposed technique over the conventional dose escalation scheme is demonstrated. Our calculations revealed that it is technically feasible to produce deliberately nonuniform dose distributions with consideration of biological information. Compared with the conventional dose escalation schemes, the new technique is capable of generating biologically conformal IMRT plans that significantly improve the TCP while reducing or keeping the NTCPs at their current levels. Biologically conformal radiation therapy (BCRT) incorporates patient specific biological information and provides an outstanding opportunity for us to truly individualize radiation treatment. The proposed formalism lays a technical foundation for BCRT and allows us to maximally exploit the technical capacity of IMRT to more intelligently escalate the radiation dose.

Key word: Inverse Planning, Biological Model, TCP, NTCP, IMRT

I. INTRODUCTION

Intensity modulated radiation therapy (IMRT) has been used clinically to provide a highly conformal radiation dose to the target volume while reducing the doses to the surrounding sensitive structures[1-13]. The current IMRT inverse planning is typically aimed at producing a homogeneous target dose under the assumption of uniform biology within the target volume. In reality, it is known that the spatial biology distributions in most tumors and normal tissues are rarely homogeneous. To maximize the efficacy of IMRT, it is desirable to take the inhomogeneous biological information into account and to produce customized nonuniform dose distributions on a patient specific basis. This type of radiation treatment is referred to as biologically conformal radiotherapy (BCRT)[14-19]. The simultaneous integrated boost (SIB) to elective volumes recently appeared in the literature[11, 17, 20] represents a simple example of BCRT. However, an underlying deficiency of the current SIB approach is that the boost doses are based on previous experience, not patient-specific biological information characterizing the spatial tumor burden distribution.

To establish the BCRT treatment planning scheme, three major aspects must be addressed: (i) Determination of the distribution of biological properties of the tumor and critical structures; (ii) Prescription of the desired dose distribution for inverse planning; and (iii) Inverse planning to generate most faithfully the prescribed nonuniform dose distribution. Recently spurred efforts in biological imaging, such as positron emission tomography (PET), single photon emission computed tomography (SPECT), and magnetic resonance spectroscopy imaging (MRSI), are aimed at providing solutions to the first problem[21-31]. To give a few examples, the clonogen density in malignant glioma can be obtained based on the choline/creatine ratio through MRSI[29, 30], tumor hypoxia can be quantified using PET imaging with fluorinated misonidazole (FMISO)[27, 28], tumor proliferation rate can be obtained based on the voxel activity level in DNA proliferation imaging (e.g., fluoro-L-thymidine PET)[25, 26, 32], and lung functional importance distributions can be obtained by perfusion imaging[33]. While the development of molecular imaging techniques is critically important in mapping out biology distributions, the successful integration of this information into IMRT planning through

steps (ii) and (iii) is also indispensable to fully exploit the obtained biology information to improve patient care. In this study we focus our efforts on the last two problems, with the optimistic assumption that spatial biology distributions within a patient has already been determined from biological imaging or other means. Our goal is to establish a theoretical framework for quantitatively incorporating the biological data into IMRT inverse optimization and to show the advantage of the selective dose escalation scheme in enhancing tumor control probability (TCP) and reducing the normal tissue complication probability (NTCP). In conjunction with the rapid development of molecular imaging techniques, this study lays a technical foundation for BCRT and provides a basis for clinically realizing the new treatment strategy in the future.

II. METHODS AND MATERIALS

A. Biological characterization and nonuniform target dose prescription

We assume that biological properties influencing radiation treatment are characterized phenomenologically by three radiobiology parameters: clonogen density (ρ), radiosensitivity (α), and proliferation rate (γ). Generally, these parameters are voxel dependent. In this work we concentrate on their spatial variation within tumor, and ignore the time dependence of the last two parameters.

To accomplish BCRT, an important step is to derive the desired dose distribution that maximizes the cell killing based on (ρ, α, γ) metrics. In the case of uniform biology, it is well known that the target dose should be uniformly distributed. It is, however, not clear at all what form of dose distribution should be used to maximize the cell killing for an arbitrary biology distribution. We start from a linear quadratic (LQ) model[34-36] with inclusion of the tumor cell proliferation. According to this model, the tumor clonogen survival S_i in a voxel of volume V_i after an irradiating dose D_i is given by

$$S_i = \rho_i V_i \exp(-\alpha_i' D_i + \gamma_i \Delta T), \qquad (1)$$

where $\alpha_i' = \alpha_i[1 + d_i/(\alpha_i/\beta_i)]$, ρ_i is the initial clonogen density, d_i is the fractional dose, α_i and β_i are the linear-quadratic coefficients of the cell survival curve, $\gamma_i = \ln 2 / T_p$ is the

cell proliferation rate, T_p is the potential cell doubling time and ΔT is the overall treatment time. The TCP of a voxel i can be expressed as

$$TCP_i = \exp[-\rho_i V_i \exp(-\alpha_i' D_i + \gamma_i \Delta T)]. \qquad (2)$$

The TCP for the whole tumor is product of the TCP_i of all voxels within the tumor volume, *i.e.*,

$$TCP = \prod_i TCP_i . \qquad (3)$$

For a given set of $\{\rho, \alpha, \gamma\}$, the task is to find the dose distribution that maximizes the TCP. Because of the limitation of normal tissue dose tolerances, an arbitrarily high dose to the tumor cannot be achieved and certain constraints need to be imposed[36-41]. In line with previous researchers[36, 37, 40], we restrict the integral dose to the tumor volume to a constant. Mathematically, the constraint is written as

$$\sum_i m_i D_i = E_t , \qquad (4)$$

where m_i is the mass of voxel i, and E_t is the integral target dose.

With the above formulation, the task becomes the maximization of the TCP under the constraint (4). The Lagrange multiplier method is employed to solve the problem. In this approach, a function

$$L(TCP_1,...TCP_i,...) = \prod_i TCP_i + \lambda(\sum_i m_i D_i - E_t) \qquad (5)$$

is introduced, where λ is the Lagrange multiplier, and the solution is obtained by solving the equations

$$\frac{\partial L}{\partial TCP_i} = 0 . \qquad (6)$$

When mass and volume are equal for all voxels in the target, using a process similar to Ebert and Hoban [40] (see appendix), we obtained a general formula for determining the desired dose, $D_0^T(i)$, at the voxel i:

$$D_0^T(i) = \frac{\alpha_{ref}'}{\alpha_i'} D_{ref} - \frac{1}{\alpha_i'}(\gamma_{ref} - \gamma_i)\Delta T - \frac{1}{\alpha_i'} \ln\left(\frac{\alpha_{ref}' \rho_{ref}}{\alpha_i' \rho_i}\right), \qquad (7)$$

where D_{ref} is the reference dose for the voxel with reference radiobiological parameters (ρ_{ref}, α_{ref}, γ_{ref}). In general, D_{ref} should be set to a value that yields a clinically sensible

TCP at the reference voxel. For a given disease site, the radiation dose used in current clinical practice with "intent to cure" can be used as a good starting point in selecting the value of D_{ref}. Using Eq. (7), it is straightforward to determine the desired target prescription dose once the radiobiological parameter (ρ, α, γ) metrics and D_{ref} are known. Note that the desired dose distribution represents an ideal situation without considering the specific dosimetric tolerances of the sensitive structures. In reality, this dose distribution may or may not be exactly realizable. Nevertheless, it sets a landmark and serves as the prescription dose in inverse planning to guide the dose optimization process.

The fractional dose, d_i, is required to obtain the parameter α_i' in Eq. (7). On the other hand, d_i is not known until $D_0^T(i)$ is known. We use a simple iterative method to solve the dilemma. First, the fractional dose is initially set to $d_i=D_{ref}/N_f$, N_f being the fractional number. Second, $D_0^T(i)$ is calculated using Eq. (7) and $d_i= D_0^T(i)/N_f$ is updated. The new $D_0^T(i)$ is then obtained using the updated d_i. We find that $D_0^T(i)$ converges to the solution in less than 5 iterations. In this study we set α/β=10 Gy for all target voxels. The formalism proposed here is, however, general and can be extended to deal with nonuniform distributions of the α/β ratio.

B. Inverse planning with spatially nonuniform dose prescription

The next logical step after obtaining the calculated prescription dose is to use inverse planning to derive the optimal beam profiles that will produce the prescribed dose distribution. To proceed, we construct an objective function to take the known biological information into account. In addition to the voxel-specific prescription as determined by Eq. (7), the nonlinear dose responses of tumor and normal structures are considered using the concept of equivalent volume[42-48] of a voxel, which is defined as

$$(\Delta V_{eff})_i = V_i \phi(i)(D(i)/D_t)^{1/n}, \qquad (8)$$

where $(\Delta V_{eff})_i$ is the effective volume for voxel i with volume V_i and dose $D(i)$, D_t is the desired dose for a target voxel or the $TD_{5/5}$ of the corresponding organ, and $\phi(i)$ is the functional unit density. The value of n characterizes the dose-volume effect of an organ and reflects its architecture (serial or parallel) of the sensitive structure. It is obtained by fitting to clinical dose-volume data. For a sensitive structure, n is a positive number ($n>0$)

while for a target, n should be assigned with a small negative value ($-1<n<0$). $\phi(i) \equiv 1$ for a target voxel.

A general form of the inverse planning objective function in the voxel domain is written as

$$F = \sum_{\tau=1}^{t_\tau} r_\tau \frac{1}{N_\tau} \sum_{i=1}^{N_\tau} \{1 + [D_c(i)/D_0^T(i)]^{1/n_\tau}\}[D_c(i) - D_0^T(i)]^2$$

$$+ \sum_{\sigma=1}^{s_\sigma} r_\sigma \frac{1}{N_\sigma} \sum_{i=1}^{N_\sigma} \{1 + \phi_\sigma(i)[D_c(i)/TD_{\sigma,5/5}]^{1/n_\sigma}\} D_c(i)^2 , \qquad (9)$$

where r_τ and r_σ are the structure specific importance factor of target τ and sensitive structure σ, respectively, t_τ and s_σ the number of targets and sensitive structures, N_τ and N_σ the total number of voxels of target τ or sensitive structure σ, n_τ and n_σ the n parameter of target τ and sensitive structure σ, $D_c(i)$ the calculated dose in voxel i, $D_0^T(i)$ the prescription dose in a target voxel i given by Eq. (7), and $TD_{\sigma,5/5}$ the $TD_{5/5}$ of sensitive structure σ. The objective function becomes the conventional quadratic objective function if the term in the bracket inside each summation is set to unity (this is true when the dose-volume effect is negligible, *i.e.*, when $n_\tau = n_s = +\infty$). More detailed information about the optimization algorithm can be found in Ref. 49.

C. Implementation

A software module for optimizing the objective function (9) is implemented in the platform of the PLUNC treatment planning system (University of North Carolina, Chapel Hill, NC). The dose calculation engine and a variety of image/beam/plan display and evaluation tools of PLUNC are used to review and compare the optimization results. The ray-by-ray iterative algorithm (SIITP) reported earlier[50, 51] is employed to obtain the optimal beam intensity profiles. The dose volume histograms (DVHs) of the involved organs are displayed at the end of each iterative step to visually monitor the optimization process.

D. Plan review tools

It is desirable to extend the currently used plan review tools to deal with a biologically

heterogeneous system. For a target, we define the effective dose at a voxel as the physical dose normalized by the desired dose determined by Eq. (7). The effective-dose volume histogram (EDVH), which is obtained by replacing the dose with the effective dose in conventional DVH, is a useful tool for assessing BCRT plans. For a sensitive structure we replace the fractional volume by $\phi_i V_i$ to construct a functional dose volume histogram (FDVH), similar to that proposed by Lu et al[52] and Marks et al[33]. After including the heterogeneous biological information into the EDVH or FDVH, the wisdom used in interpreting a conventional DVH can be applied to assess the BCRT plans. In addition to the effective dose and the EDVH or FDVH, a cluster of DVHs, each corresponding to a given set of biological parameters $\{\rho, \alpha, \gamma\}$, are also useful to assess dosimetric behavior of the system as a function of the biological status of the system.

Besides the dosimetric evaluation tools, we also used the TCP and NTCPs for plan evaluation. In calculating TCP and NTCP, the heterogeneous biology distributions need to be taken into account. TCP is calculated using equations (2) and (3) and NTCP is assessed using Lyman's model. The Kutcher-Burman effective-volume DVH reduction method[44] is extended to include the non-uniform functional unit density distribution using Eq. (8) when transforming a nonuniform dose distribution into a uniform irradiation of an effective partial volume. Model parameters from Burman *et al*[53] are listed in Table I for the NTCP calculation.

E. Case studies

A prostate case with two different hypothetical distributions of radiobiological parameters is used to test the proposed BRCT inverse planning scheme. In each study, the target consists of the prostate gland with a few intra-prostatic lesions. The sensitive structures include the rectum, bladder and femoral heads. Figures 1a and 3a show the geometric shapes and locations of the structures in the two examples.

In the first example the target includes four biologically different regions, and the functional unit density distributions in the sensitive structures are uniform. Region 1 represents the basis reference target volume with typical parameters[54, 55] $\rho_{0i} = 5\times10^5$ clonogen/cm^3, α_i=0.26 Gy^{-1}, and γ_i=ln2/40 day^{-1}. The radiobiological parameters of the

intra-prostatic lesions are listed in Table II. The parameters n_σ characterizing the dose-volume effect of the sensitive structures in the objective function (9) can be found in Table I. The parameter n_τ is chosen to be –0.2. For comparison, five IMRT plans, indexed by Plan-1, -2, -3, -4, and –5, are generated. Plan-1 is obtained using the BCRT optimization scheme described above with D_{ref}=70 Gy. Plan-2 is obtained by prescribing the whole target a uniform dose of 70 Gy. Plan-3 and -4 are similar to Plan-2 except that the dose is escalated to 81 Gy and 91 Gy[12, 14], respectively. Plan-5 is the SIB IMRT plan with the same prescribed doses as that of the BCRT. In Plan-1 to –4, the objective function expressed in Eq. (9) is used and in Plan-5 the conventional dose-based quadratic objective function is adopted. The optimization parameters (maximum dose constraints and importance factors) in the dose-based method were adjusted by trial-and-error to obtain the "optimal" plan. The same beam configuration (five equally spaced 15MV photon beams with gantry angles of 0°, 72°, 144°, 216°, and 288° in IEC convention) is used in generating the five plans.

In the second example we hypothetically introduced a higher functional unit density region in the rectum (R_Region 2 as shown in figure 3a) in addition to three biologically different target regions. The functional unit density of the R_Region 1 is assigned a value of 1 and that of the R_Region 2 is set to be 4. The same set (ρ_{0i}, α_i, γ_i) as the previous example and a reference dose of 70 Gy are assigned to the prostate gland. The parameters for other target regions are listed in Table II. Once again, five IMRT plans are generated: Plan-1 is obtained using the proposed selective dose escalation scheme, Plan-2, -3, and –4 are generated using different uniform prescription doses (70, 81, and 91 Gy) and Plan-5 is SIB plan with the same prescription as Plan-1 but is optimized using the conventional quadratic objective function. In generating these five plans, seven equally spaced 15MV photon beams (0°, 51°, 103°, 154°, 206°, 257°, and 309°) are employed.

III. RESULTS

A. Example 1: Prostate case with four biologically different regions

In the first example, based on Eq. (7) and the parameters listed in Table II, the prescription doses to the target region 2, 3 and 4 are determined to be 85 Gy, 119 Gy and 75 Gy, respectively. In order to examine the capability of the BCRT inverse planning system in producing an extremely nonuniform dose within a target volume, we have used an "extreme" combination of $\{\rho, \alpha, \gamma\}$, which leads to an exceedingly high prescription dose in region 3 (119 Gy). Figures 1b-d show the isodose distributions of Plan-1 in a transverse slice and two sagittal slices. The EDVH of the target and the DVHs of the sensitive structures are plotted in figure 2 for Plan-1 in solid curves. For comparison, the corresponding EDVHs and DVHs of Plan-2, -3, -4, and -5 are also shown in the figures as dashed, dotted, dash-dotted and dash-dot-dotted curves. As seen from figure 1, all regions in the prostate are well covered by their prescription doses and the sensitive structures are well spared. Even in this "extreme" case, it seems that the inverse planning system can satisfy the biological requirement. A steep dose gradient is found at the interface between the target and the rectum. A comparison of the target EDVH in figure 2a indicates that above 98.5% of the target voxels achieved their desired doses in Plan-1 and Plan-5. However, for the uniform dose escalation scheme, the desired doses in some regions (region 2, 3 and part of region 4 in Plan-2; region 2 and 3 in Plan-3; and region 3 in Plan-4) are not achieved. We found that, in Plan-1, the doses to the surrounding sensitive structures are not significantly increased compared with those of Plan-2, despite of the fact that some voxels in region 4 receive a dose as high as 119 Gy. In Plan-1, the rectum, bladder and femoral heads are better spared in comparison with Plan-3, -4. However, by comparing the DVHs of Plan-1 and –5, it is noticed that, although the target coverage in Plan-5 is similar to that in Plan-1, the sensitive structures in Plan-5 receive much higher doses than Plan-1, indicating that the proposed approach can increase the sensitive structure sparing compared with the conventional dose-based quadratic objective function. In addition, as can be expected, the target doses in Plan-1 and –5 are less uniform in the target volume in comparison with that of Plan-2, -3, and –4. This is more pronounced in the target region 1, where about 50% of the volume receives a dose larger than 85 Gy as shown in figure 2b, resulting in an effective doses above 120% in

~50% of the target voxels (see figure 2a). However, the increase of dose homogeneity is desirable here provided that the NTCPs are not compromised.

Table III lists the calculated TCPs for the targets and NTCPs for the sensitive structures with consideration of heterogeneous biology in all plans. It is seen that the overall TCPs for the three plans with uniform target dose prescriptions (Plan-2, -3, and -4) are all less than that of the BCRT plan (Plan-1) and SIB plan (Plan-5). This is understandable because, in Plan-2, -3 and –4, some target regions (such as target region 3) receive doses much less than the desired doses. For example, in Plan-4, the TCP for target region 3 is only 0.461. Even if the TCPs for region 1, 2, and 4 are all close to 1.00, the resultant total TCP for Plan-4 is 0.461. In contrast, the TCPs of Plan-1 and Plan-5 are 0.984 and 0.981, respectively. Furthermore, we found that the NTCPs of the sensitive structures in Plan-1 are very close to Plan-2, significantly less than Plan-3, -4 and -5. For example, the rectum NTCPs are 0.21% for Plan-1 and 0.20% for Plan-2. These are increased to 0.65%, 1.84% and 0.89% for Plan-3, -4 and -5, respectively. Again, although similar overall TCPs are achieved for the BCRT and dose-based SIB IMRT plans when the same dose prescriptions are used, the rectum NTCPs are significantly reduced using the proposed formulism. This is consistent with our previous study of the objective function in the context of conventional IMRT aiming to deliver a uniform dose to the target volume (49).

B. Example 2: Prostate case with three biologically different regions and nonuniform importance in rectum

In the second hypothetical example, there are three biologically different regions in the prostate and two functionally different regions in the rectum. The prescription doses for the three target regions are 70 (reference dose), 99 and 121 Gy, as determined by Eq. (7) with the biological parameters listed in table II. Figures 3b-f show the isodose distributions of Plan-1 in three transverse slices and two sagittal slices. The EDVHs and DVHs of the target and sensitive structures for Plan-1 to Plan-5 are plotted in figure 4 as solid, dashed, dotted, dash-dotted and dash-dot-dotted curves. Similar to the previous example, in Plan-1, all regions in the prostate are well covered by a dose comparable to the prescription and the sensitive structures are well spared. The dose gradient at the

interface between the target and the rectum is very sharp for all the plans. From figure 4a we find that above 98% of the target voxels achieved their desired doses in Plan-1. As a consequence of incorporating functional unit density information in inverse planning, the rectum sparing is even better than that of Plan-2, much better than that of Plan-3, -4. However, we notice that the sparing of the femoral heads in Plan-1 is not as good as that in Plan-2, -3 and -4. This is because high intensity beamlets that pass through the femoral heads are needed to adequately irradiate the target region 3, as seen from figures 3b and 3c. In addition, similar to the first example, the target coverage in Plan-5 is close to that in Plan-1, but the doses to the sensitive structures in Plan-5 are much higher than that in Plan-1.

Table IV lists the calculated TCPs and NTCPs for all plans. Once again, we found that the TCP of the target in the proposed BCRT technique is much higher and the NTCP of the rectum is lower compared with those obtained using the conventional uniform dose escalation schemes. Remarkably, the overall TCP for the target is increased from 0.823 to 0.982 and the NTCP of the rectum is reduced from 3.1% to 0.40% when Plan-4 is replaced by the selective dose escalation scheme (Plan-1). Again, we found that, for similar overall TCPs, the rectum NTCPs of the BCRT plan are much lower in comparison with that obtained using dose-based SIB scheme.

IV. DISCUSSION

Eq. (7) provides a general formula for determining the desired target dose distribution based on the known biology information of the system and represents one of the main results of this study. A few special cases are worth discussing here. First, when the biology distribution is uniform in the target, a uniform dose of D_{ref} is desired. This is consistent with previous studies[37] and existing clinical knowledge.

When the clonogen density ρ is nonuniform while the values of α and γ are constant across the target, we have

$$D_0^T(i) = D_{ref} - \frac{1}{\alpha} \ln\left(\frac{\rho_{0ref}}{\rho_{0i}}\right), \qquad (10)$$

which is identical to the formula obtained by Webb and Nahum[36]. Eq. (10) indicates that the desired dose depends on the tumor cell density logarithmically and is thus relatively insensitive to a variation in the clonogen density. For α'_{ref}=0.312, for example, even if the clonogen density in a tumor voxel is 10 times higher than that of the reference situation, the desired dose is only about 7 Gy higher than the reference value. A detailed discussion of this special situation has been presented by Webb and Nahum[36].

Another special case is that the tumor clonogen density and the proliferation rate are constant and the radiosensitivity α is spatially nonuniform. Eq. (7) now becomes

$$D_0^T(i) = \frac{\alpha'_{ref}}{\alpha'_i} D_{ref} - \frac{1}{\alpha'_i} \ln\left(\frac{\alpha'_{ref}}{\alpha'_i}\right). \qquad (11)$$

The desired dose is approximately inversely proportional to the parameter α'_i and is thus sensitively dependent on the value of parameter α'_i. This is similar to the conclusions of Ebert and Hoban[40] and Levin-Plotnik and Hamilton[41]. For example, if α'_i is reduced from 0.312 (corresponding to α =0.26, fractional dose d_i =2.0Gy and α/β ratio=10 Gy) to 0.18 (corresponding to α =0.15, d_i =2.0Gy, and α/β =10 Gy), the desired dose is increased by about 70% (from 70 Gy to about 118 Gy).

If we keep the tumor clonogen density and radiosensitivety α' constant and only allow the proliferation rate γ to vary spatially, then

$$D_0^T(i) = D_{ref} + \frac{1}{\alpha'_i}(\gamma_i - \gamma_{ref})\Delta T. \qquad (12)$$

Thus the desired dose increases linearly with the proliferation rate. In this work the potential cell-doubling times, T_p, used by King *et al*[54] are adopted. Since T_p for a prostate tumor is relatively longer, its influence on the desired dose is not very significant. However, for other more rapidly proliferating tumors, the proliferation rate may play an important role. In such situations, reducing the overall treatment time ΔT (e.g., using an accelerated scheme) is helpful to minimize the influence of the proliferation rate.

We emphasize that the quadratic term in the linear-quadratic model plays an important role in accounting for the fractionation effect. If only the linear term is kept, the total dose $D_0^T(i)$ in Eq. (7) is no longer entangled with the fractional dose d_i. When the

quadratic term is "switched on", the value of $D_0^T(i)$ depends not only the total reference dose but also the fractional dose. For a large fractional dose, the total dose will be less, and *vice versa*. In other words, the total dose received by a voxel is determined by two contributing factors, one being the local biological parameters $\{\rho,\alpha,\gamma\}$, and the other being the coupling between the fractional dose and the total dose. The latter is responsible for the phenomenon that the total dose needs to be decreased when the number of fractions is reduced. If the quadratic term were ignored, according to Eq. (7), the dose required at a voxel would be much higher. For example, the desired doses for target region 3 in Example 1 are determined to be 119 Gy and 135 Gy with and without inclusion of the quadratic term, respectively.

We also would like to emphasize that in this study, the radiosensitivity α' and proliferation rate γ are assumed to be constants during the whole treatment course. In reality, both α' and γ may change with time due to such biological processes as tumor cell redistribution[56] and reoxygenation[57]. The time dependence of these factors may result in a reduction of the desired prescription dose, and this effect should be investigated in the future.

Comparing with the uniform dose escalation scheme, our study clearly suggests that deliberately incorporating an inhomogeneous dose distribution significantly enhances the TCP and reduces the NTCP. Physically, we believe that the significant improvement arises from the more effective use of radiation in the newly proposed treatment scheme. A great deal of dose is "wasted" in the conventional uniform dose escalation scheme. For example, in the first example the increased doses in the target region 1 and 4 have almost no contributions to the enhancement of the TCP when Plan-2 (70 Gy uniform dose to the prostate gland) is replaced by Plan-3 (81 Gy) or Plan-4 (91 Gy). Even though part of the prostate receives high doses in the selective dose escalation scheme (for example, 119 Gy in target region 3 of the first example), the total deposited energy in the targets is still less than that of Plan-3 or -4. It is thus not difficult to understand why deliberately nonuniform dose distributions can, in general, reduce the radiation side-effects and represent a more intelligent way to irradiate the tumor target.

A similar deficiency also exists in the current SIB approach. Although it is clear that the regions with different tumor burdens should be given different doses, the specific

values for the regions are determined in an ad hoc manner. The empirical boost dose could be too low, in which case the tumor control is sacrificed, or too high, in which case other parts of the system are compromised. The problem is aggravated when the tumor burden varies continuously from point to point. In the proposed BCRT approach, the prescribed dose is voxel-dependent and is determined based on the tumor biology distribution. In addition, a more sophisticated objective function is developed to take the dose volume effect and functional density information of the sensitive structures into account, resulting in better sparing of the sensitive structures.

Finally, it should be recognized that our knowledge of radiobiological parameters for tumors or normal tissues is still very crude and the validity of the model is still under establishment. Therefore, the LQ model and the parameters adopted in the paper are fine for a proof of principle but they should not be taken as more than that.

V. CONCLUSION

In the presence of nonuniform biology distributions, IMRT inverse planning is complicated by the fact that it is not clear what represents the appropriate spatial dose prescription, which is generally used as a landmark to guide the dose optimization process. In this work, we have described a technique for deriving the prescription dose based on a LQ model with consideration of the cell proliferation. The relation is quite general and can be used as prescription dose to guide an arbitrary inverse planning objective function aimed to produce customized dose distribution in accordance with the spatial biology information. For a given patient, IMRT inverse planning now consists of two steps: Derivation of the prescription dose, and beam profile optimization that produces as closely as possible this prescription dose. The formalism proposed here lays a technical foundation for future BCRT development, allowing us to escalate tumor dose more intelligently and effectively. When combined with state-of-the-art biological imaging techniques, which promise to reveal detailed patient-specific biology distribution information, this study may have significant implication for the management of cancer in the future.

Acknowledgement

The authors wish to thank Dr. B. Thorndyke for carefully reading the manuscript. We would also like to thank Drs S. Hancock, A. Koong, C. King, Q. T. Le, A. Boyer, and D. Spielman for useful discussion. This research is supported in part by the National Cancer Institute (5 R01 CA98523-01) and Department of Defense (DAMD17-03-1-0019 and -0023).

Appendix

We present the detailed derivation process for Eq. (7) under the condition of equal mass and volume for all target voxels.

Substituting Eq. (5) into the Eq. (6), we obtain,

$$\lambda TCP_i \frac{\partial(m_i D_i)}{\partial TCP_i} = \lambda TCP_{ref} \frac{\partial(m_{ref} D_{ref})}{\partial TCP_{ref}} = -TCP . \qquad \text{(A1)}$$

Since $\lambda \neq 0$, otherwise, TCP becomes zero according to the requirement of Eq. (6), which corresponds to a minimum. If we assumed that mass for all target voxels is equal, then Eq. (A1) becomes

$$TCP_i \frac{\partial D_i}{\partial TCP_i} = TCP_{ref} \frac{\partial D_{ref}}{\partial TCP_{ref}} . \qquad \text{(A2)}$$

From Eq. (2) we have

$$D_i = \frac{-1}{\alpha_i'} \ln\left\{ -\gamma_i \Delta T + \ln\left[\frac{-1}{\rho_i V_i} \ln TCP_i \right] \right\} . \qquad \text{(A3)}$$

Substituting the expressions from Eq. (A3) for both D_i and D_{ref} into Eq. (A2), we have

$$\alpha_i' \ln(TCP_i) = \alpha_{ref}' \ln(TCP_{ref}) . \qquad \text{(A4)}$$

The desired doses, $D_0^T(i)$, producing maximum TCP with the constraint of constant integral dose, can be obtained by substituting TCP_i and TCP_{ref} expressed in Eq. (2) into Eq. (A4)

$$D_0^T(i) = \frac{\alpha_{ref}'}{\alpha_i'} D_{ref} - \frac{1}{\alpha_i'}(\gamma_{ref} - \gamma_i)\Delta T - \frac{1}{\alpha_i'} \ln\left(\frac{\alpha_{ref}' \rho_{ref} V_{ref}}{\alpha_i' \rho_i V_i} \right) . \qquad \text{(A5)}$$

When volume for all target voxels is equal, Eq. (A5) becomes Eq. (7).

References:

1 S. Webb. Intensity-Modulated Radiation Therapy volume xv: Bristol: Institute of Physics Publishing, 2001

2 C. C. Ling, C. Burman, C. S. Chui, G. J. Kutcher, S. A. Leibel, T. LoSasso, R. Mohan, T. Bortfeld, L. Reinstein, S. Spirou, X. H. Wang, Q. Wu, M. Zelefsky and Z. Fuks, "Conformal radiation treatment of prostate cancer using inversely-planned intensity-modulated photon beams produced with dynamic multileaf collimation," International Journal of Radiation Oncology, Biology, Physics 35, 721-730 (1996).

3 S. Y. Woo, W. H. Grant, 3rd, D. Bellezza, R. Grossman, P. Gildenberg, L. S. Carpentar, M. Carol and E. B. Butler, "A comparison of intensity modulated conformal therapy with a conventional external beam stereotactic radiosurgery system for the treatment of single and multiple intracranial lesions," International Journal of Radiation Oncology, Biology, Physics 35, 593-597 (1996).

4 N. Lee, P. Xia, J. M. Quivey, K. Sultanem, I. Poon, C. Akazawa, P. Akazawa, V. Weinberg and K. K. Fu, "Intensity-modulated radiotherapy in the treatment of nasopharyngeal carcinoma: an update of the UCSF experience," Int J Radiat Oncol Biol Phys 53, 12-22 (2002).

5 Q. T. Le, L. Xing and A. L. Boyer, Head and Neck IMRT. In: Purdy J. GI, and Palta J, ed. 3D Conformal Radiation Therapy & Intensity Modulated Radiation Therapy in the Next Millennium. Madison, WI: Medical Physics Publishing, 1999; 190-195

6 E. Huang, B. S. Teh, D. R. Strother, Q. G. Davis, J. K. Chiu, H. H. Lu, L. S. Carpenter, W. Y. Mai, M. M. Chintagumpala, M. South, W. H. Grant, 3rd, E. B. Butler and S. Y. Woo, "Intensity-modulated radiation therapy for pediatric medulloblastoma: early report on the reduction of ototoxicity," International Journal of Radiation Oncology, Biology, Physics 52, 599-605 (2002).

7 J. G. Rosenman, J. S. Halle, M. A. Socinski, K. Deschesne, D. T. Moore, H. Johnson, R. Fraser and D. E. Morris, "High-dose conformal radiotherapy for treatment of stage IIIA/IIIB non-small-cell lung cancer: technical issues and results of a phase I/II trial," Int J Radiat Oncol Biol Phys 54, 348-356 (2002).

8 A. J. Mundt, A. E. Lujan, J. Rotmensch, S. E. Waggoner, S. D. Yamada, G. Fleming and J. C. Roeske, "Intensity-modulated whole pelvic radiotherapy in women with gynecologic malignancies," International Journal of Radiation Oncology, Biology, Physics 52, 1330-1337 (2002).

9 M. J. Krasin, B. T. Crawford, Y. Zhu, E. S. Evans, M. R. Sontag, L. E. Kun and T. E. Merchant, "Intensity-modulated radiation therapy for children with intraocular retinoblastoma: potential sparing of the bony orbit," Clin Oncol (R Coll Radiol) 16, 215-222 (2004).

10 J. Meyer, M. H. Phillips, P. S. Cho, I. Kalet and J. N. Doctor, "Application of influence diagrams to prostate intensity-modulated radiation therapy plan selection," Phys Med Biol 49, 1637-1653 (2004).

11 A. Eisbruch, "Intensity-modulated radiotherapy of head-and-neck cancer: encouraging early results," Int J Radiat Oncol Biol Phys 53, 1-3 (2002).

12 M. J. Zelefsky, Z. Fuks, M. Hunt, Y. Yamada, C. Marion, C. C. Ling, H. Amols, E. S. Venkatraman and S. A. Leibel, "High-dose intensity modulated radiation therapy for prostate cancer: early toxicity and biochemical outcome in 772 patients," Int J Radiat Oncol Biol Phys 53, 1111-1116 (2002).

13 S. M. Zhou, L. B. Marks, G. S. Tracton, G. S. Sibley, K. L. Light, P. D. Maguire and M. S. Anscher, "A new three-dimensional dose distribution reduction scheme for tubular organs," Med Phys 27, 1727-1731 (2000).

14 C. C. Ling, J. Humm, S. Larson, H. Amols, Z. Fuks, S. Leibel and J. Koutcher, "Towards multidimensional radiotherapy (MD-CRT): biological imaging and biological conformality," International Journal of Radiation Oncology, Biology, Physics 47, 551-560 (2000).

15 A. Brahme, "Individualizing cancer treatment: biological optimization models in treatment planning and delivery," Int J Radiat Oncol Biol Phys 49, 327-337. (2001).

16 L. Xing, C. Cotrutz, S. Hunjan, A. L. Boyer, E. Adalsteinsson and D. Spielman, "Inverse planning for functional image-guided intensity-modulated radiation therapy," Phys Med Biol 47, 3567-3578. (2002).

17 K. S. Chao, S. Mutic, R. L. Gerber, C. A. Perez and J. A. Purdy, "A novel approach to overcome hypoxic tumor resistance: Cu-ATSM-guided intensity-modulated radiation therapy," International Journal of Radiation Oncology, Biology, Physics 49, 1171-1182 (2001).

18 R. Macklis, M. Weinhous and G. Harnisch, "Intensity-modulated radiotherapy: rethinking basic treatment planning paradigms.," International Journal of Radiation Oncology, Biology, Physics 48, 317-318 (2000).

19 M. Alber, F. Paulsen, S. M. Eschmann and H. J. Machulla, "On biologically conformal boost dose optimization," Phys Med Biol 48, N31-35 (2003).

20 Q. Wu, R. Mohan, A. Niemierko and R. Schmidt-Ullrich, "Optimization of intensity-modulated radiotherapy plans based on the equivalent uniform dose," Int J Radiat Oncol Biol Phys 52, 224-235. (2002).

21 S. R. Cherry, "In vivo molecular and genomic imaging: new challenges for imaging physics," Phys Med Biol 49, R13-48 (2004).

22 J. Kurhanewicz, M. G. Swanson, S. J. Nelson and D. B. Vigneron, "Combined magnetic resonance imaging and spectroscopic imaging approach to molecular imaging of prostate cancer," J Magn Reson Imaging 16, 451-463 (2002).

23 C. H. Contag and B. D. Ross, "It's not just about anatomy: in vivo bioluminescence imaging as an eyepiece into biology," J Magn Reson Imaging 16, 378-387 (2002).

24 S. J. DiBiase, K. Hosseinzadeh, R. P. Gullapalli, S. C. Jacobs, M. J. Naslund, G. N. Sklar, R. B. Alexander and C. Yu, "Magnetic resonance spectroscopic imaging-guided brachytherapy for localized prostate cancer," Int J Radiat Oncol Biol Phys 52, 429-438 (2002).

25 J. G. Tjuvajev, H. A. Macapinlac, F. Daghighian, A. M. Scott, J. Z. Ginos, R. D. Finn, P. Kothari, R. Desai, J. Zhang, B. Beattie and et al., "Imaging of brain tumor proliferative activity with iodine-131-iododeoxyuridine," J Nucl Med 35, 1407-1417 (1994).

26 A. F. Shields, J. R. Grierson, B. M. Dohmen, H. J. Machulla, J. C. Stayanoff, J. M. Lawhorn-Crews, J. E. Obradovich, O. Muzik and T. J. Mangner, "Imaging proliferation in vivo with [F-18]FLT and positron emission tomography," Nat Med 4, 1334-1336 (1998).

27 J. S. Rasey, W. J. Koh, M. L. Evans, L. M. Peterson, T. K. Lewellen, M. M. Graham and K. A. Krohn, "Quantifying regional hypoxia in human tumors with positron emission tomography of [18F]fluoromisonidazole: a pretherapy study of 37 patients," Int J Radiat Oncol Biol Phys 36, 417-428 (1996).

28 W. J. Koh, K. S. Bergman, J. S. Rasey, L. M. Peterson, M. L. Evans, M. M. Graham, J. R. Grierson, K. L. Lindsley, T. K. Lewellen, K. A. Krohn and et al., "Evaluation of oxygenation status during fractionated radiotherapy in human nonsmall cell lung cancers using [F-18]fluoromisonidazole positron emission tomography," Int J Radiat Oncol Biol Phys 33, 391-398 (1995).

29 B. L. Miller, L. Chang, R. Booth, T. Ernst, M. Cornford, D. Nikas, D. McBride, and D.J. Jenden, In vivo 1H MRS choline: correclation with in vitro chemistry/histology, Life Sciences 58, 1929-35 (1996).

30 R.K. Gupta, T.F. Cloughesy, U. Sinha, J. Garakian, J. Lazareff, G. Rubino, L. Rubino, D.P. Becker, H.V. Vinters, and J.R. Alger, Relationships between holine magnetic

resonance spectroscopy, apparent diffusion coefficient and quantitative histopathology in human glioma, Journal of Neuro-Oncology 50, 215-26 (2000).

31 R. J. Hamilton, M. J. Blend, C. A. Pelizzari, B. D. Milliken and S. Vijayakumar, "Using vascular structure for CT-SPECT registration in the pelvis," J Nucl Med 40, 347-351 (1999).

32 A. F. Shields, D. A. Mankoff, J. M. Link, M. M. Graham, J. F. Eary, S. M. Kozawa, M. Zheng, B. Lewellen, T. K. Lewellen, J. R. Grierson and K. A. Krohn, "Carbon-11-thymidine and FDG to measure therapy response," J Nucl Med 39, 1757-1762 (1998).

33 L. B. Marks, G. W. Sherouse, M. T. Munley, G. C. Bentel, D. P. Spencer and C. Scarfone, "Incorporation of functional status into dose-volume analysis," Medical Physics 26, 196-199 (1999).

34 T. E. Schultheiss, G. K. Zagars and L. J. Peters, "An explanatory hypothesis for early- and late-effect parameter values in the LQ model," Radiother Oncol 9, 241-248 (1987).

35 J. F. Fowler, "The linear-quadratic formula and progress in fractionated radiotherapy," Br J Radiol 62, 679-694 (1989).

36 S. Webb and A. E. Nahum, "A model for calculating tumour control probability in radiotherapy including the effects of inhomogeneous distributions of dose and clonogenic cell density," Physics in Medicine & Biology 38, 653-666 (1993).

37 S. Webb, P. M. Evans, W. Swindell and D. J. O., "A proof that uniform dose gives the greatest TCP for fixed integral dose in the planning target volume," Physics in Medicine & Biology 39, 2091-2098 (1994).

38 A. Brahme and A. K. Agren, "Optimal dose distribution for eradication of heterogeneous tumours," Acta Oncol 26, 377-385 (1987).

39 N. A. Stavreva, P. V. Stavrev and W. H. Round, "A mathematical approach to optimizing the radiation dose distribution in heterogeneous tumours," Acta Oncol 35, 727-732 (1996).

40 M. A. Ebert and P. W. Hoban, "Some characteristics of tumour control probability for heterogeneous tumours," Phys Med Biol 41, 2125-2133 (1996).

41 D. Levin-Plotnik and R. J. Hamilton, "Optimization of tumour control probability for heterogeneous tumours in fractionated radiotherapy treatment protocols," Phys Med Biol 49, 407-424 (2004).

42 T. E. Schultheiss, C. G. Orton and R. A. Peck, "Models in radiotherapy: volume effects," Medical Physics 10, 410-415 (1983).

43 J. T. Lyman and A. B. Wolbarst, "Optimization of radiation therapy, III: A method of assessing complication probabilities from dose-volume histograms," International Journal of Radiation Oncology, Biology, Physics 13, 103-109 (1987).

44 G. J. Kutcher and C. Burman, "Calculation of complication probability factors for non-uniform normal tissue irradiation: the effective volume method.," International Journal of Radiation Oncology, Biology, Physics 16, 1623-1630 (1989).

45 R. Mohan, G. S. Mageras, B. Baldwin, L. J. Brewster, G. J. Kutcher, S. Leibel, C. M. Burman, C. C. Ling and Z. Fuks, "Clinically relevant optimization of 3-D conformal treatments," Medical Physics 19, 933-944 (1992).

46 J. O. Deasy, K. S. Chao and J. Markman, "Uncertainties in model-based outcome predictions for treatment planning," International Journal of Radiation Oncology, Biology, Physics 51, 1389-1399 (2001).

47 M. K. Martel, W. M. Sahijdak, R. K. Ten Haken, M. L. Kessler and A. T. Turrisi, "Fraction size and dose parameters related to the incidence of pericardial effusions," International Journal of Radiation Oncology, Biology, Physics 40, 155-161 (1998).

48 L. Jones and P. Hoban, "A comparison of physically and radiobiologically based optimization for IMRT," Med Phys 29, 1447-1455 (2002).

49 Y. Yang and L. Xing, "Clinical knowledge-based inverse treatment planning," Phys Med Biol 49, 5101-5117 (2004).

50 L. Xing and G. T. Y. Chen, "Iterative algorithms for Inverse treatment planning," Physics in Medicine & Biology 41, 2107-2123 (1996).

51 L. Xing, R. J. Hamilton, D. Spelbring, C. A. Pelizzari, G. T. Chen and A. L. Boyer, "Fast iterative algorithms for three-dimensional inverse treatment planning," Medical Physics 25, 1845-1849 (1998).

52 Y. Lu, D. R. Spelbring and G. T. Chen, "Functional dose-volume histograms for functionally heterogeneous normal organs," Phys Med Biol 42, 345-356 (1997).

53 C. Burman, G. J. Kutcher, B. Emami and M. Goitein, "Fitting of normal tissue tolerance data to an analytic function," Int J Radiat Oncol Biol Phys 21, 123-135. (1991).

54 C. R. King, T. A. DiPetrillo and D. E. Wazer, "Optimal radiotherapy for prostate cancer: predictions for conventional external beam, IMRT, and brachytherapy from radiobiologic models," Int J Radiat Oncol Biol Phys 46, 165-172 (2000).

55 A. E. Nahum, B. Movsas, E. M. Horwitz, C. C. Stobbe and J. D. Chapman, "Incorporating clinical measurements of hypoxia into tumor local control modeling of prostate cancer: implications for the alpha/beta ratio," Int J Radiat Oncol Biol Phys 57, 391-401 (2003).

56 S. L. Scott, P. H. Gumerlock, L. Beckett, Y. Li and Z. Goldberg, "Survival and cell cycle kinetics of human prostate cancer cell lines after single- and multifraction exposures to ionizing radiation," Int J Radiat Oncol Biol Phys 59, 219-227 (2004).

57 R. F. Kallman and M. J. Dorie, "Tumor oxygenation and reoxygenation during radiation therapy: their importance in predicting tumor response," Int J Radiat Oncol Biol Phys 12, 681-685 (1986).

Table I Dose-volume parameters of various sensitive structures used for calculating NTCP in this study.

Sensitive structures	n	m	$D_{50/5}$ (Gy)
Bladder	0.50	0.11	80
Rectum	0.12	0.15	80
Femoral head	0.25	0.12	65

Table II Radiological parameters for the target regions in the two examples.

Targets		ρ_{0i} (clonogen/cm^3)	α_i (Gy^{-1})	γ_i (day^{-1})
Example 1	Region 2	5×10^8	0.26	ln2/40
	Region 3	5×10^5	0.13	ln2/40
	Region 4	5×10^5	0.26	ln2/10
Example 2	Region 2	5×10^6	0.20	ln2/10
	Region 3	5×10^3	0.10	ln2/60

Table III Comparison of TCP and NTCP for the four IMRT plans for Example 1.

		Plan-1 (BCRT plan)	Plan-2 (70 Gy Uniform)	Plan-3 (81 Gy Uniform)	Plan-4 (91 Gy Uniform)	Plan-5 (SIB plan)
TCP	Region 1	0.997	0.995	1.000	1.000	0.994
	Region 2	0.998	0.642	0.995	1.000	0.999
	Region 3	0.989	0.000	0.002	0.461	0.989
	Region 4	1.000	0.997	1.000	1.000	0.998
	Overall	0.984	0.000	0.002	0.461	0.981
NTCP (%)	Rectum	0.212	0.196	0.652	1.84	0.885
	Bladder	1.6×10^{-5}	1.4×10^{-5}	2.3×10^{-5}	4.2×10^{-5}	3.6×10^{-5}
	Femoral head (R)	2.0×10^{-5}	2.1×10^{-6}	2.6×10^{-4}	1.75×10^{-4}	3.9×10^{-5}
	Femoral head (L)	1.2×10^{-5}	2.0×10^{-6}	7.0×10^{-4}	5.26×10^{-4}	6.9×10^{-5}

Table IV Comparison of TCP and NTCP for the four IMRT plans for Example 2.

		Plan-1 (BCRT plan)	Plan-2 (70 Gy Uniform)	Plan-3 (81 Gy Uniform)	Plan-4 (91 Gy Uniform)	Plan-5 (SIB Plan)
TCP	Region 1	0.997	0.995	1.000	1.000	0.968
	Region 2	0.989	0.000	0.587	0.981	0.987
	Region 3	0.996	0.006	0.408	0.839	0.990
	Overall	0.981	0.000	0.239	0.823	0.946
NTCP (%)	Rectum	0.397	0.414	1.46	3.12	1.25
	Bladder	1.5×10^{-5}	1.2×10^{-5}	1.8×10^{-5}	4.3×10^{-5}	3.9×10^{-5}
	Femoral head (R)	3.7×10^{-5}	1.5×10^{-5}	1.8×10^{-5}	5.3×10^{-5}	2.3×10^{-5}
	Femoral head (L)	4.9×10^{-5}	1.1×10^{-5}	3.0×10^{-5}	4.5×10^{-5}	3.6×10^{-5}

Legends

Figure 1. A hypothetical prostate case with four biologically different regions (Example 1). (a) Geometric shapes and locations of the targets and sensitive structures; (b)-(d): Isodose distributions in an axial slice and two sagittal slices for Plan-1, generated by optimizing the objective function with a nonuniform dose prescription derived from Eq. (7).

Figure 2. Comparison of EDVHs and DVHs of the BCRT plan (Plan-1), three uniform IMRT plans (Plan-2: 70Gy, Plan-3: 81Gy, and Plan-4: 91Gy) and the SIB plan (Plan-5) in example 1. (a): Target EDVHs for the five plans (Insert is the regular DVHs of the prostate target). The normalized doses to the target region 1, 2, 3 and 4 are 70, 85, 119 and 75 Gy, respectively; (b)-(e): DVHs of different target regions and sensitive structures for the five plans. The solid, dashed, dotted, dash-dotted and dash-dot-dotted curves represent the results of Plan-1, -2, -3, -4 and –5, respectively. The effective dose is defined as the physical dose at a voxel normalized by its desired dose determined by Eq. (7).

Figure 3. A hypothetical prostate case with three biologically different regions and nonuniform importance in the rectum (Example 2). (a) Geometric shapes and locations of the targets and sensitive structures; (b)-(d): Isodose distributions in three axial slices and two sagittal slices for Plan-1, generated by optimizing the objective function with nonuniform dose prescription derived from Eq. (7).

Figure 4. Comparison of EDVHs, FDVHs and DVHs of the BCRT plan (Plan-1), three uniform IMRT plans (Plan-2: 70Gy, Plan-3: 81Gy, and Plan-4: 91Gy) and the SIB plan (Plan-5) in example 2. (a):The target EDVHs for the five plans (Insert is the regular DVHs of the prostate target). The normalized doses to the target region 1, 2, and 3 are 70, 99 and 121 Gy, respectively; (b): The rectum FDVHs for the five plans (Insert is the regular DVHs of the rectum); (c) -(e): DVHs of different target regions and sensitive structures for the five plans. The solid, dashed, dotted, dash-dotted and dash-dot-dotted curves represent the results of Plan-1, -2, -3, -4 and –5, respectively.

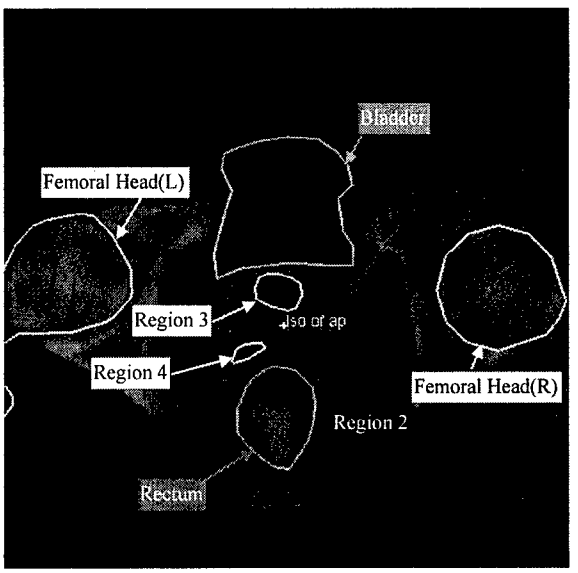

(a)

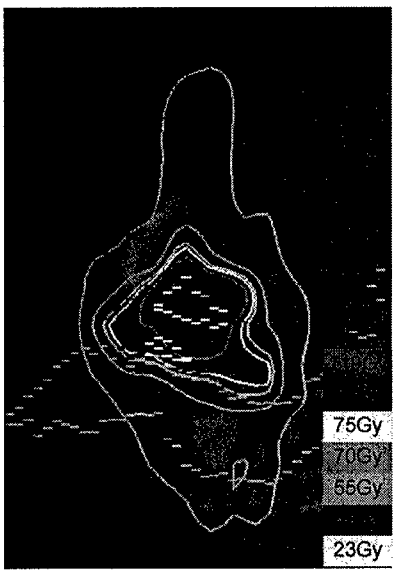

(c) Sagittal 1

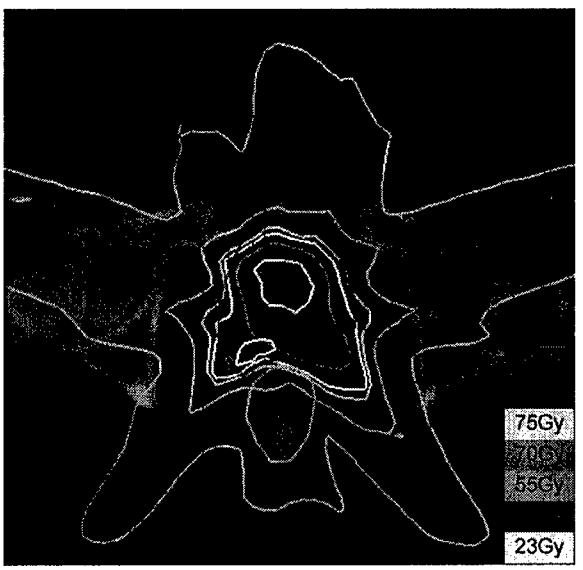

(b) Axial

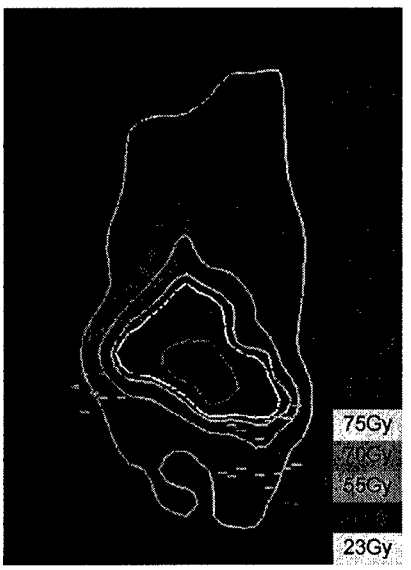

(d) Sagittal 2

Figure 1

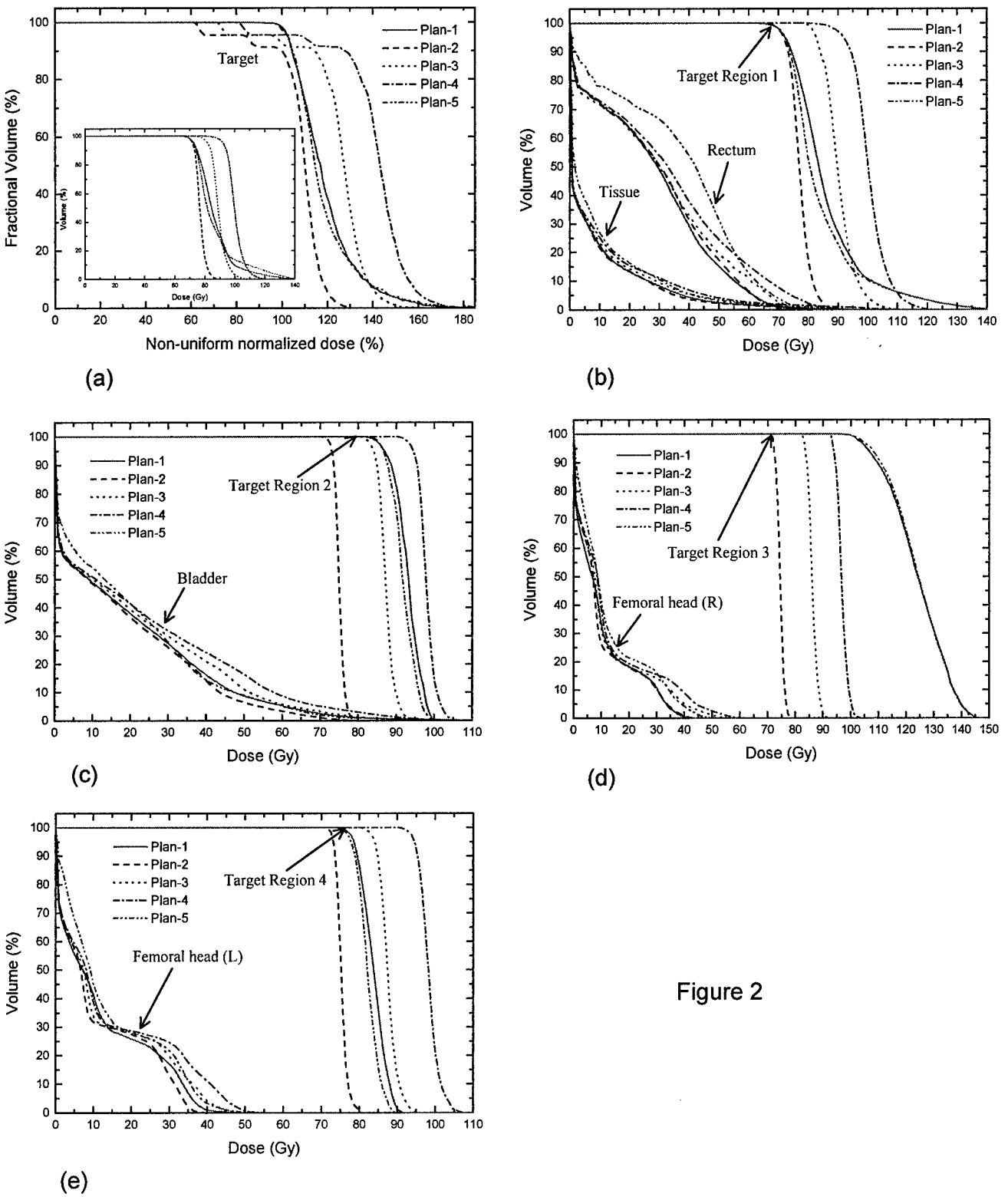
Plan-1
Plan-2
Plan-3
Plan-4
Plan-5
Target
Fractional Volume (%)
Non-uniform normalized dose (%)
(a)
Target Region 1
Rectum
Tissue
Volume (%)
Dose (Gy)
(b)
Target Region 2
Bladder
(c)
Target Region 3
Femoral head (R)
(d)
Target Region 4
Femoral head (L)
(e)

Figure 2

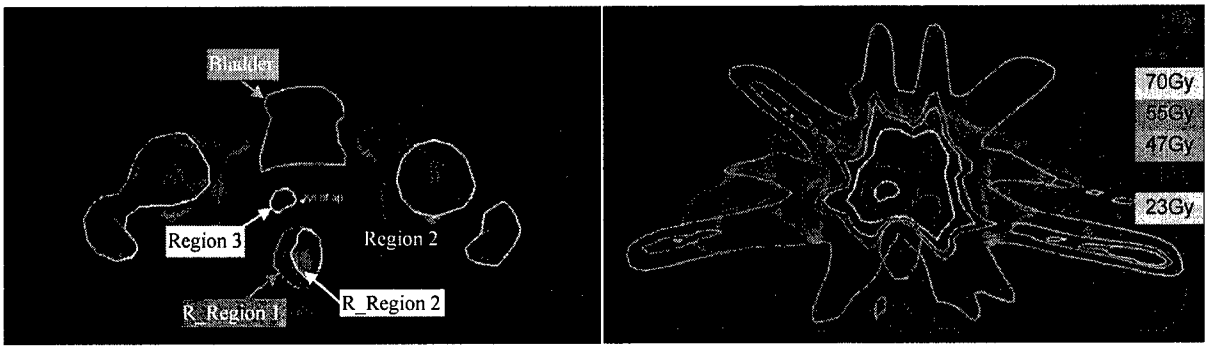

(a) (b) Axial 1

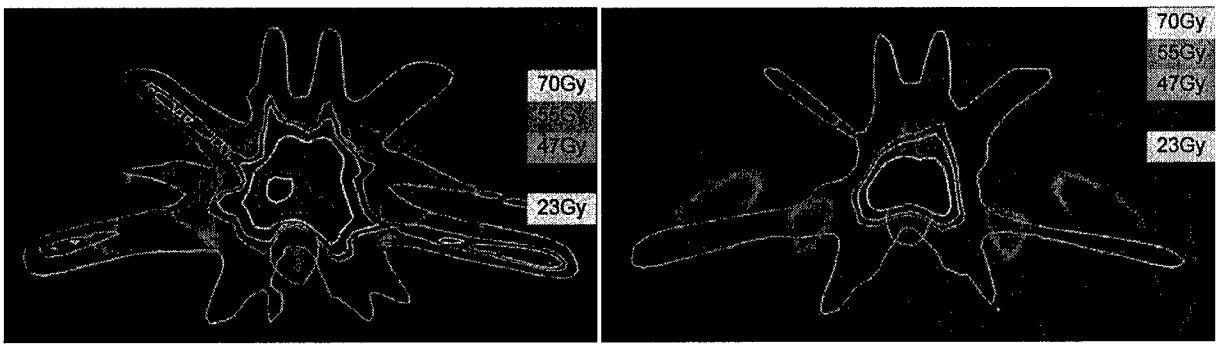

(c) Axial 2 (d) Axial 3

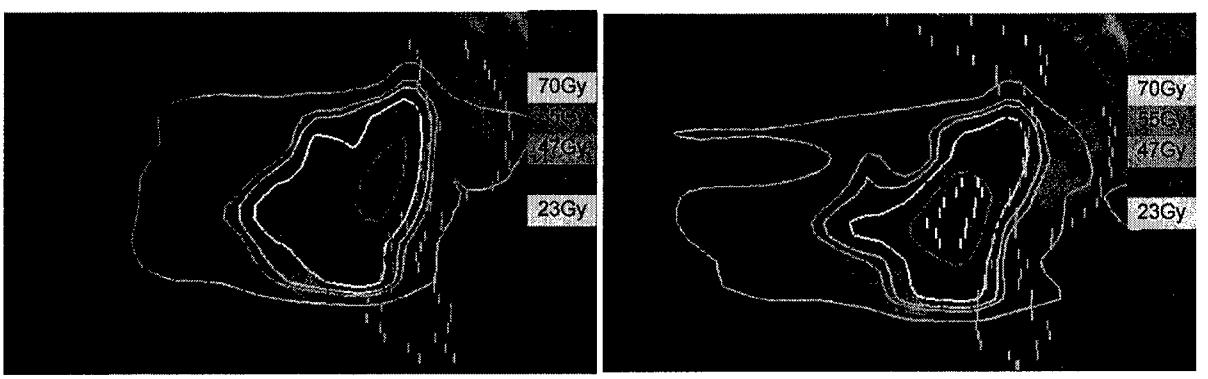

(e) Sagittal 1 (f) Sagittal 2

Figure 3

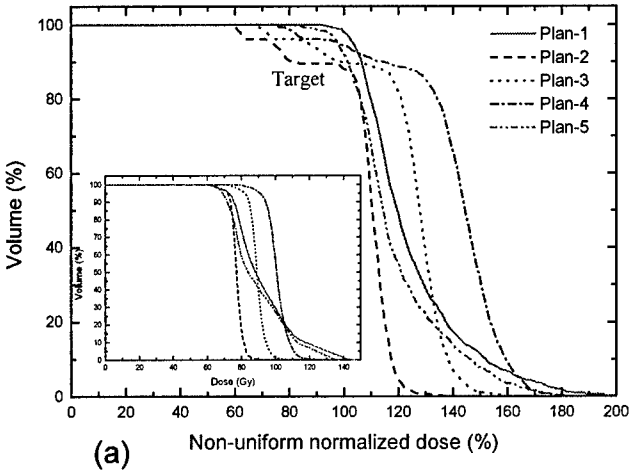
Target
Plan-1
Plan-2
Plan-3
Plan-4
Plan-5
Volume (%)
Non-uniform normalized dose (%)
(a)

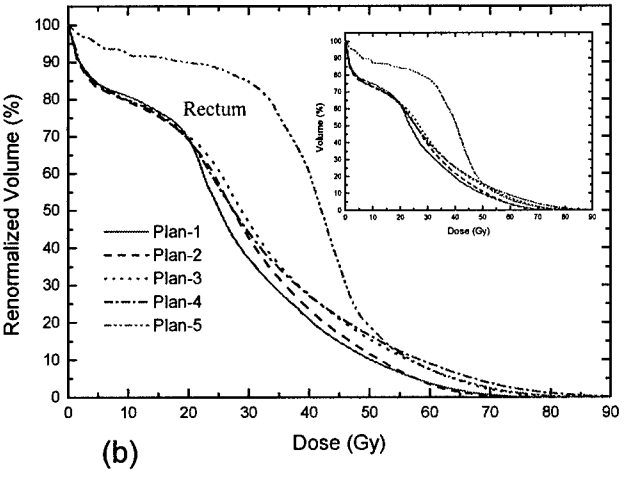
Rectum
Plan-1
Plan-2
Plan-3
Plan-4
Plan-5
Renormalized Volume (%)
Dose (Gy)
(b)

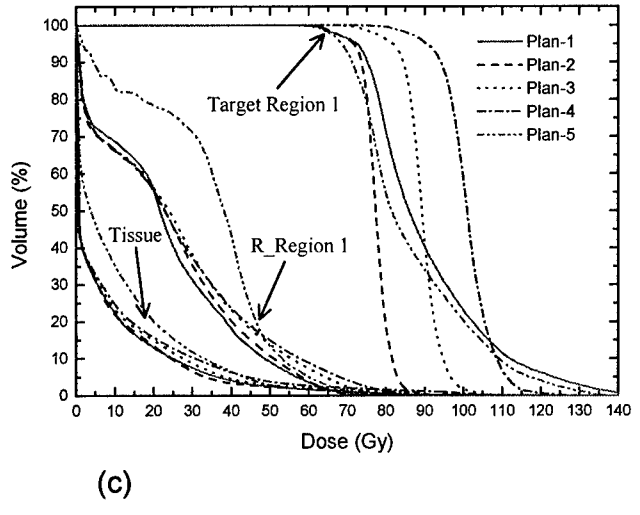
Target Region 1
Tissue
R_Region 1
Plan-1
Plan-2
Plan-3
Plan-4
Plan-5
Volume (%)
Dose (Gy)
(c)

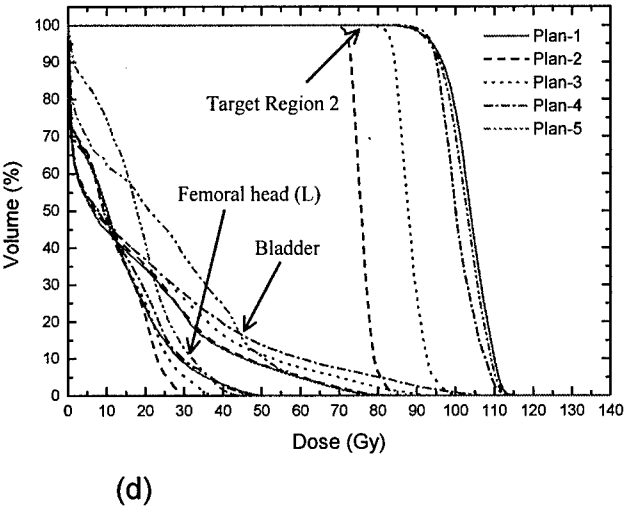
Target Region 2
Femoral head (L)
Bladder
Plan-1
Plan-2
Plan-3
Plan-4
Plan-5
Volume (%)
Dose (Gy)
(d)

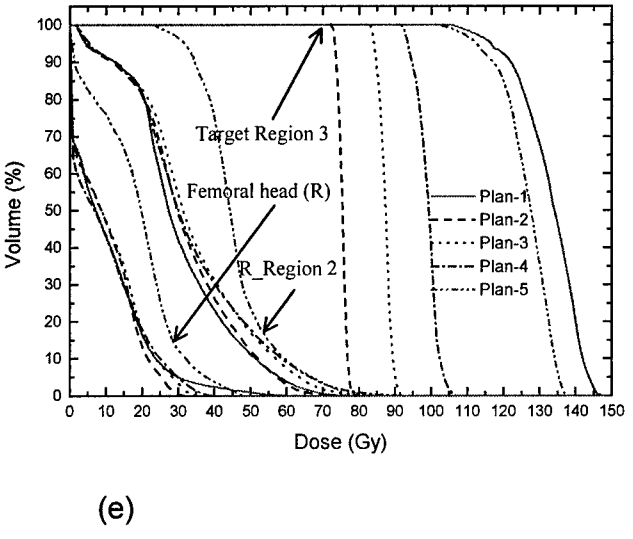
Target Region 3
Femoral head (R)
R_Region 2
Plan-1
Plan-2
Plan-3
Plan-4
Plan-5
Volume (%)
Dose (Gy)
(e)

Figure 4

INSTITUTE OF PHYSICS PUBLISHING PHYSICS IN MEDICINE AND BIOLOGY

Phys. Med. Biol. **49** (2004) 5101–5117 PII: S0031-9155(04)81634-8

Clinical knowledge-based inverse treatment planning

Yong Yang and Lei Xing

Department of Radiation Oncology, Stanford University School of Medicine, Stanford, CA 94305-5847, USA

E-mail: lei@reyes.stanford.edu

Received 1 June 2004, in final form 20 September 2004
Published 25 October 2004
Online at stacks.iop.org/PMB/49/5101
doi:10.1088/0031-9155/49/22/006

Abstract

Clinical IMRT treatment plans are currently made using dose-based optimization algorithms, which do not consider the nonlinear dose–volume effects for tumours and normal structures. The choice of structure specific importance factors represents an additional degree of freedom of the system and makes rigorous optimization intractable. The purpose of this work is to circumvent the two problems by developing a biologically more sensible yet clinically practical inverse planning framework. To implement this, the dose–volume status of a structure was characterized by using the effective volume in the voxel domain. A new objective function was constructed with the incorporation of the volumetric information of the system so that the figure of merit of a given IMRT plan depends not only on the dose deviation from the desired distribution but also the dose–volume status of the involved organs. The conventional importance factor of an organ was written into a product of two components: (i) a generic importance that parametrizes the relative importance of the organs in the ideal situation when the goals for all the organs are met; (ii) a dose-dependent factor that quantifies our level of clinical/dosimetric satisfaction for a given plan. The generic importance can be determined *a priori*, and in most circumstances, does not need adjustment, whereas the second one, which is responsible for the intractable behaviour of the trade-off seen in conventional inverse planning, was determined automatically. An inverse planning module based on the proposed formalism was implemented and applied to a prostate case and a head–neck case. A comparison with the conventional inverse planning technique indicated that, for the same target dose coverage, the critical structure sparing was substantially improved for both cases. The incorporation of clinical knowledge allows us to obtain better IMRT plans and makes it possible to auto-select the importance factors, greatly facilitating the inverse planning process. The new formalism proposed also reveals the relationship between different inverse planning schemes and gives important insight into the problem of therapeutic plan optimization.

0031-9155/04/225101+17$30.00

In particular, we show that the EUD-based optimization is a special case of the general inverse planning formalism described in this paper.

(Some figures in this article are in colour only in the electronic version)

1. Introduction

An important issue in inverse planning is how to formalize the clinical goals to objectively evaluate the figures of merit of different IMRT plans. Despite intense research effort in modelling the clinical decision-making strategies (Amols and Ling 2002, Deasy *et al* 2002, Earl *et al* 2003, Hou *et al* 2003, Lahanas *et al* 2003, Langer *et al* 1993, 1998, Lee *et al* 2000, Llacer *et al* 2001, Mohan *et al* 1994, Webb 2004, Xing *et al* 1999, Yan *et al* 2003), the appropriate form of the objective function remains illusive. Presently, two types of objective functions are widely used: dose or dose–volume histogram (DVH)-based (physical objective functions) (Chen *et al* 2002, Cho *et al* 1998, Holmes *et al* 1995, Hristov *et al* 2002, Michalski *et al* 2004, Starkschall *et al* 2001, Shepard *et al* 2002, Xing *et al* 1998) and dose–response-based objective functions (biological objective functions) (Brahme 2001, Kallman *et al* 1992, Miften *et al* 2004, Mohan *et al* 1992, Wang *et al* 1995, Webb and Nahum 1993). The underlying difference between these models lies in what endpoints are used to evaluate the treatment or which fundamental quantities are used to define the optimality. The physical approach emphasizes the difference between the calculated and prescribed doses and does not consider the nonlinear effects for tumours and normal structures. Dose–volume constraints are often introduced to select a solution with certain shapes of the DVHs for the target and sensitive structures. However, it is important to note that the construction of the DVH constraints is *a priori* in nature. The use of constraints can only passively restrict the accessible DVHs by narrowing the solution space, and the figures of merits of the physically realizable plans are not changed as long as they satisfy the constraints. To reflect our preference over certain DVHs for a structure, it is necessary to express the objective of the structure as a function of the volumetric status, which has not been achieved up to this point. On the other hand, biological model-based optimization proponents argue that plan optimization should be guided by estimates of biological effects, which depend on the radiation dose through the dose–response function. The treatment objective in biological model-based inverse planning is usually stated as the maximization of the tumour control probability (TCP) while maintaining the normal tissue complication probability (NTCP) to within acceptable levels (Brahme 2001, Kallman *et al* 1992, Langer *et al* 1998, Mohan *et al* 1992, Wang *et al* 1995). In principle, the biologically based models are most relevant for radiotherapy plan ranking. However, the dose–response function of various structures is not sufficiently understood and, at this point, there is considerable controversy about the models for computing dose–response indices and their use in optimization. In reality, the use of dose–response indices for optimization may lead to very inhomogeneous target dose distributions. Furthermore, it is difficult for clinicians to specify the optimization criteria in terms of dose–response indices. This becomes compounded when two or more independently optimized plans are to be combined. Because of the problems, the use of biological model-based optimization has mainly been limited in the research community and little effort has been made to implement the model in commercial planning systems. Given the fact that biological outcome is the ultimate endpoint of radiation therapy, the importance of the biological modelling and the biological model-based inverse planning can never be overstated.

To pin down the underlying problem of the current inverse planning formalism and illustrate the need for a clinically more relevant approach, let us take parotid glands as an example. It is well known that the clinical endpoint is the same if the glands are irradiated with 15 Gy to 67%, or 30 Gy to 45%, or 45 Gy to 24% of the total volume (Eisbruch *et al* 1999). If a dose-based metric, such as the commonly used quadratic objective function, is used, the rankings for the three different scenarios would be completely different. Even with the use of dose–volume constraints, it is difficult, if not impossible, to incorporate this type of knowledge to correctly model the behaviour of the organ in response to radiation. Indeed, a constraint in optimization acts as a 'boundary condition' during the optimization and does not change the rankings of dosimetrically different plans. This example clearly reveals the inadequacy of the conventional dose-based objective function and suggests the urgent need for a clinically more sensible model. Obviously, a minimum requirement for the model is that it should be consistent with the existing clinical outcome data. For parotid glands, for instance, the three different DVHs mentioned above should be scored equally. This type of 'degeneracy' can be achieved by effectively integrating clinical endpoint data into the inverse planning formulation. For a given patient, the specific DVH selection will be determined by the optimization algorithm with the consideration of the dosimetric/clinical requirements of other structures and the results will, of course, depend on the geometric and dosimetric details of the given patient. The example, however, underscores the important role of the existing clinical data in inverse planning and emphasizes the essential ingredients for a clinically realistic objective function. Towards developing a biologically more sensible yet clinically practical inverse planning formalism, in the following we propose a method to incorporate clinical endpoint data into the construction of the objective function and attempt to bridge the gap between the clinical decision-making process and the computational modelling. Our study indicates that the clinical knowledge-based modelling allows us to objectively rank IMRT plans according to their clinical merits and makes it possible to obtain truly optimal IMRT plans with much reduced efforts.

2. Methods and materials

2.1. Dose–volume effect

Generally, the dose response of a structure with respect to the irradiated dose and volume is complicated. The fact that the dose distribution in tumour or a sensitive structure is generally inhomogeneous makes the establishment of such a relationship even more intractable. Over the last two decades, attempts have been made by many researchers to capture the main feature(s) of the dose–volume effects. A power-law model represents one of the successful techniques in dealing with the dose–volume effects of sensitive structures (Lyman and Wolbarst 1987). In this model an equivalent dose uniformly irradiating the whole organ, D_{eq}, can be used to represent the situation in which a fractional partial volume, v, is irradiated to a dose, D, by a simple power-law model: $D_{eq} = v^{1/n}D$. A remarkable characteristic of this model is that, although only a single organ-specific parameter, n, is used, clinical and biological data have shown that this power law holds well at low complication levels (Lyman and Wolbarst 1987, Schultheiss *et al* 1983). On the basis of this relation, Mohan *et al* (1992) introduced the concept of effective dose to represent a non-uniform dose distribution in a sensitive structure. Kutcher and Burman (1989) applied the same power model independently to each volume element of the histogram and introduced the concept of effective volume to reduce the DVH of an inhomogeneous dose distribution in a sensitive structure to a uniform dose distribution.

Following their study, in this work we define the effective volume $(\Delta V_{\text{eff}})_i$ for a voxel i with volume ΔV and dose $D_c(i)$ as follows:

$$(\Delta V_{\text{eff}})_i = \Delta V (D_c(i)/D_{\text{ref}})^{1/n} \tag{1}$$

and extend this concept to handle the voxels in the tumour target, where n is an organ-dependent parameter, and D_{ref} is the reference dose. For a sensitive structure, n is a small positive number ($0 < n < 1$) and the value of parameter n reflects the architecture (serial or parallel) of the sensitive structure. For a target, n should be assigned with a small negative value ($-1 < n < 0$). The biological meaning of equation (1) is that for a sensitive structure a small volume receiving a higher dose than a reference dose would be equivalent to a larger volume receiving the reference dose; for a target, a volume with a lower dose would have a larger effective volume. The effective volumes of all voxels reflect the DVH status of the given organ, and for inverse planning, this permits us to deal with the complicated dose–volume effect in the voxel domain.

2.2. *Dose–volume-based objective function*

The objective function, f, expressed as a function of the effective volume in the voxel domain for an organ should take the form of

$$f = f(\{(\Delta V_{\text{eff}})_i\}). \tag{2}$$

Generally, the dose–volume effect suggests that the voxels receiving different doses are inequivalent: the one with a larger effective volume (higher dose for a critical organ) should be penalized more when compared to a voxel with a smaller effective volume (lower dose). Thus we heuristically write the f in the following form:

$$f = 1 + \eta_1 \sum_i r_i [D_c(i)/D_{\text{ref}}]^{1/n} + \eta_2 \left\{ \sum_i r_i [D_c(i)/D_{\text{ref}}]^{1/n} \right\}^2 + \cdots, \tag{3}$$

where equation (1) has been incorporated, r_i is the importance factor of the ith voxel, representing the intrastructural trade-off due to physical/clinical requirements other than the dose–volume-based penalty, η_1 and η_2 are phenomenological parameters of the model. In equation (3), the third (and higher order) term emphasizes more the voxels with high effective volumes, whereas the first and second terms ensure that the voxels with low effective volumes receive an adequate penalty. We typically set $r_i \equiv 1$, unless there are other physical/clinical considerations (e.g., when the density of clonogens varies spatially (Xing *et al* 2002)). In this work, we set $\eta_1 = 1$ and $\eta_2 = \eta_3 = \cdots = 0$.

2.3. *Hybrid of dose-based and dose–volume-based objective functions*

Equation (3) provides a good description of the dose–volume effect. With proper choice of the parameter, n, the clinically observed dose–volume effect can be reproduced by the objective function. In reality, other requirements, such as the target dose uniformity, should also be considered. A more general form of inverse planning objective function can be written as a hybrid of the dose–volume-based and the dose-based functions. In this situation, the overall objective function of the system takes the form of

$$F = \sum_{\tau=1}^{t_\tau} r_\tau \frac{1}{N_\tau} \sum_{i=1}^{N_\tau} \left\{ 1 + \eta_1^t [D_c(i)/D_{\tau,\text{ref}}]^{1/n_\tau} \right\} \left| D_c(i) - D_0^T(i) \right|^{k_\tau} + \sum_{\sigma=1}^{s_\sigma} r_\sigma \frac{1}{N_\sigma} \sum_{i=1}^{N_\sigma} \left\{ 1 + \eta_1^s [D_c(i)/D_{\sigma,\text{ref}}]^{1/n_\sigma} \right\} D_c(i)^{k_\sigma}, \tag{4}$$

where t_τ and s_σ are the numbers of targets and sensitive structures, $D_0^T(i)$ is the prescription dose in target voxel i, subscripts τ and σ represent target τ and sensitive structure σ, N_τ, N_σ, r_τ, r_σ, n_τ, n_σ, $D_{\tau,\mathrm{ref}}$, $D_{\sigma,\mathrm{ref}}$, k_τ and k_σ represent the total numbers of voxels, structure specific importance factors, n parameters, reference doses, power of dosimetric deviation from the specified criteria for target τ and sensitive structure σ, respectively. The factor $\left|D_c(i) - D_0^T(i)\right|^{k_\tau}$ for target or $D_c(i)^{k_\sigma}$ for a sensitive structure represents the contribution from dosimetric deviation from the ideal situation. If the k_τ and k_σ are set to zero, the objective function becomes purely dose–volume driven. In particular, if we set k_σ to zero and k_τ to a nonzero value, the objective function for a target becomes a hybrid of dose–volume and dose, whereas the objective functions for critical structures remain purely dose–volume based. On the other hand, when all the n parameters in equation (4) are set to be $+\infty$, no dose–volume effects are considered and equation (4) is reduced to the conventional dose-based objective function.

2.4. Automatic determination of structure specific importance factors

The selection of structure specific importance factors, r_τ or r_σ in equation (4), is generally done empirically by trial and error. Here we describe an automated approach for solving the problem. The key to success is to establish an effective method to express the structural importance factor in terms of physically or clinically more meaningful quantities. For this purpose, we write the importance of a structure into a product of two components: (i) a generic factor parametrizing the relative importance of the organs in an ideal situation when the goals for the organs are met; and (ii) a dose-dependent factor quantifying our level of clinical/dosimetric satisfaction for a given plan. The first factor can be determined *a priori*, and in most circumstances, does not need adjustment (generally speaking, the value of r_σ^g is determined on the basis of the treatment modality and the patient's overall condition), whereas the second one is responsible for the intractable behaviour of the trade-off in conventional planning and can be automatically determined. This decomposition is essentially to normalize the conventional importance factor in terms of our clinical goals for the structures under discussion. Because of this decomposition, the meaning of the importance factor becomes more transparent and the determination of the factors becomes straightforward. Mathematically, we write $r_\sigma = r_\sigma^g r_\sigma^d$, where r_σ^g represents the first contribution described above (the desired weighting among different structures in an ideal situation), and r_σ^d is the second component and is defined as a function of NTCP for a sensitive structure. In this study r_σ^g was set empirically (see tables 2 and 3 for examples). r_σ^d is updated according to the DVH or the dose distribution during the optimization process and reflects the most current status of trade-off in the system. Generally, the importance of a sensitive structure should be increased in the next iteration if NTCP is high, and *vice versa*. We found that a simple linear relation between r_σ^d and NTCP,

$$r_\sigma^d = \mathrm{NTCP}_\sigma + \delta, \tag{5}$$

describes the trade-off behaviour of the system well, where the value of NTCP_σ depends on the dose distribution at the current iteration for structure σ, and δ is a cut-off factor for NTCP, which is introduced to ensure the sensitive structure receives a minimum penalty even if its NTCP is close to zero. We set δ as an organ-independent constant of 0.01%.

The NTCP was assessed using Lyman's model in this study. For non-uniform irradiation, the Kutcher–Burman (1989) effective-volume DVH reduction method is used to transform a DVH into a uniform irradiation on an effective partial volume. Model parameters (n, m,

$TD_{50/5}$) used in this study were those fitted to the model by Burman *et al* (1991) for the normal tissue tolerance data compiled by Emami *et al* (1991).

2.5. Computational algorithm

After considering the automatic trade-off strategy, the generalized objective function takes the following form:

$$F = \sum_{\tau=1}^{t_\tau} r_\tau \frac{1}{N_\tau} \sum_{i=1}^{N_\tau} \left\{1 + \eta_1^t [D_c(i)/D_{\tau,\mathrm{ref}}]^{1/n_\tau}\right\} \left|D_c(i) - D_0^T(i)\right|^{k_\tau} + \sum_{\sigma=1}^{s_\sigma} r_\sigma^g r_\sigma^d \frac{1}{N_\sigma} \sum_{i=1}^{N_\sigma} \left\{1 + \eta_1^s [D_c(i)/D_{\sigma,\mathrm{ref}}]^{1/n_\sigma}\right\} D_c(i)^{k_\sigma}. \quad (6)$$

We implemented a software module to optimize the objective function (6) in the PLUNC treatment planning system (University of North Carolina, Chapel Hill, NC). The ray-by-ray iterative algorithm (SIITP) reported earlier (Xing *et al* 1998) was employed to obtain the optimal beam intensity profiles. The values of k_τ and k_σ in equation (6) were set to be 2, but the behaviour of the system for a few other combinations of k_τ and k_σ were also checked for the prostate case. The reference dose, $D_{\sigma,\mathrm{ref}}$, was chosen to be $TD_{5/5}$ of the corresponding critical organ. For the target, $D_{\tau,\mathrm{ref}}$ was set as the prescription dose. Figure 1 shows the flow chart of the calculation process. In the current study we specify a maximum number of iterations as the termination condition of the optimization process. The DVHs can be inspected in each iterative step to visually monitor the optimization process.

2.6. Case studies

Two cases, a prostate case and a head–neck case, were used to evaluate the proposed inverse planning formalism. The optimization results were compared with those obtained using the conventional dose-based optimization method, which was described in detail by Xing *et al* (1998). The optimization parameters in the dose-based method were adjusted by trial-and-error to obtain an 'optimal' plan.

In the prostate case, the target volume included the prostate and seminal vesicles. The sensitive structures included rectum, bladder and femoral heads. All the IMRT plans used identical configuration of five equally spaced 15 MV photon beams with gantry angles of 0°, 72°, 144°, 216° and 288° (in IEC convention). The plans were normalized to deliver the prescription dose of 70 Gy to 99% of the target volume. The parameter n_τ was chosen to be -0.2 for the target. The parameters used in the NTCP calculations of the rectum, bladder and femoral heads are listed in table 1. Table 2 summarizes the optimization parameters for both the newly proposed and dose-based approaches.

For the prostate case, we also studied the influence of two more combinations of k_σ and k_τ. These included ($k_\sigma = 2$, $k_\tau = 4$) and ($k_\sigma = 0$, $k_\tau = 2$). In the latter case, we have included a higher order term of the dose–volume effect (the third term in equation (3) with $\eta_2 = 1$) to ensure that the high effective volume voxels are penalized enough in the absence of the dose-based factor.

In the head-and-neck case, the organs at risk included the eyes, optic nerves, optic chiasm, brainstem, spinal cord and parotids. Two targets were the gross target volume (GTV) and the clinical target volume (CTV), which includes the microscopic disease region surrounding the GTV. The plan was normalized to deliver a prescription dose of 70 Gy to at least 99% of the GTV and 62 Gy to at least 95% of the CTV. Nine equally spaced 6 MV coplanar beams

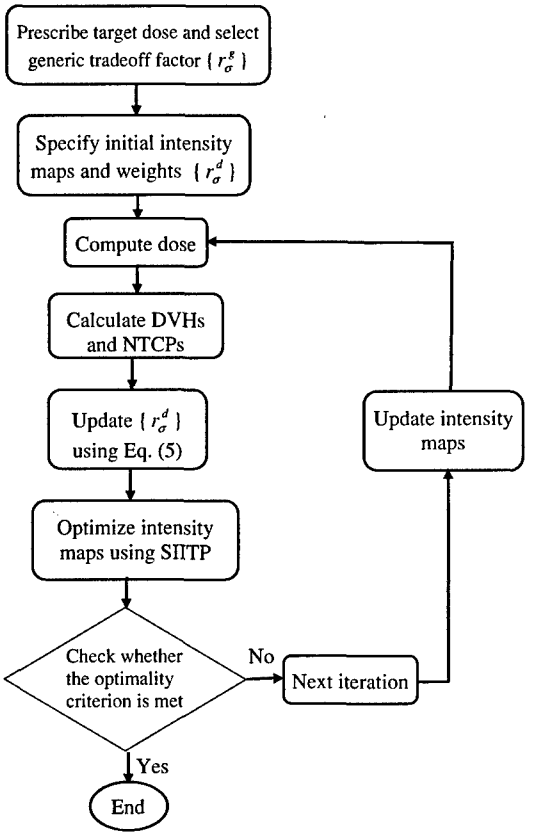

Figure 1. A flow chart of the proposed optimization process.

Table 1. The radiological parameters for various sensitive structures used in this study.

Sensitive structures	n	m	$D_{50/5}$ (Gy)	$D_{5/5}$ (Gy)
Bladder	0.50	0.11	80	65
Rectum	0.12	0.15	80	60
Femoral head	0.25	0.12	65	52
Eye lens	0.3	0.27	18	10
Optic nerve	0.25	0.14	65	50
Optic chiasm	0.25	0.14	65	50
Spinal cord	0.05	0.175	66.5	47
Brainstem	0.16	0.14	65	50
Parotid	0.70	0.18	46	32

(0°, 40°, 80°, 120°, 160°, 200°, 240°, 280° and 320°) were used for this case. The parameter n_τ was -0.5 for both GTV and CTV. The parameters used for the computation of the NTCPs of the sensitive structures are also obtained from the same source stated earlier and are listed in table 1. The optimization parameters for both the two techniques are summarized in table 3.

Table 2. Summary of the optimization parameters used in the dose-based and proposed approaches for the prostate case.

	The dose-based approach		The proposed approach
Organs	Relative importance factors	Target prescription and OAR tolerance doses (Gy)	Generic importance factors (r_o^g)
Target	5.0	78	5
Bladder	1.2	48	2
Rectum	1.8	43	2
Femoral head (R)	1.0	32	1
Femoral head (L)	1.0	32	1
Normal tissue	0.5	65	0.3

Table 3. Summary of the optimization parameters used in the dose-based and proposed approaches for the head-and-neck case.

	The dose-based approach		The proposed approach
Organs	Relative importance factors	Target prescription and OAR tolerance doses (Gy)	Generic importance factors (r_o^g)
GTV	3.0	70	4.0
CTV	4.0	62	6.0
Spinal cord	2.0	30	3.0
Brainstem	1.5	30	2.0
Left optic nerve	1.0	25	1.0
Right optic nerve	1.0	25	1.0
Left eye	2.0	6	3.0
Right eye	2.0	6	3.0
Left parotid	1.2	25	1.0
Right parotid	1.2	25	1.0
Optic chiasm	1.0	25	1.0
Normal tissue	0.5	40	0.5

3. Results

3.1. Prostate IMRT plans

Figures 2 and 3 summarize the results of the two IMRT plans obtained using the newly proposed and conventional techniques. Figure 2 compares the isodose distributions in two transverse slices and a sagittal slice for the two plans. The DVHs of the target and sensitive structures are plotted in figure 3, in which the solid and dashed lines represent the DVHs obtained using the new and conventional approaches, respectively. The calculated NTCPs of rectum, bladder and femoral heads for both IMRT plans are listed in table 4. According to the table, it is seen that the NTCPs of the sensitive structures are improved significantly. For the rectum, for example, the NTCP is reduced from 0.45% to 0.03%. Our results also indicate that the main compromise in a prostate IMRT treatment seems to be between the tumour coverage and the rectum complication because the NTCP of the rectum is much higher than that of other sensitive structures.

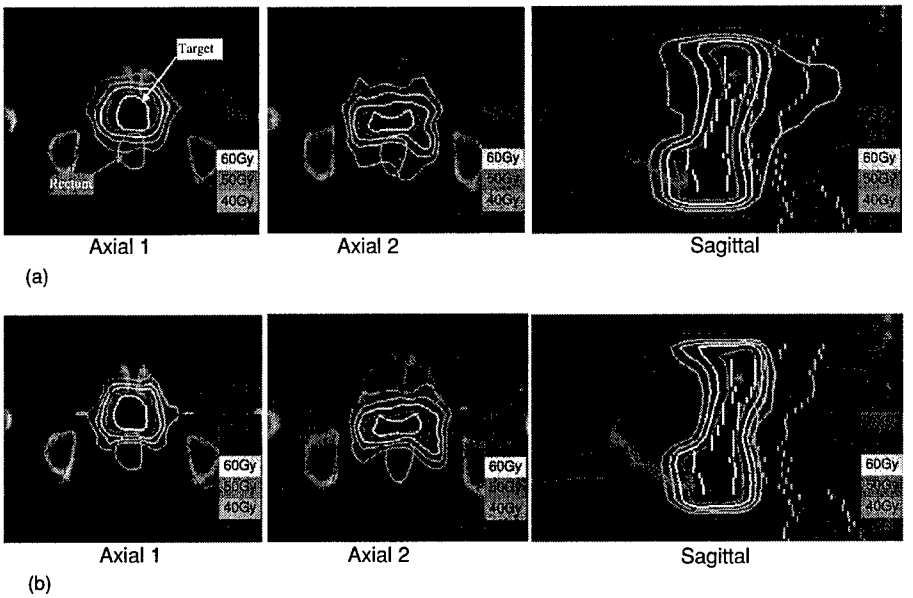

Figure 2. Comparison of the isodose distributions of the two prostate IMRT plans: (a) the conventional dose-based approach; (b) the newly proposed approach.

Table 4. Comparison of the NTCP for the two IMRT plans for the prostate case.

NTCP (%)	The dose-based IMRT plan	The proposed IMRT plan
Bladder	0.017	0.000 30
Rectum	0.45	0.029
Femoral head (R)	0.000 076	0.000 0038
Femoral head (L)	0.000 032	0.000 015

The above results demonstrate that, for comparable target coverage, the new inverse planning technique greatly improves the critical structure sparing, especially the rectum sparing. By comparing the isodose distributions of the two plans (figure 2), it is seen that the dose gradient at the interface between the target and the rectum is much steeper for the IMRT plan obtained with the new formalism. Furthermore, it is intriguing that the non-sensitive structure normal tissue also receives fewer doses in comparison with that of the dose-based optimization. Our results suggest that the improvement in the critical structure sparing is achieved not at the cost of higher target dose inhomogeneity, which is commonly seen in IMRT plan optimization.

The resultant DVHs when $k_\sigma = 2$ and k_τ was increased from 2 to 4 in equation (6) are plotted in figure 3 as the dotted curves. While the target dose uniformity is improved when the k_τ increases, the doses to the rectum and bladder are worsened. The results make intuitive sense as when the k_τ increases, more penalty is applied towards dosimetric deviation from the prescription. The DVHs when the objective function for the target is a hybrid of dose–volume- and dose-based functions ($k_\tau = 2$) and that for the sensitive structures are purely dose–volume based ($k_\sigma = 0$) are shown in figure 3 as dash-dotted curves. In this case, a high order term

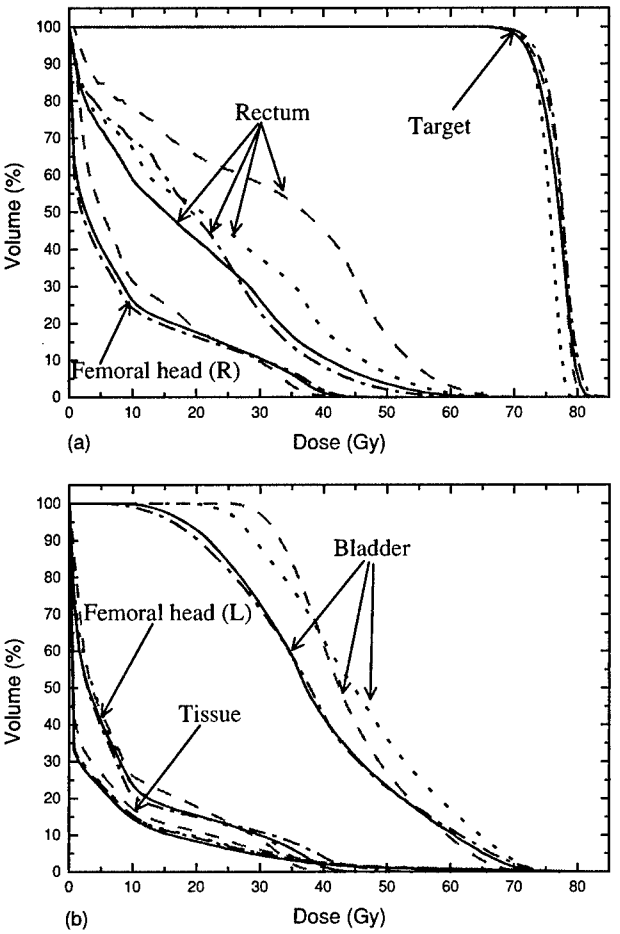

Figure 3. Comparison of DVHs of the prostate IMRT plans obtained using the proposed approach (solid curves) and the conventional dose-based approach (dashed curves). The dotted curves represent the results obtained with $k_\tau = 4$ and $k_\sigma = 2$ in equation (6). The dash-dotted curves are the DVHs with $k_\tau = 2$ and $k_\sigma = 0$ (a higher order term, the third term in equation (3), was included during the optimization).

of the dose–volume effect in equation (3) was added to ensure that the high effective volume voxels are penalized enough in the absence of the dose-based factor. Interestingly, as can be seen from figure 3, the results so obtained were very similar to that obtained with the hybrid objective function.

3.2. Head-and-neck IMRT plans

Figure 4 shows the isodose distributions obtained using the two different planning techniques in three transverse slices, one sagittal slice and one coronal slice for the two plans. Figure 5 compares the DVHs of the targets and sensitive structures, in which the solid and dashed lines represent the DVHs obtained using the newly proposed and conventional approaches,

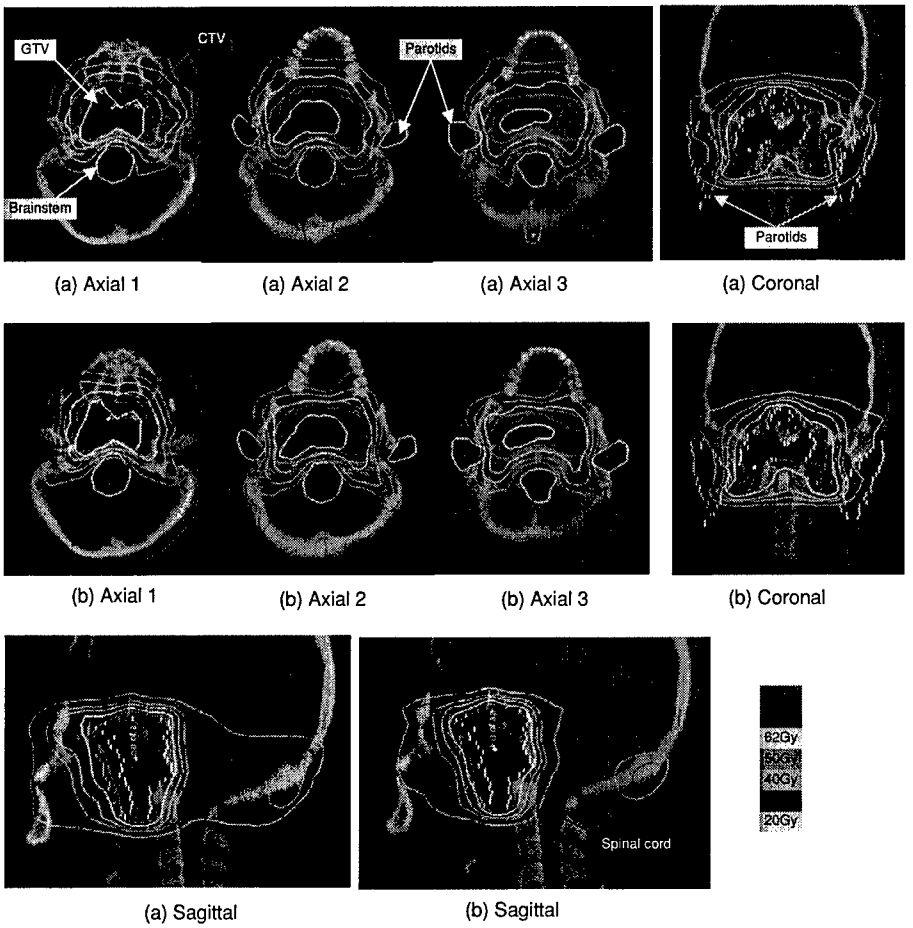

Figure 4. Comparison of the isodose distributions of the two head-and-neck IMRT plans: (a) the conventional dose-based approach; (b) the newly proposed approach.

Table 5. Comparison of the NTCP for the two IMRT plans for the head-and-neck case.

NTCP (%)	The dose-based IMRT plan	The proposed IMRT plan
Spinal cord	0.043	0.002 5
Brainstem	0.012	0.004 0
Left Eye	0.27	0.18
Right Eye	0.24	0.12
Left parotid	0.21	0.056
Right parotid	0.22	0.064
Optic chiasm	0.000 24	0.000 064
Left optic nerve	0.000 064	0.000 0075
Right optic nerve	0.000 043	0.000 025

respectively. The calculated NTCPs of eyes, optical nerves, optical chiasm, brainstem, spinal cord and parotids for both plans are shown in table 5. As seen from the isodose distributions

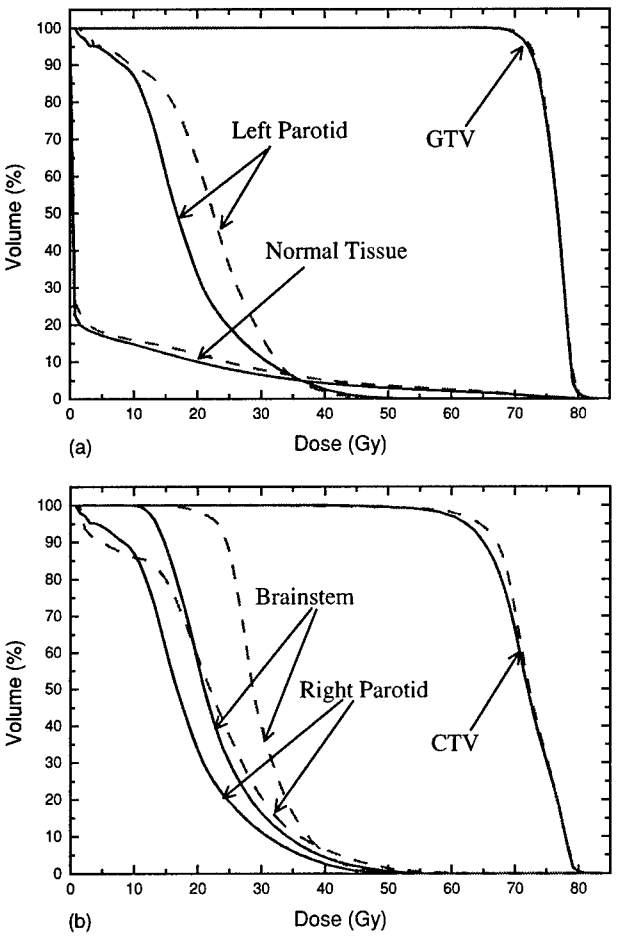

Figure 5. Comparison of the DVHs of the two head-and-neck IMRT plans obtained using our newly proposed approach (solid curves) and the conventional dose-based approach (dashed curves).

(figure 4) and DVHs (figure 5), with comparable GTV and CTV dose coverage and dose homogeneity, the doses to the sensitive structures are dramatically reduced. The dose reduction is particularly pronounced in the spinal cord, brainstem, parotids and eyes. For the left and right parotids, for example, the fractional volume receiving a dose above 25 Gy is reduced from 35% to 20% and 15%, respectively. Consistent with the enhanced dosimetric conformality and similar to the prostate case, much steeper dose gradient occurs near the boundary of the target volume. The dose to the non-sensitive structure normal tissue is also lower in comparison with the conventional IMRT plan. While the NTCPs of the optical nerves and optical chiasm are small and it is difficult to draw a conclusion, from table 5, it is quite clear that the NTCPs of the eyes, parotids, spinal cord and brainstem are improved significantly. We emphasize once again that the significant improvement in sensitive structure sparing is achieved without deteriorating the dose coverage of the GTV and CTV.

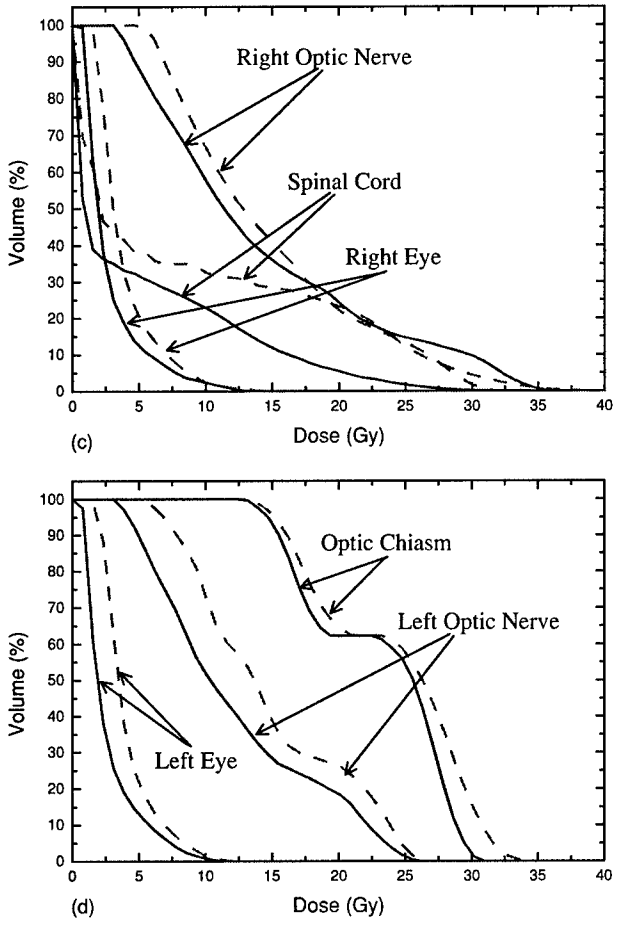

Figure 5. (Continued.)

4. Discussion

The currently available dose-based objective functions do not truly reflect the nonlinear relationship between the dose and the response of tumours and tissues, and it is highly desirable to incorporate clinical outcome data in the formulation of inverse planning to guide the plan optimization process. While the dose dependence of a clinical endpoint may be degenerate in the sense that it may be caused by a variety of dose distributions or DVHs, there exists no mechanism in conventional inverse planning to model the phenomenon. The irradiation of parotid glands mentioned in the introduction represents an example of this. On the other hand, the conventional objective function may impose some unrealistic degeneracy that is inconsistent with clinical experience. For example, assume that in a treatment plan the prescription dose to the target is 70 Gy and that the tumour is divided into two parts with the same volume, one receiving a dose 60 Gy and another 80 Gy. The penalty values of the two scenarios would be the same according to the conventional quadratic function. Obviously, the

two different dose distributions would lead to different outcomes. The cold part, which would greatly diminish the tumour control, is more detrimental than the hot spot.

In this paper we have established a general inverse planning framework in which the penalty at a voxel depends not only on the dose deviation from the desired value but also the dose–volume status of the involved organs. The technique circumvents the problems mentioned above and makes it possible to take advantage of the clinical outcome data. Our study shows that the incorporation of existing clinical knowledge can greatly facilitate the inverse planning process and allows us to obtain better IMRT plans. For the same target dose coverage, the critical structure sparing was substantially improved for both cases. Physically, we believe that the superior performance of the new formalism arises from the adequate modulation of the voxel dependent weighting induced by the dose–volume factor f (see equations (3) and (4)). In conventional dose-based objective function, $f \equiv 1$, and a tacit assumption that all points within a structure are equivalent has been made. The use of dose–volume factor f given by equation (3) enables us to weight different voxels according to the local doses. In this way, we can effectively 'boost' those target regions where the doses are low or penalize more those sensitive structure regions where the doses are high. The dose–volume induced voxel inequality is an important feature of the new inverse planning formalism and is the main driving-force in improving the dose distributions.

The use of clinical knowledge can also facilitate the determination of the structure specific importance factors. While the general influence of the importance factors on the solution is known, the specific response of the plan to a variation in the factors is not clear until the dose optimization is done, which necessitates a manual trial-and-error adjustment of the factors to achieve an acceptable trade-off. The underlying deficiency of the conventional approach is that the importance factors are purely heuristic and lack physical/clinical meanings. In this work we proposed a new scheme for modelling the trade-off and develop an algorithm to auto-determine the factors. The importance of an organ was written into a product of a generic and a dose-dependent factor. The latter was related to the corresponding TCP or NTCP. After the beam optimization, the dose-dependent factors were increased or decreased according to the values of TCPs/NTCPs. This procedure is similar to that reported by Xing *et al* (1999), where a DVH-based 'distance' was used for the assessment of the trade-off status after each optimization. In reality, other types of plan evaluation indices, such as mean/maximum/minimum doses, can also be employed for the purpose. We noted that, with the use of a new objective function, the final solution becomes much less sensitive to choice of $\{r_\sigma^g\}$. This feature may have practical implications in simplifying the inverse planning process.

We should acknowledge that the new technique, just like any other dose response-based technique, may be limited by the scarcity and uncertainty of biological data and the limited predictive power of the TCP/NTCP models. It is important to note, however, that the TCP/NTCP is used as a relative ranking in our plan optimization algorithm instead of a clinical decision-making tool. Because of the phenomenological nature of the modelling, one may further modify the structure specific importance manually to achieve a certain clinical goal. The proposed technique can, at least, provide us with a good starting point for the fine-tuning. Our experience, along with the results shown in the above section, indicates that the technique proposed in this work is capable of generating clinically sensible plans and is much more efficient than the manual selection process.

Finally, we mention that the equivalent uniform dose (EUD)-based dose optimization (Niemierko 1997, Wu *et al* 2002, Thieke *et al* 2003, Lian and Xing 2004) can be cast into the realm of the above inverse planning framework and represents a special case of the general formalism described in this work. Indeed, assuming $\text{EUD} = \left(\frac{1}{N}\sum_i^N D_c^a(i)\right)^{1/a}$, $a = 1/n$ and

setting k_τ and k_σ in equation (4) to zero, we can rewrite equation (4) into

$$F = \sum_{\tau=1}^{t_\tau} r_\tau \left[1 + \eta_1^t (\mathrm{EUD}/\mathrm{EUD}_{\tau,\mathrm{ref}})^{a_\tau} + \eta_2^t (\mathrm{EUD}/\mathrm{EUD}_{\tau,\mathrm{ref}})^{2a_\tau} + \cdots\right] + \sum_{\sigma=1}^{s_\sigma} r_\sigma \left[1 + \eta_1^s (\mathrm{EUD}/\mathrm{EUD}_{\sigma,\mathrm{ref}})^{a_\sigma} + \eta_2^s (\mathrm{EUD}/\mathrm{EUD}_{\sigma,\mathrm{ref}})^{2a_\sigma} + \cdots\right], \quad (7)$$

which becomes a function of EUD. Different from the EUD-based model, the general hybrid objective function given in equation (6) treats the dose–volume effect at a more fundamental voxel level with the actual radiation dose considered, which is more flexible than the EUD defined at a structure level. Because of this, other clinical/dosimetric requirements can easily be integrated. Our study for the prostate case suggests that it is necessary to include the higher order contribution(s) if equation (3) or (7) is used to appropriately model a sensitive structure. Alternatively, a hybrid of dose–volume and dose-based objective function, as given by equation (6), can yield equally good plans. In practice, equation (6) is quite broad and seems to model the inverse planning system effectively. It may also find a natural application in functional image-guided IMRT, where the goal is generally to produce a spatially inhomogeneous dose distribution (Xing *et al* 2002). Finally, we note that the formalism does not involve the prescription of EUD, which could be problematic for practical implementation of an EUD-based model.

5. Conclusion

Inverse planning is an important step in IMRT and its performance crucially determines the quality of IMRT treatment plans. In this work, we provide a mechanism for incorporating clinical endpoint data into the inverse treatment planning process and established a clinically practicable inverse planning framework. We employed the effective volume in voxel domain to take the dose–volume effect of the involved organs into account. The new formalism gives important insight into the problem of therapeutic plan optimization. An algorithm for using computers to aid the determination of structure specific importance factors was also developed. A key step for accomplishing the auto-determination of the importance factors is the decomposition of the conventional importance factor into a generic importance and a dose-dependent component. Two case studies were presented to demonstrate the advantages of the proposed objective function. Comparison of the newly proposed approach with the conventional inverse planning technique indicated that the algorithm is capable of greatly improving the sensitive structure sparing with comparable target dose coverage and homogeneity.

Acknowledgments

Support from the National Cancer Institute (1R01 CA98523-01), the American Cancer Society (IGR-58-008-40), and Department of Defense (DAMD17-03-1-0019 and -0023) is gratefully acknowledged.

References

Amols H I and Ling C C 2002 EUD but not QUD *Int. J. Radiat. Oncol. Biol. Phys.* **52** 1–2

Brahme A 2001 Individualizing cancer treatment: biological optimization models in treatment planning and delivery *Int. J. Radiat. Oncol. Biol. Phys.* **49** 327–37

Burman C, Kutcher G J, Emami B and Goitein M 1991 Fitting of normal tissue tolerance data to an analytic function *Int. J. Radiat. Oncol. Biol. Phys.* **21** 123–35

Chen Y, Michalski D, Houser C and Galvin J M 2002 A deterministic iterative least-squares algorithm for beam weight optimization in conformal radiotherapy *Phys. Med. Biol.* **47** 1647–58

Cho P, Lee S, Marks R II, Oh S, Sutlief S and Phillips M 1998 Optimization of intensity modulated beams with volume constraints using two methods: cost function minimization and projections onto convex sets *Med. Phys.* **25** 435–43

Deasy J, Niemierko A, Herbert D, Yan D, Jackson A, Ten Haken R, Langer M and Sapareto S 2002 Methodological issues in radiation dose–volume outcome analyses: summary of a joint AAPM/NIH workshop *Med. Phys.* **29** 2109–27

Earl M A, Shepard D M, Naqvi S, Li X A and Yu C 2003 Inverse planning for intensity-modulated arc therapy using direct aperture optimization *Phys. Med. Biol.* **48** 1075–89

Eisbruch A, Ten Haken R, Kim H, Marsh L and Ship J 1999 Dose, volume, and function relationships in parotid salivary glands following conformal and intensity-modulated irradiation of head and neck cancer *Int. J. Radiat. Oncol. Biol. Phys.* **45** 577–87

Emami B, Lyman J, Brown A, Coia L, Goitein M, Munzenrider J E, Shank B, Solin L J and Wesson M 1991 Tolerance of normal tissue to therapeutic irradiation *Int. J. Radiat. Oncol. Biol. Phys.* **21** 109–22

Holmes T W, Mackie T R and Reckwerdt P 1995 An iterative filtered backprojection inverse planning algorithm for tomotherapy *Int. J. Radiat. Oncol. Biol. Phys.* **32** 1215–25

Hou Q, Wang J, Chen Y and Galvin J M 2003 An optimization algorithm for IMRT—the simulated dynamics with dose–volume constraints *Med. Phys.* **30** 61–8

Hristov D, Stavrev P, Sham E and Fallone B 2002 On the implementation of dose–volume objectives in gradient algorithms for inverse planning *Med. Phys.* **29** 848–56

Kallman P, Lind B K and Brahme A 1992 An algorithm for maximizing the probability of complication-free tumour control in radiation therapy *Phys. Med. Biol.* **37** 871–90

Kutcher G J and Burman C 1989 Calculation of complication probability factors for non-uniform normal tissue irradiation: the effective volume method. *Int. J. Radiat. Oncol. Biol. Phys.* **16** 1623–30

Lahanas M, Schreibmann E and Baltas D 2003 Multiobjective inverse planning for intensity modulated radiotherapy with constraint-free gradient-based optimization algorithms *Phys. Med. Biol.* **48** 2843–71

Langer M, Brown R, Kijewski P and Ha C 1993 The reliability of optimization under dose–volume limits *Int. J. Radiat. Oncol. Biol. Phys.* **26** 529–38

Langer M, Morrill S and Lane R 1998 A test of the claim that plan rankings are determined by relative complication and TCP *Int. J. Radiat. Oncol. Biol. Phys.* **41** 451–7

Lee E K, Fox T and Crocker I 2000 Optimization of radiosurgery treatment planning via mixed integer programming *Med. Phys.* **27** 995–1004

Lian J and Xing L 2004 Incorporating model parameter uncertainty into inverse treatment planning *Med. Phys.* **31** 2711–20

Llacer J, Solberg T and Promberger C 2001 Comparative behaviour of the dynamically penalized likelihood algorithm in inverse planning *Phys. Med. Biol.* **46** 2637–63

Lyman J and Wolbarst A 1987 Optimization of radiation therapy. III: A method of assessing complication probabilities from dose–volume histograms *Int. J. Radiat. Oncol. Biol. Phys.* **13** 103–9

Michalski D, Xiao Y, Censor Y and Galvin J 2004 The dose–volume constraint satisfaction problem for inverse planning with field segments *Phys. Med. Biol.* **49** 601–16

Miften M M, Das S K, Su M and Marks L B 2004 Incorporation of functional imaging data in the evaluation of dose distributions using the generalized concept of EUD *Phys. Med. Biol.* **49** 1711–21

Mohan R, Mageras G S, Baldwin B, Brewster L J, Kutcher G J, Leibel S, Burman C M, Ling C C and Fuks Z 1992 Clinically relevant optimization of 3D conformal treatments *Med. Phys.* **19** 933–44

Mohan R, Wang X, Jackson A, Bortfeld T, Boyer A, Kutcher G, Leibel S A, Fuks Z and Ling C C 1994 The potential and limitations of the inverse radiotherapy technique *Radiother. Oncol.* **32** 232–48

Niemierko A 1997 Reporting and analyzing dose distributions: a concept of equivalent uniform dose *Med. Phys.* **24** 103–10

Schultheiss T E, Orton C G and Peck R A 1983 Models in radiotherapy: volume effects *Med. Phys.* **10** 410–5

Shepard D, Earl M, Li X, Naqvi S and Yu C 2002 Direct aperture optimization: a turn-key solution for step-and-shoot delivery *Med. Phys.* **29** 1007–18

Starkschall G, Pollack A and Stevens C 2001 Treatment planning using a dose–volume feasibility search algorithm *Int. J. Radiat. Oncol. Biol. Phys.* **49** 1419–27

Thieke C, Bortfeld T, Niemierko A and Nill S 2003 From physical dose constraints to EUD constraints in inverse radiotherapy planning *Med. Phys.* **30** 2332–9

Wang X H, Mohan R, Jackson A, Leibel S A, Fuks Z and Ling C C 1995 Optimization of intensity-modulated 3D conformal treatment plans based on biological indices *Radiother. Oncol.* **37** 140–52

Webb S 2004 Direct aperture optimization for a variable aperture collimator for intensity-modulated radiation therapy *Phys. Med. Biol.* **49** N47–55

Webb S and Nahum A E 1993 A model for calculating tumour control probability in radiotherapy including the effects of inhomogeneous distributions of dose and clonogenic cell density *Phys. Med. Biol.* **38** 653–66

Wu Q, Mohan R, Niemierko A and Schmidt-Ullrich R 2002 Optimization of intensity-modulated radiotherapy plans based on the EUD *Int. J. Radiat. Oncol. Biol. Phys.* **52** 224–35

Xing L, Cotrutz C, Hunjan S, Boyer A, Adalsteinsson E and Spielman D 2002 Inverse planning for functional image-guided IMRT *Phys. Med. Biol.* **47** 3567–78

Xing L, Hamilton R J, Spelbring D, Pelizzari C, Chen G T and Boyer A L 1998 Fast iterative algorithms for 3D inverse treatment planning *Med. Phys.* **25** 1845–9

Xing L, Li J G, Donaldson S, Le Q T and Boyer A 1999 Optimization of importance factors in inverse planning *Phys. Med. Biol.* **44** 2525–36

Yan H, Yin F F, Guan H Q and Kim J 2003 AI-guided parameter optimization in inverse treatment planning *Phys. Med. Biol.* **48** 3565–80

Incorporating model parameter uncertainty into inverse treatment planning

Jun Lian[a] and Lei Xing[b]
Department of Radiation Oncology, Stanford University School of Medicine, 875 Blake Wilbur Drive, Stanford, California 94305-5847

(Received 28 October 2003; revised 28 April 2004; accepted for publication 1 July 2004; published 27 August 2004)

Radiobiological treatment planning depends not only on the accuracy of the models describing the dose-response relation of different tumors and normal tissues but also on the accuracy of tissue specific radiobiological parameters in these models. Whereas the general formalism remains the same, different sets of model parameters lead to different solutions and thus critically determine the final plan. Here we describe an inverse planning formalism with inclusion of model parameter uncertainties. This is made possible by using a statistical analysis-based frameset developed by our group. In this formalism, the uncertainties of model parameters, such as the parameter a that describes tissue-specific effect in the equivalent uniform dose (EUD) model, are expressed by probability density function and are included in the dose optimization process. We found that the final solution strongly depends on distribution functions of the model parameters. Considering that currently available models for computing biological effects of radiation are simplistic, and the clinical data used to derive the models are sparse and of questionable quality, the proposed technique provides us with an effective tool to minimize the effect caused by the uncertainties in a statistical sense. With the incorporation of the uncertainties, the technique has potential for us to maximally utilize the available radiobiology knowledge for better IMRT treatment. © *2004 American Association of Physicists in Medicine.* [DOI: 10.1118/1.1785451]

Key words: inverse planning, dose optimization, biological models, IMRT

INTRODUCTION

Most intensity-modulated radiotherapy (IMRT) optimization systems at present use dose and/or dose volume-based objective functions,[1–6] which guide the IMRT planning by imposing a penalty according to the difference between the computed and prescribed doses. A well-known drawback of the dose-based inverse planning is that the nonlinear dose response of tumor or normal structures is not fully considered. A number of mathematical models have been developed over the years to better describe the biological effect of radiation, which include tumor control probability (TCP),[7] normal tissue complication probability (NTCP),[8] equivalent uniform dose (EUD)[9] and the probability of uncomplicated tumor control (P_+).[10,11] In parallel to these modeling efforts, considerable works have also been done to use these biological models to construct more meaningful objective functions for therapeutic dose optimization.[1–16]

Generally speaking, radiobiological formalism involves the use of model parameters that are of considerable uncertainty.[7,17–22] For instance, the radiosensitivity α of Webb's TCP model varies from 0.157 to 0.090 Gy^{-1} when model parameters were fit to 103 patients' data.[7] Biological "margins" have been used to account for the variability in radiation sensitivity. Similar to the use of a safety margin to account for the potential uncertainties in targeting a tumor, this method assigns more conservative radiosensitivity values to the tumor or sensitive structures to deal with the potential uncertainty of the parameter.[23] Kåver *et al.* proposed a stochastic optimization to account for clinical uncertainties, including the varying radiosensitivity.[24,25] The objective function was constructed based on a linear quadratic Poisson model which approximates the probability of curing the patient or inflicting injury. Two parameters in the model could be calculated if the standard deviation of dose per faction was known. The optimization was thus executed corresponding to different standard deviations.

We have recently presented a general statistical analysis-based inverse planning framework[26,27] and applied it to investigate the influence of model parameter uncertainties in biologically based dose optimization.[28] The purpose of this paper is to provide a detailed description of the technique and addresses several important issues related to the dose optimization in the presence of model parameter uncertainties. In our approach, the uncertainty of a model parameter is quantified by a probability density function and its influence is then incorporated into inverse planning through the use of a statistical inference theorem.[26] The technique is illustrated by using a hypothetical C-shaped tumor case, a prostate tumor case and a paraspinal tumor case with an EUD-based model. Considering that currently available models for computing biological effects of radiation are simplistic, and the data they rely on are sparse and of questionable quality, the proposed technique provides us with an effective tool to minimize the effect caused by the uncertainties in a statistical sense. The treatment plans so obtained are generally less sensitive to the inter-patient variation and other types of uncertainties that may otherwise influence the final treatment plan greatly.

METHODS AND MATERIALS

Statistical analysis-based inverse planning

The inverse problem as posed for IMRT consists of the determination of the beamlet weight vector $\boldsymbol{w}$ when a desired plan is prescribed. In a vectorial form, the dose to the points in the treatment region depends upon the beamlet weights $\boldsymbol{w}$ as

$$\boldsymbol{D}_c = \boldsymbol{d} \cdot \boldsymbol{w}, \tag{1}$$

where $\boldsymbol{d}$ represents the dose deposition coefficients matrix, expressing the dose deposited to any patient point when irradiated with a unit weight beamlet. The total number of physically realizable dose distributions $\boldsymbol{D}_c$ in IMRT is enormous and increases exponentially with the number of beamlets. Inverse planning is essentially a plan selection process from the vast pool of physically realizable solutions. In a recent paper, Xing *et al.*[26] introduced a statistical analysis-based inverse planning technique. In this approach the commonly used objective function is reformulated into a probability density function whose value gives the figure of merit of a dose distribution. A virtue of the approach is that it allows us to obtain solution in the presence of uncertainties of the prescription parameters or other model parameters using a statistical inference technique. Application of the technique to deal with a system with a set of variable dose prescriptions has been described in another work of our group.[27] Here we use the formalism for biological modeling based-inverse planning in the presence of model parameter uncertainties. To be specific, we use an equivalent uniform dose (EUD)-based objective function employed by Wu *et al.*[13,29] and discuss the consequences of the variation of model parameter a and how to incorporate the fluctuations into inverse planning dose optimization to obtain statistically optimal solutions.

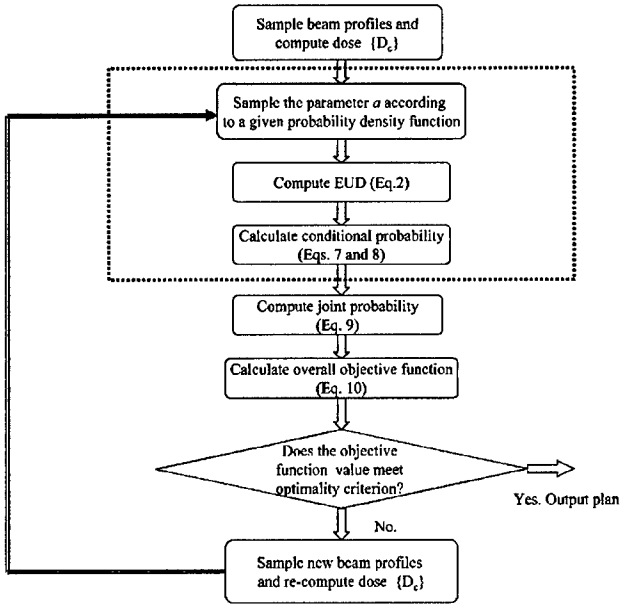

FIG. 1. The flow chart of the optimization process with the inclusion of model parameter uncertainty.

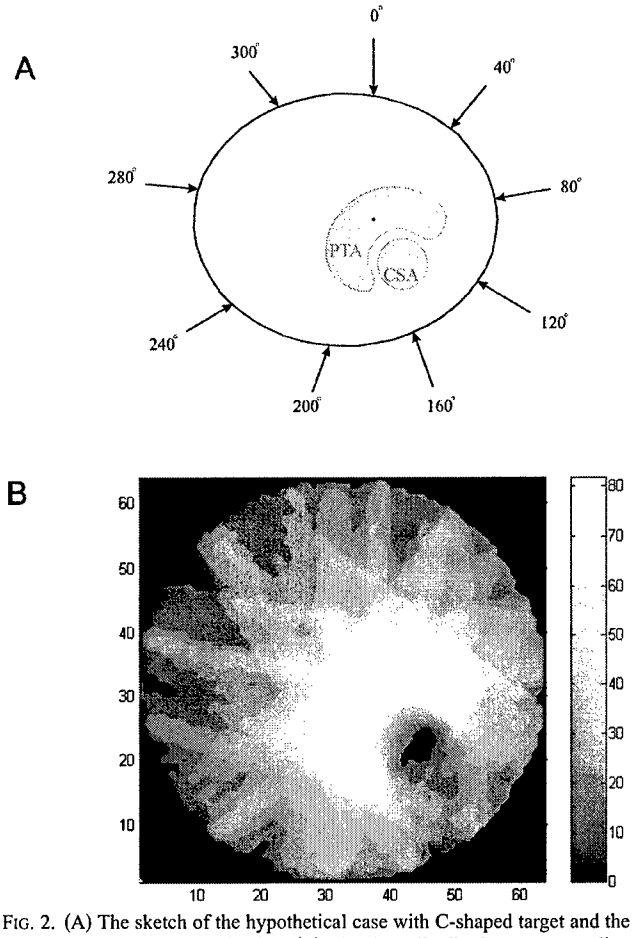

FIG. 2. (A) The sketch of the hypothetical case with C-shaped target and the beam setup for dose optimization. (B) The dose distribution corresponding to the parameters listed in Table I and the probabilistic distribution shown in Fig. 3 d2.

EUD model and EUD-based objective function

The concept of equivalent uniform dose (EUD) for tumor was originally introduced by Niemierko as the biologically equivalent dose that, if given uniformly, would lead to the same cell kill in the tumor volume as the actual nonumiform dose distribution. Recently, Niemierko *et al.* suggested a phenomenological form[9,13,30]

$$\mathrm{EUD} = \left(\frac{1}{N} \sum_i D_i^a \right)^{1/a}, \tag{2}$$

for both tumor and normal tissues, where N is the number of voxels in the structure, D_i is the dose delivered to the ith voxel, a is the tumor or normal tissue-specific parameter that describes the dose-volume effect. EUD described in Eq. (2) is the general mean of the non-uniform dose distribution. According to the mathematic properties of the function,[31] for $a = \infty$, the EUD is equal to the maximum dose, and for $a = -\infty$, the EUD is equal to the minimum dose. Tumors generally have large negative values of a, whereas serial critical structures (e.g., spinal cord and rectum) have large positive values and parallel critical structures that exhibit a large dose-volume effect (e.g., liver, parotids, and lungs) have small positive values.

TABLE I. The conventional EUD-based optimization parameter for the hypothetical IMRT treatment of a C-shaped tumor.

	PTV	PTV[a]	OAR	NT
a	−10.0	10.0	6.0	6.0
EUD_0 (Gy)	72	76	35	35
n	20	20	6	6

[a]Contains parameters for the target treated as virtual normal tissue to limit dose inhomogeniety.

TABLE II. The conventional EUD-based optimization parameter for prostate cancer.

	PTV	PTV[a]	Bladder	Rectum	NT
a	−10.0	10.0	6.0	24	6.0
EUD_0 (Gy)	72	76	35	35	35
n	20	20	6	6	6

[a]Contains parameters for the target treated as virtual normal tissue to limit dose inhomogeniety.

The objective function or figure of merit used to measure the goodness of a dose distribution and guide the optimization.[1] In the present paper, the system objective function is given by[13]

$$F=\prod_j f_j, \tag{3}$$

where the component subcore f_j may be either

$$f_T=\frac{1}{1+\left(\frac{EUD_0}{EUD}\right)^n}, \tag{4}$$

for tumors, or

$$f_{OAR}=\frac{1}{1+\left(\frac{EUD}{EUD_0}\right)^n}, \tag{5}$$

for normal tissues and organs at risk (OARs). EUD_0 is the desired dose parameter for the target volume and the maximum tolerable uniform dose for normal structures. Parameter n is akin to the structure specific importance factor[32] in the conventional inverse planning formalism that parameterizes our tradeoff strategy of different structure. The large n indicates high importance.

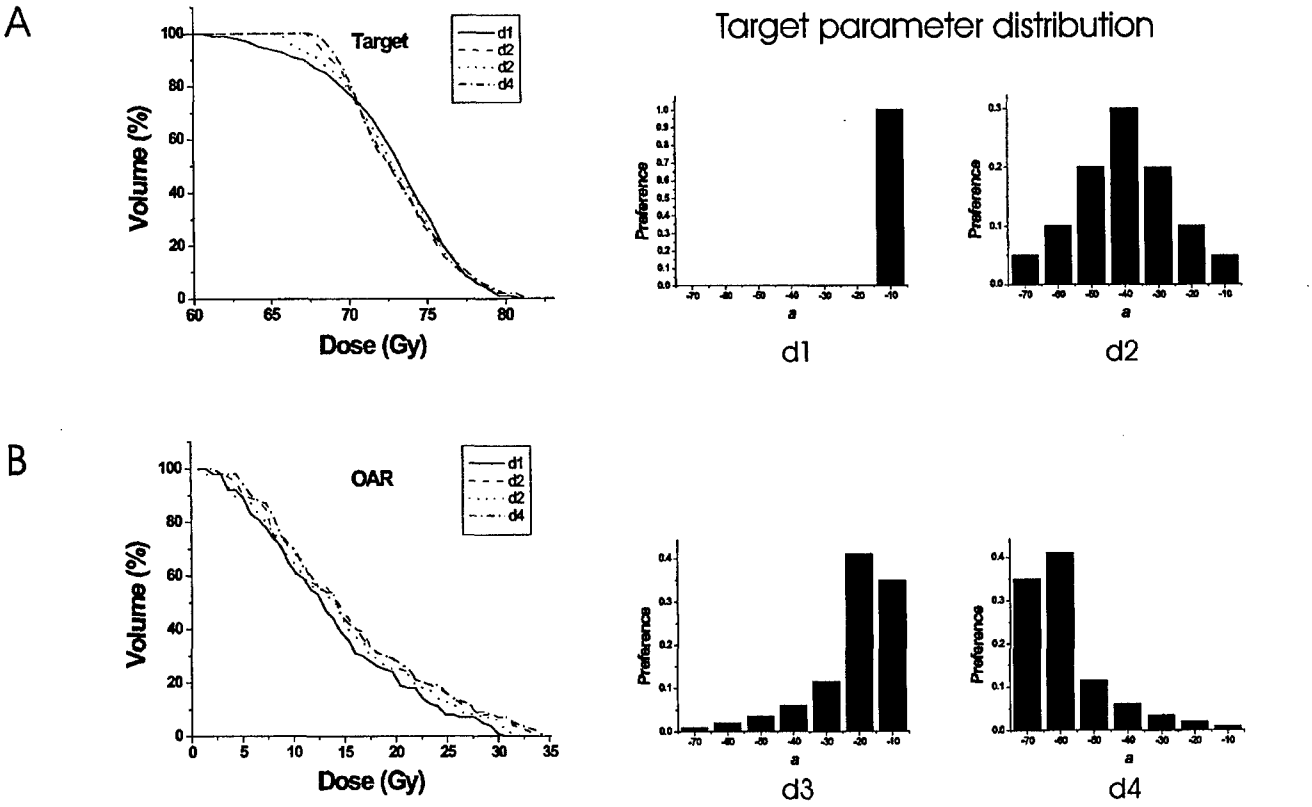

FIG. 3. The target and OAR DVHs of four optimal plans when parameter a is a fixed value (bar chart d1) and varies according to three different probabilistic distributions (bar chart d2, d3, and d4).

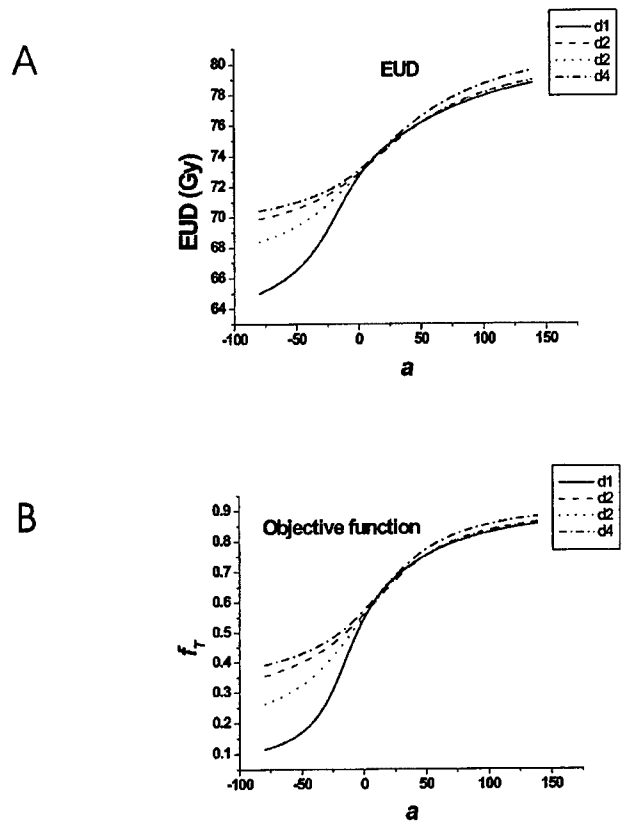

FIG. 4. The EUD of the target and objective function when parameter a is prescribed according to Fig. 3.

Incorporation of the variation distribution of the model parameter into inverse planning

We assume that a_k in the EUD model varies according to a simple Gaussian distribution

$$P_n(a_k)=P'_{0n}\exp\{-r_n[a_k-a_0]^2\}, \tag{6}$$

where a_0 is the mean value, P'_{0n} is a normalization constant and a_k is one of the sampling values of a. For a given distribution, the EUD and the corresponding figure of merit of an IMRT plan vary with the sampling of a. We thus rewrite Eqs. (4) and (5) as conditional probabilities for a sampled a_k:

$$P_T(\mathrm{EUD}|a_k)=\frac{1}{1+\left(\frac{\mathrm{EUD}_0}{\mathrm{EUD}}\right)^n}, \tag{7}$$

$$P_{\mathrm{OAR}}(\mathrm{EUD}|a_k)=\frac{1}{1+\left(\frac{\mathrm{EUD}}{\mathrm{EUD}_0}\right)^n}. \tag{8}$$

The objective function for a structure m in the presence of uncertainty in a is expressed as the summation of a series of joint probabilities

$$P_m(\mathrm{EUD})=\sum_k P_m(\mathrm{EUD}|a_k)\cdot P_m(a_k), \tag{9}$$

and the overall objective function P of the system is a product of $P_m(\mathrm{EUD})$ defined in Eq. (9). That is

$$F=\ln(1/P)=-\ln\prod_m P_m(\mathrm{EUD})$$

$$=-\sum_m \ln\sum_k P_m(\mathrm{EUD}|a_k)\cdot P_m(a_k). \tag{10}$$

Optimization method

As described above, the uncertainties of model parameters, $\{a_k\}$, are described by probability density functions and they are incorporated into the overall objective function of the system through the joint probability given by Eq. (9). To obtain the optimal solution in the presence of model parameters, all we need to do is to minimize the overall objective function given by Eq. (10).

The calculation process is schematically shown in Fig. 1. For the computational purpose, the probability density function for each structure is discreted into seven equally spaced points. We use the Fletcher–Reeves conjugate gradient optimization algorithm[33] to optimize the system. But any other iterative or stochastic optimization can be also employed to optimize the system. A common step in all optimization algorithms is the evaluation of the objective function for a trial beam profiles (or computed dose distribution), which is somewhat tedious here because of the appearance of multiple a_k's of the involved structures. Briefly, for a given trial beam profiles or dose distribution, the evaluation of the objective function consists of four steps: (i) For a structure m, calculate the EUD corresponding to each possible a_k; (ii) calculate the conditional probability for the target and OAR using Eqs. (7) and (8), respectively; (iii) sum over all possible a_k to obtain the joint probability, given by Eq. (9); and (iv) sum over all structures to obtain the overall objective function value. After the dose optimization, a set of optimal beam profiles and the corresponding dose distribution and other plan indices are provided for the planner to assess the clinical relevance of the obtained treatment plan.

Test cases

The new algorithm was tested using a hypothetical phantom case with a C-shaped target and two clinical cases (a prostate case and a paraspinal tumor boost treatment). The size of the pencil beam defined at the isocenter was 0.5 cm. The configuration of the C-shaped tumor case is shown in Fig. 2(A). Nine 6 MV equi-spaced beams were used for the treatment (0°, 40°, 80°, 120°, 160°, 200°, 240°, 280°, and 320°—respecting the International Electrotechnical Commission (IEC) convention). The values of n and a in the EUD-based objective function are listed in Table I. The parameter a in EUD model characterizes the dose-volume effect but its value is generally not known accurately even for clinically well studied organs. The influence of the uncertainty in the a value of a target or sensitive structure to the final treatment plan was studied and analyzed.

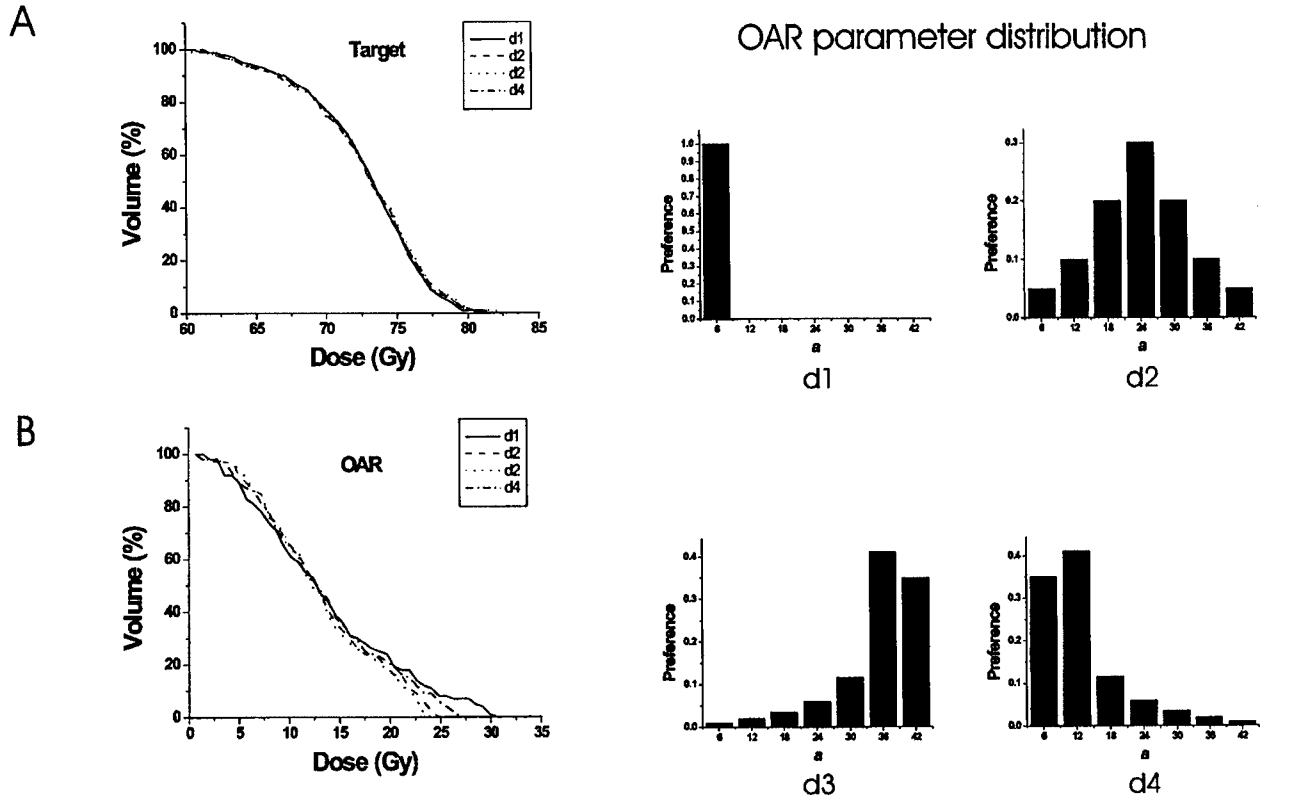

FIG. 5. The target and OAR DVHs of four optimal plans when parameter a is a fixed value (bar chart d1) and varies according to three different probabilistic distributions (bar chart d2, d3, and d4).

Similar study was carried out for the two clinical cases. The six 6 MV beam angles used for the IMRT prostate treatment were 0°, 55°, 135°, 180°, 225°, and 305°. Table II lists some relevant parameters used for planning the case. For the IMRT paraspinal boost treatment, five 6 MV nonequally spaced coplanar beams were placed at the following angular positions: 95°, 140°, 175°, 225°, and 275°. The target boost dose was prescribed to 16 Gy. Relevant parameters are listed in Table II. The planning goal was to find a dose distribution that covered the tumor volume as uniformly as possible, while maximally sparing the spinal cord, liver, and kidney.

RESULTS AND DISCUSSIONS

The C-shaped tumor case

We first investigated the behavior of the system when the parameter a of the target EUD takes four different distributions, as depicted in the bar charts shown on the right of Fig. 3, while keeping the parameter a of the OAR at a constant $a_0=6.0$. In the case shown in Fig. 3 d1, the parameter a takes only a single value, $a_0=-10$, which is a simple case studied by Wu *et al.*[13] The optimal plans for the four distributions of parameter a differ significantly, as indicated by the target and OAR DVHs shown in Figs. 3(A) and 3(B). The isodose plot corresponding to the a-distribution shown in Fig. 3 d2 is plotted in Fig. 2(B).

To estimate the degree of sensitivity of the solutions against a variation in a, we computed the target EUD and the objective function, f_T, as a function of parameter a for the four optimal dose distributions under different types of uncertainty distributions. The results are plotted in Fig. 4. For plan d1, the EUD changes from 65 to 71 Gy when a is varied from -10 to -70 and to 79 Gy when a is equal to 140. The objective function varies from 0.11 to 0.85 in the range of variation in a. For plan d4, the EUD is narrowed to a range between 70 and 79 Gy. The EUD variations of plans d2 and d3 are similarly reduced. These results suggest that the EUD becomes much less sensitive to the variation in parameter a in the plans obtained with some "built-in" distributions in parameter a (i.e., plans corresponding to Figs. 3 d2 to d4).

The uncertainty of parameter a of the OAR can be similarly included in the dose optimization process when its distribution is known. In the second study, we fixed the target EUD parameter $a=-10$ and allowed the parameter a of the OAR to take four different distributions as plotted in the right of Fig. 5. The target and OAR DVHs for the four possible scenarios are shown in A and B. Once again, we found that the final solution strongly depends on the distributions of the parameter a.

The maximum doses of the OAR of the four plans vary from 24 to 30 Gy. Note that the doses to the OAR in plans d2, d3, and d4 are less than that of plan A, where the parameter a is restricted to a single value, $a_0=6$. This is explainable since the parameters a in plans d2, d3, and d4 are shifted up to higher values. As a increases, the EUD puts more em-

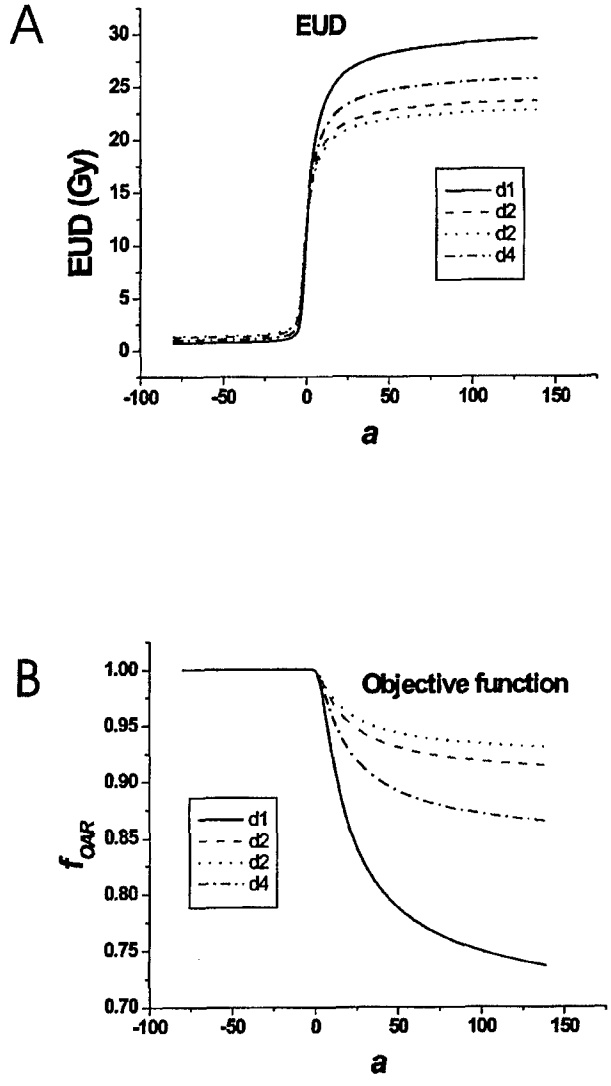

FIG. 6. The EUD of the OAR and objective function when parameter a is prescribed according to Fig. 5.

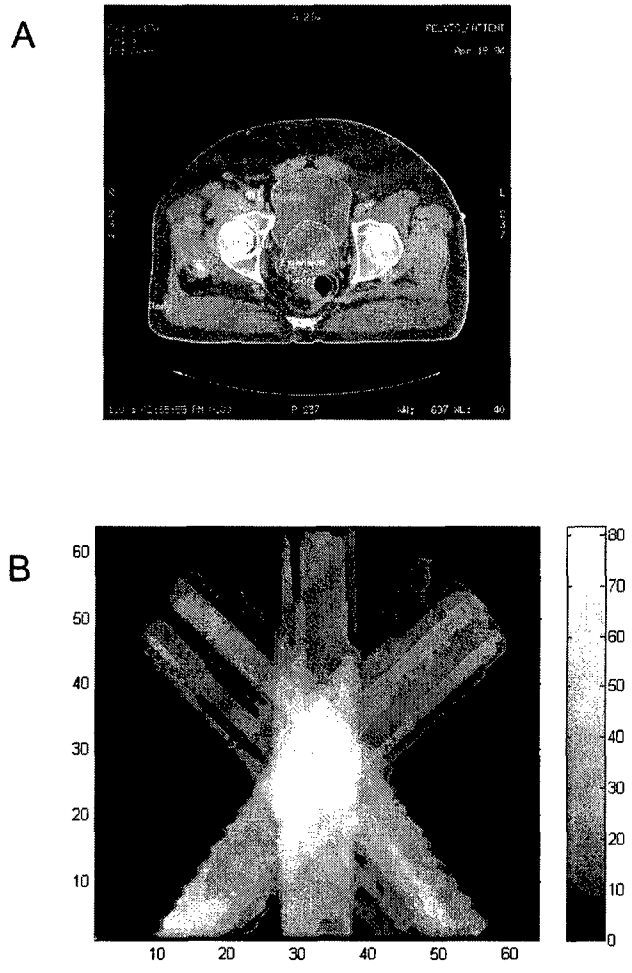

FIG. 7. A transverse slice showing the anatomical structures delineated for the prostate tumor (A) and the corresponding optimized dose distribution with the parameters listed in Table II and the probabilistic distribution shown in Fig. 8(B).

phasis on the high dose (recall that EUD becomes the maximum dose when $a=\infty$). As a consequence of the increased "effective" a value in the distributions shown in Fig. 5, d2, d3, and d4, the OAR dose is improved in comparison with the plan obtained under the assumption of a fixed a value (Fig. 5, d1). Interestingly, the target DVHs shows that four distinct plans have very similar target coverage. It is well known that in dose optimization there is generally no net gain: an improvement in the dose to a structure is often accompanied by a dosimetrically adverse effect(s) at other points in the same or different structures. The result here suggests that, from a clinical point of view, it is possible to have a great gain in one structure with a little sacrifice in another structure. How to find the truly optimal tradeoff represents a practical subject that is worth of studying in the future.

As can be expected from the discussion in previous paragraphs, the solution obtained with $a_0=6$ (Fig. 5, d1) is more sensitive to a variation in parameter a. Indeed, as seen from Fig. 6, the EUD for this plan varies from 1 to 30 Gy when a is changed from -80 to 140. On the other hand, the EUD changes for the rest three situations are much less for the same variation in a. The upper bound of the EUD is reduced to 26 Gy for plan d4, 24 Gy for plan d2, and 23 Gy for plan d3. The objective functions of four plans show a similar trend.

The prostate tumor case

Four IMRT plans with different types of pre-assumed uncertainties were generated for a prostate tumor case [Fig. 7(A)]. These include: (i) The a-parameters for both prostate target and OARs are restricted to single values as listed in Table II. This plan serves as a reference whose DVHs are shown in Figs. 8(A)–8(C) as dotted curves; (ii) Only the a-parameter of the prostate target takes a range of values, as depicted in the right of Fig. 8(A); (iii) Only the a-parameter of the rectum takes a range of values, as depicted in the right of Fig. 8(B); and (iv) The a-parameters of both prostate target and the rectum were allowed to take a range of values, as depicted in the right of Fig. 8(C).

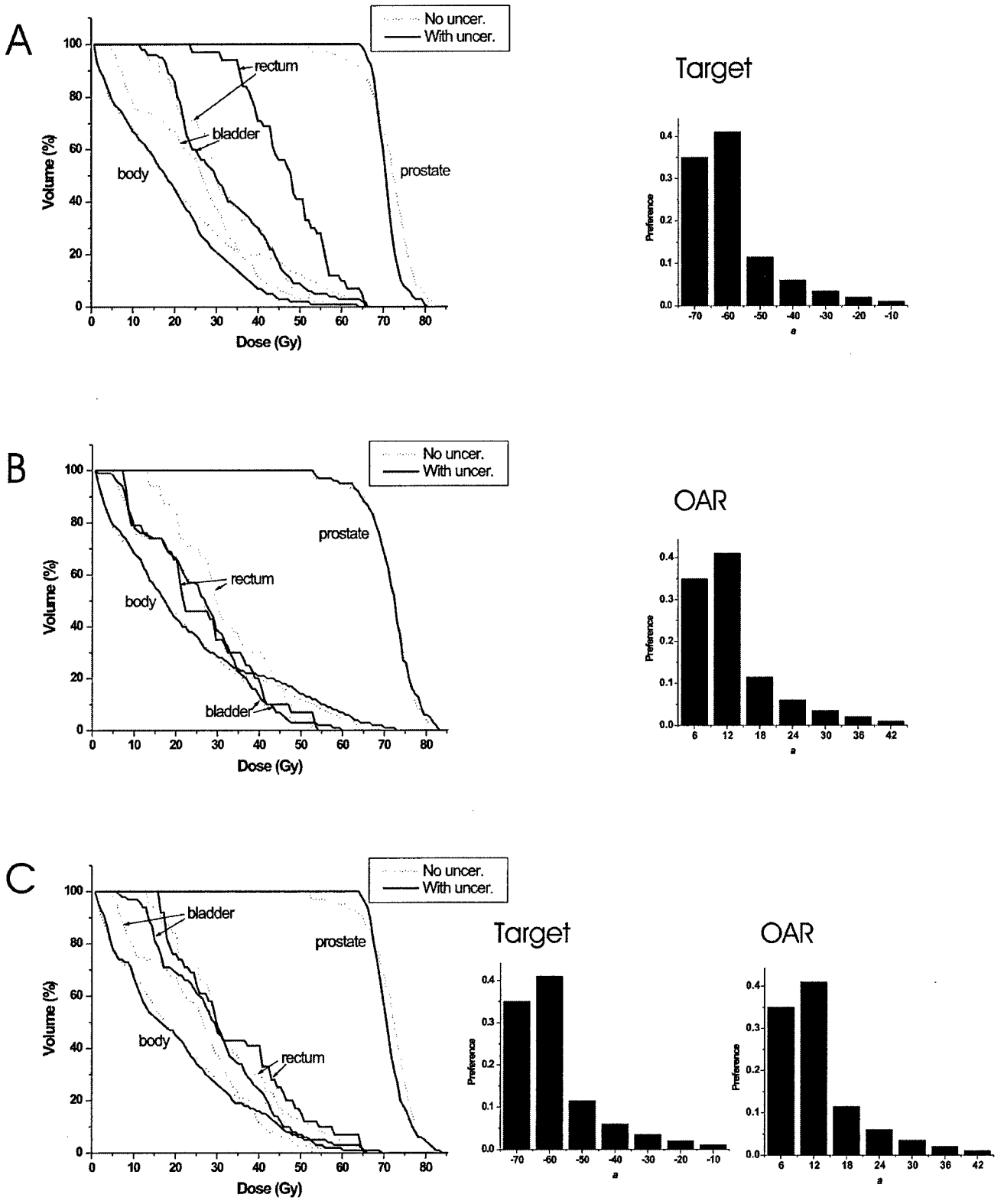

FIG. 8. DVHs for a prostate cancer case using the conventional optimization with fixed a-value (dotted line) and the newly proposed approach with the inclusion of model parameter uncertainty (solid line). (A) Only the a-parameter for the target is assigned with a probabilistic distribution; (B) Only the a-parameter for the OAR is assigned with a probabilistic distribution; (C) Uncertainties in the a-parameter are introduced for both the target and OAR.

DVHs for the plan using parameters defined in Table II are plotted with dotted curves and plans with the inclusion of parameter uncertainty are drawn with solid curves (Fig. 8). When the parameter a in target EUD takes a Poisson distribution as shown in the bar chart of Fig. 8(A), prostate dose homogeneity is significantly improved. The minimum dose

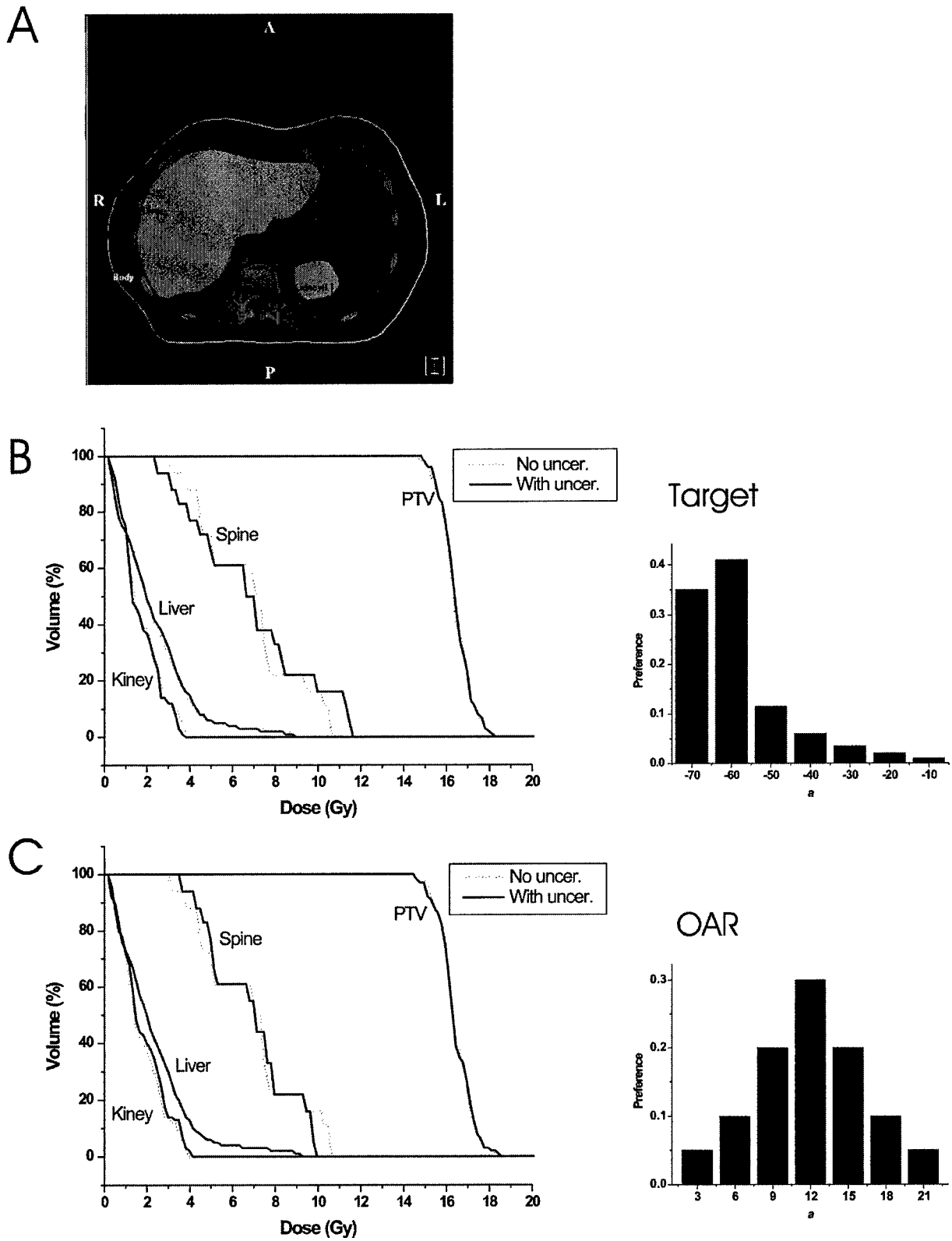

FIG. 9. (A) A transverse slice showing the anatomical structures for a paraspinal case; (B) DVHs when the a-parameter for the target is assigned with a probabilistic distribution; (C) DVHs when the a-parameter for the OAR is assigned with a probabilistic distribution.

increases from 55 to 67 Gy, and the maxim dose decreases slightly from 82 to 80 Gy. However the volumes receiving radiation dose for rectum, bladder and normal tissue all increase significantly though the maximum dose remains similar. The improvement of the target coverage and compromise of OAR sparing is a natural outcome of the competitive re-

TABLE III. The conventional EUD-based optimization parameter for paraspinal tumor.

	PTV	PTV[a]	Spine	Liver	Kidney
a	−10.0	10.0	6.0	6.0	6.0
EUD_0 (Gy)	16	17	12	6.4	4.8
n	20	20	6	6	6

[a]Contains parameters for the target treated as virtual normal tissue to limit dose inhomogeniety.

quirements for targets and OARs imposed on the system. The corresponding dose distribution with the target parameter defined in the bar chart A is shown in Fig. 7(B).

Next we considered the inclusion of parameter a uncertainty in EUD calculation in one of the critical structures-rectum [Fig. 8(B)]. The irradiated rectum volume for a dose below 60 Gy is less than that of a conventional plan with the parameter a fixed at 24. DVHs for the bladder, normal tissue and prostate do not change significantly compared to the plan without inclusion of parameter uncertainty.

Lastly, we simultaneously replaced target and rectum parameters with the distributions shown in Fig. 8(C). Similar to that corresponds the prescription of Fig. 8(A), the prostate coverage is improved. However, the rectum DVH in this case is not worsen greatly because parameter a of rectum EUD was allowed to take a spectrum of values. For bladder and normal tissue, although their irradiated volumes in the low dose region are higher than those of the conventional plan, the volumes receiving high doses are reduced.

The paraspinal tumor case

Three IMRT plans were generated for a paraspinal tumor case [Fig. 9(A)]. These include: (i) The a-parameters for both target and OARs are restricted to single values as listed in Table III. This plan serves as a reference whose DVHs are shown in Figs. 9(B) and 9(C) as dotted curves; (ii) Only the a-parameter of the target takes a range of values, as depicted in the right of Fig. 9(B); and (iii) Only the a-parameter of the spinal cord takes a range of values, as depicted in the right of Fig. 9(C).

When a in target EUD takes a Poisson distribution as shown in the bar chart of Fig. 9(B), dose homogeneity is slightly improved. However, this is achieved at the expense of more irradiation to the cord. The inclusion of parameter a uncertainty in EUD calculation in the spinal cord [Fig. 9(C)] reduced the maximum cord dose by 100 cGy. The DVHs of the target, kidney, and liver were not changed significantly compared to the plan without inclusion of parameter uncertainty.

The influence of various uncertainties on the patient treatment has been a subject of intense study. Fenwick and Nahum have included the model parameter uncertainty with a standard deviation when calculating the NTCP of rectum.[34,35] Similarly, the inclusion of uncertainties in the patient setup and dose calculation has also been demonstrated.[36–38] Deasy *et al.* have used a bootstrap-based method to estimate the influence of biological parameter uncertainties on predicting long-term salivary function.[21] The statistical method proposed here provides a general framework to include various uncertainties in the dose optimization process. With minor modification, the technique can be extended to derive statistically optimal solutions in the presence of other types of uncertainties.

As can be intuitively imagined, the inclusion of a-distribution will definitely change the final dose. Whether it will improve or worsen the final dose distribution will generally depend on the specific form of the a-distribution, and also the metric used to judge the goodness of a plan. If the original EUD-based objective function is used as the sole metric for the judgment, the inclusion of a-distribution may make the plan worse. However, clinical decision-making is not made by a single function and a "worse" plan judged by the EUD-objective function may turn out to be clinically more favorable. In other words, there is a gap between mathematical dose optimization and clinical decision-making. The study seems to suggest that, while it is generally true that there is no net gain in dose optimization,[27] it is important to develop a method that is capable of optimizing not only the objective function but also the next level of decision-making. This kind of optimization will allow us to find the solution that may sacrifice a little (i.e., clinically insignificant) in one or a few structures but gain a lot in other structures.

CONCLUSIONS

We have proposed and implemented a technique for incorporating biological model parameter uncertainties into inverse treatment planning. The formalism is quite general and does not prerequisite the specific form of uncertainty distributions of the involved model parameters. By including model parameter uncertainties, the final solution becomes more robust and the treatment outcome will be less likely influenced by inter-patient variation of biological characteristics. With the increasing interest in radiation therapy community to use biologically based models for treatment planning, this work provides an effective way to better account for the known uncertainties in the model parameters and allows us to maximally utilize the available radiobiology knowledge to facilitate patient care.

ACKNOWLEDGMENTS

We would like to thank the useful discussion with C. Cotrutz, Y. Yang, and J. Both. This work was in part supported by a research grant from the prostate cancer research program of U.S. Department of Defense (DAMD17-03-1-0019) to Jun Lian and a research grant from the National Cancer Institute (5 R01 CA98523-02) to Lei Xing.

[a]Present address: Department of Radiation Oncology, The University of North Carolina, Chapel Hill, NC 27599-7512. Telephone: (919) 966 1101; Fax: (919) 966 7681. Electronic mail: Jun_Lian@med.unc.edu

[b]Author to whom correspondence should be addressed. Stanford University School of Medicine, Department of Radiation Oncology, 875 Blake Wilbur Drive, Stanford, CA 94305-5847. Telephone: (650) 498 7896; Fax: (650) 498 4015. Electronic mail: lei@reyes.stanford.edu

[1] Q. Wu and R. Mohan, "Algorithms and functionality of an intensity

modulated radiotherapy optimization system," Med. Phys. **27**, 701–711 (2000).
[2] G. Starkschall, A. Pollack, and C. W. Stevens, "Treatment planning using a dose-volume feasibility search algorithm," Int. J. Radiat. Oncol., Biol., Phys. **49**, 1419–1427 (2001).
[3] L. Xing, R. J. Hamilton, D. Spelbring, C. A. Pelizzari, G. T. Chen, and A. L. Boyer, "Fast iterative algorithms for three-dimensional inverse treatment planning," Med. Phys. **25**, 1845–1849 (1998).
[4] P. S. Cho, S. Lee, R. J. Marks II, S. Oh, S. G. Sutlief, and M. H. Phillips, "Optimization of intensity modulated beams with volume constraints using two methods: cost function minimization and projections onto convex sets," Med. Phys. **25**, 435–443 (1998).
[5] T. Bortfeld, "Optimized planning using physical objectives and constraints," Semin Radiat. Oncol. **9**, 20–34 (1999).
[6] S. Webb, "Optimization of conformal radiotherapy dose distributions by simulated annealing," Phys. Med. Biol. **34**, 1349–1370 (1989).
[7] S. Levegrun, A. Jackson, M. J. Zelefsky, M. W. Skwarchuk, E. S. Venkatraman, W. Schlegel, Z. Fuks, S. A. Leibel, and C. C. Ling, "Fitting tumor control probability models to biopsy outcome after three-dimensional conformal radiation therapy of prostate cancer: pitfalls in deducing radiobiologic parameters for tumors from clinical data," Int. J. Radiat. Oncol., Biol., Phys. **51**, 1064–1080 (2001).
[8] J. T. Lyman, "Complication probability as assessed from dose-volume histograms," Radiat. Res., Suppl. **8**, S13–S19 (1985).
[9] A. Niemierko, "Reporting and analyzing dose distributions: a concept of equivalent uniform dose," Med. Phys. **24**, 103–110 (1997).
[10] G. O. De Meerleer, L. A. Vakaet, W. R. De Gersem, C. De Wagter, B. De Naeyer, and W. De Neve, "Radiotherapy of prostate cancer with or without intensity modulated beams: a planning comparison," Int. J. Radiat. Oncol., Biol., Phys. **47**, 639–648 (2000).
[11] C. Fiorino, S. Broggi, D. Corletto, G. M. Cattaneo, and R. Calandrino, "Conformal irradiation of concave-shaped PTVs in the treatment of prostate cancer by simple 1D intensity-modulated beams," Radiother. Oncol. **55**, 49–58 (2000).
[12] M. Alber and F. Nusslin, "An objective function for radiation treatment optimization based on local biological measures," Phys. Med. Biol. **44**, 479–493 (1999).
[13] Q. Wu, R. Mohan, A. Niemierko, and R. Schmidt-Ullrich, "Optimization of intensity-modulated radiotherapy plans based on the equivalent uniform dose," Int. J. Radiat. Oncol., Biol., Phys. **52**, 224–235 (2002).
[14] A. Brahme, J. Nilsson, and D. Belkic, "Biologically optimized radiation therapy," Acta Oncol. **40**, 725–734 (2001).
[15] X. H. Wang, R. Mohan, A. Jackson, S. A. Leibel, Z. Fuks, and C. C. Ling, "Optimization of intensity-modulated 3D conformal treatment plans based on biological indices," Radiother. Oncol. **37**, 140–152 (1995).
[16] C. Thieke, T. Bortfeld, A. Niemierko, and S. Nill, "From physical dose constraints to equivalent uniform dose constraints in inverse radiotherapy planning," Med. Phys. **30**, 2332–2339 (2003).
[17] C. Burman, G. J. Kutcher, B. Emami, and M. Goitein, "Fitting of normal tissue tolerance data to an analytic function," Int. J. Radiat. Oncol., Biol., Phys. **21**, 123–135 (1991).
[18] S. Webb and A. E. Nahum, "A model for calculating tumour control probability in radiotherapy including the effects of inhomogeneous distributions of dose and clonogenic cell density," Phys. Med. Biol. **38**, 653–666 (1993).
[19] P. M. Wu, D. T. Chua, J. S. Sham, L. Leung, D. L. Kwong, M. Lo, A. Yung, and D. T. Choy, "Tumor control probability of nasopharyngeal carcinoma: a comparison of different mathematical models," Int. J. Radiat. Oncol., Biol., Phys. **37**, 913–920 (1997).
[20] J. D. Fenwick, "Predicting the radiation control probability of heterogeneous tumour ensembles: data analysis and parameter estimation using a closed-form expression," Phys. Med. Biol. **43**, 2159–2178 (1998).
[21] J. O. Deasy, K. S. Chao, and J. Markman, "Uncertainties in model-based outcome predictions for treatment planning," Int. J. Radiat. Oncol., Biol., Phys. **51**, 1389–1399 (2001).
[22] R. Jeraj and P. Keall, "The effect of statistical uncertainty on inverse treatment planning based on Monte Carlo dose calculation," Phys. Med. Biol. **45**, 3601–3613 (2000).
[23] A. Brahme, "Optimized radiation therapy based on radiobiological objectives," Semin Radiat. Oncol. **9**, 35–47 (1999).
[24] G. Kåver, B. K. Lind, J. Lof, A. Liander, and A. Brahme, "Stochastic optimization of intensity modulated radiotherapy to account for uncertainties in patient sensitivity," Phys. Med. Biol. **44**, 2955–2969 (1999).
[25] J. Lof, B. K. Lind, and A. Brahme, "An adaptive control algorithm for optimization of intensity modulated radiotherapy considering uncertainties in beam profiles, patient set-up and internal organ motion," Phys. Med. Biol. **43**, 1605–1628 (1998).
[26] L. Xing, J. G. Li, A. Pugachev, Q. T. Le, and A. L. Boyer, "Estimation theory and model parameter selection for therapeutic treatment plan optimization," Med. Phys. **26**, 2348–2358 (1999).
[27] J. Lian, C. Cotrutz, and L. Xing, "Therapeutic treatment plan optimization with probability density-based dose prescription," Med. Phys. **30**, 655–666 (2003).
[28] L. Xing, J. Lian, and C. Cotrutz, *Inverse treatment planning with inclusion of model parameter uncertainty*, in *the 44th Annual AAPM Meeting*, Montreal (2002).
[29] B. Choi and J. O. Deasy, "The generalized equivalent uniform dose function as a basis for intensity-modulated treatment planning," Phys. Med. Biol. **47**, 3579–3589 (2002).
[30] P. Mavroidis, B. K. Lind, and A. Brahme, "Biologically effective uniform dose (D) for specification, report and comparison of dose response relations and treatment plans," Phys. Med. Biol. **46**, 2607–2630 (2001).
[31] M. Abramowitz and I. A. Stegun, *Handbook of mathematical functions with formulas, graphs, and mathematical tables* (Wiley-Interscience, New York, 1984), p. 1046.
[32] L. Xing, J. G. Li, S. Donaldson, Q. T. Le, and A. L. Boyer, "Optimization of importance factors in inverse planning," Phys. Med. Biol. **44**, 2525–2536 (1999).
[33] C. Cotrutz, M. Lahanas, C. Kappas, and D. Baltas, "A multiobjective gradient-based dose optimization algorithm for external beam conformal radiotherapy," Phys. Med. Biol. **46**, 2161–2175 (2001).
[34] J. D. Fenwick, "Impact of dose-distribution uncertainties on rectal ntcp modeling. II: Uncertainty implications," Med. Phys. **28**, 570–581 (2001).
[35] J. D. Fenwick and A. E. Nahum, "Impact of dose-distribution uncertainties on rectal ntcp modeling. I: Uncertainty estimates," Med. Phys. **28**, 560–569 (2001).
[36] A. E. Lujan, E. W. Larsen, J. M. Balter, and R. K. Ten Haken, "A method for incorporating organ motion due to breathing into 3D dose calculations," Med. Phys. **26**, 715–720 (1999).
[37] P. J. Keall, J. V. Siebers, R. Jeraj, and R. Mohan, "The effect of dose calculation uncertainty on the evaluation of radiotherapy plans," Med. Phys. **27**, 478–484 (2000).
[38] J. G. Li and L. Xing, "Inverse planning incorporating organ motion," Med. Phys. **27**, 1573–1578 (2000).

Therapeutic treatment plan optimization with probability density-based dose prescription

Jun Lian, Cristian Cotrutz, and Lei Xing[a)]
Department of Radiation Oncology, Stanford University School of Medicine, 300 Pasteur Drive, Stanford, California 94305-5304

(Received 18 September 2002; accepted for publication 29 January 2003; published 26 March 2003)

The dose optimization in inverse planning is realized under the guidance of an objective function. The prescription doses in a conventional approach are usually rigid values, defining in most instances an ill-conditioned optimization problem. In this work, we propose a more general dose optimization scheme based on a statistical formalism [Xing *et al.*, Med. Phys. **21**, 2348–2358 (1999)]. Instead of a rigid dose, the prescription to a structure is specified by a preference function, which describes the user's preference over other doses in case the most desired dose is not attainable. The variation range of the prescription dose and the shape of the preference function are predesigned by the user based on prior clinical experience. Consequently, during the iterative optimization process, the prescription dose is allowed to deviate, with a certain preference level, from the most desired dose. By not restricting the prescription dose to a fixed value, the optimization problem becomes less ill-defined. The conventional inverse planning algorithm represents a special case of the new formalism. An iterative dose optimization algorithm is used to optimize the system. The performance of the proposed technique is systematically studied using a hypothetical C-shaped tumor with an abutting circular critical structure and a prostate case. It is shown that the final dose distribution can be manipulated flexibly by tuning the shape of the preference function and that using a preference function can lead to optimized dose distributions in accordance with the planner's specification. The proposed framework offers an effective mechanism to formalize the planner's priorities over different possible clinical scenarios and incorporate them into dose optimization. The enhanced control over the final plan may greatly facilitate the IMRT treatment planning process.
[DOI: 10.1118/1.1561622]

Key words: IMRT, dose optimization, inverse planning, statistical analysis

I. INTRODUCTION

Inverse planning is used in intensity modulated radiation therapy (IMRT) for deriving the optimal beam intensity profiles that produce the best possible dose distribution for a given patient.[1–16] The dose optimization process is usually performed under the guidance of an objective function, which measures the "distance" between the physical and the prescribed dose distributions.[8,17–20] One of the common objective functions for inverse planning is the quadratic objective function,[3,21,22] with importance factors assigned to the involved structures to prioritize their relative importance during the optimization process.[23–25] The objective function is defined as a global quantity based on general physical considerations. When the desired dose distribution is not attainable during optimization, a compromise solution is found using the algorithm's ranking. The compromise dose distribution, however, is often not what the planner wants and multiple trial and errors are needed to obtain a clinically acceptable IMRT plan.

A main problem of the existing IMRT planning algorithms is the lack of an effective mechanism for incorporating prior knowledge into inverse planning.[31] In the past, there have been many attempts to introduce soft/hard constraints to steer the dose optimization process toward the clinically desired solutions.[26–30,36] However, the constraints are introduced in an *ad hoc* fashion and do not fully utilize the partial information available from years of clinical investigations because of their phenomenological nature. On a more fundamental level, the constraints are imposed *a posteriori* and controls the optimization passively. Our purpose in this paper is to develop a statistical analysis-based inverse planning formalism to more effectively utilize the prior knowledge. Instead of specifying a rigid prescription dose, the formalism allows us to use a dose distribution as the input prescription to the system, providing a natural way for us to take advantage of the existing information of the system variables and promising to make the optimization outcome more predictable and controllable.

In the next section we present the details of the new dose optimization algorithm after a brief introduction of the concept of preference function. The formalism is then applied to a synthetic phantom case with C-shaped tumor target and a prostate case. Our results indicate that the statistical analysis-based formalism provides a general framework for inverse planning and is capable of producing conformal IMRT dose distribution. Coupled with the capability of the preference function in customizing/formalizing our prior clinical knowledge, it is expected that the proposed technique will have a

broad implication and potential to greatly facilitate an IMRT planning process.

II. MATERIAL AND METHODS

A. Theoretical background

In a vectorial form, the dose to the points in the treatment region depend upon the beamlet weights **w** as

$$\mathbf{D}_c = \mathbf{d}\cdot\mathbf{w}, \tag{1}$$

where **d** represents the dose deposition matrix, expressing the dose deposited to any point in the patient when irradiated with a unit weight beamlet vector. The inverse problem as posed for IMRT is to find a set of beamlet weights that produce the optimal dose distribution by minimizing a therapeutic objective function. The most used objective function has a quadratic form and reads[32] as

$$F = \frac{1}{N}\sum_{n=1}^{N} r_\sigma [D_c(n) - D_p(n)]^2, \tag{2}$$

where N is the total number of voxels, r_σ is the importance factor that controls the relative importance of a structure σ, and D_p and D_c are prescribed and calculated doses, respectively.

In inverse planning algorithm based on the quadratic objective function [Eq. (2)], the dose prescription to the target or sensitive structure takes a rigid value. The minimization of the objective function is realized by various algorithms like simulated annealing, gradient methods, etc.[17,26,32,33] Independent of the used dose optimization algorithms, we will call these methods throughout the text conventional IMRT optimization procedures. The problem is usually ill-posed and may lead to negative fluence unless hard constraints are introduced.[3] Practically, it is not uncommon that the plans computed by what are called optimization systems are not consistent with the expectation of the planner and that several trial-and-error adjustments of the system parameters might be required to achieve a clinically acceptable plan. Given a patient, the obtained plan can vary widely from one planer to the next, even within a department. In the following we describe a more adaptable and "intelligent" statistical inverse planning formalism based on the concept of a preference function to better deal with the dilemma.

B. Preference function

In a recent paper, Xing *et al.*[31] introduced the concept of preference function to weaken the rigid dose prescription commonly seen in the existing inverse planning algorithms. Its role is to allow a dose distribution to be considered instead of just a single value, and to quantify the degree of our willingness to accept a prescription dose D_p in that range. The preference function can be constructed heuristically from clinical considerations.[31] The defined preference function states that the most favorable prescription dose for a voxel n is $D_p(n)$ and that a different prescription dose is also acceptable, but with a smaller preference level. For illustration, in Fig. 1 we show a sketch of the preference functions

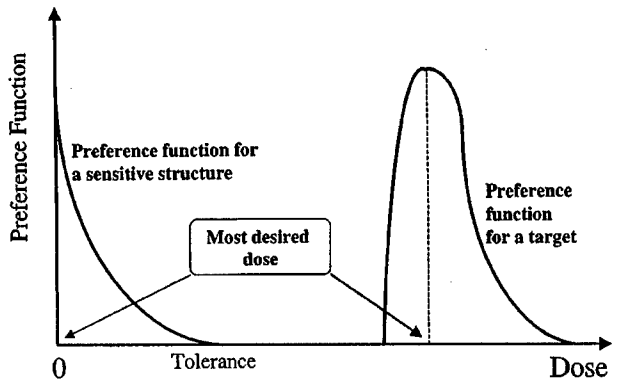

FIG. 1. A sketch of preference functions for a target and a sensitive structure.

for a target and sensitive structure. The most desirable dose for a sensitive structure should generally be set to zero. The conventional prescription scheme represents a special case of the general approach proposed here with the step function form of the preference function. That is,

$$P_n(D_p) = \begin{cases} 1, & \text{if } D_p = D_p^0, \\ 0, & \text{if } D_p \neq D_p^0. \end{cases} \tag{3}$$

To give another example, we write down the Gaussian preference function for a voxel n

$$P_n(D_p) = P_{0n}\exp\{-\gamma_n[D_p(n) - D_p^0(n)]^2\}, \tag{4}$$

where P_{0n} is a normalization constant and γ_n represents the Gaussian parameter. For a system comprising N voxels, the total preference is given by a product of the preference functions of all voxels:

$$P = \prod_n P_n(D_p)$$

$$= \prod_n P_{0n}\exp\{-\gamma_n[D_p(n) - D_p^0(n)]^2\}. \tag{5}$$

When a maximum likelihood estimator is used, it has been demonstrated that the maximization of the logarithmic function of P or minimization of $\ln(1/P)$, is equivalent to the minimization of the conventional quadratic objective function.[31,34] In this case, the Gaussian parameter γ_n in Eq. (5), which commands the "spread" of the Gaussian around D_p^0, is equivalent to the importance factor that controls the relative importance of the structure and parametrizes the clinical trade-off strategy.

C. Probability density-based dose prescription and inverse planning

The objective function defined in Eq. (2) uses a rigid dose, D_p. Since in most instances an ideal dose prescription is not physically attainable, we resort to an expansion of the prescription dose, over a certain interval. That is, we allow the prescription dose to take a "probabilistic" distribution around the most desired dose as specified by the preference function. For computational purpose, we divide the permis-

sible prescription dose into a number of discretized values, $\{D_p^i\}$, where i is the index of a possible prescription dose and $i=0$ represents the most desirable dose. The preference distribution prescription is usually normalized to unity.

In order to utilize the probability information characterized by the preference function, we formulate the conventional dose optimization into a statistical analysis problem. To proceed, let us take the quadratic objective function as an example. We rewrite the traditional quadratic objective function (2) into

$$f(D_c)=f_0\prod_n \exp\{-r_\sigma[D_c(n)-D_p(n)]^2\}. \quad (6)$$

where f_0 is a normalization constant. For a given prescribed dose distribution, Eq. (6) measures the goodness of a calculated dose distribution using an exponential scale, as compared with Eq. (2). Equation (6) can be interpreted as a conditional probability and formally rewritten as

$$f(D_c|D_p)=f_0\prod_n \exp\{-r_\sigma[D_c(n)-D_p(n)]^2\}. \quad (7)$$

When the prescription dose is no longer a rigid dose, it is conceivable that there are a number of optimum solutions, each corresponding to a sample of prescription doses. Mathematically, we now have two "probability" distribution functions. One is the preference function that characterizes our *a priori* preference over different prescription doses $P(D_p)$, and the other is Eq. (6) that ranks a calculated dose for a given prescribed dose, D_p. Our task is to find the solution that is statistically optimal with consideration of the variable prescription. For this purpose, we introduce the "joint probability" of the two "probability" distributions defined by Eqs. (5) and (7). The function at a voxel n can be written as

$$P_n(D_c)=\sum_i f_n(D_c|D_p^i)P_n(D_p^i). \quad (8)$$

The total preference function of the system is given by

$$P=\prod_n P_n(D_c). \quad (9)$$

D. Optimization strategy

Having the rigid prescription D_p in (2) replaced by a range of prescribed doses, $\{D_p^i\}$, the total preference function is now given by Eqs. (8) and (9). For convenience, we define objective function $F=\ln(1/P)$ and derive the optimal solution by minimizing the F, which is equivalent to maximize the preference function (9). The objective function now reads as

$$F=\ln(1/P)$$

$$=-\ln\prod_n P_n=-\sum_n \ln\sum_i f_n(D_c|D_p^i)\cdot P_n(D_p^i). \quad (10)$$

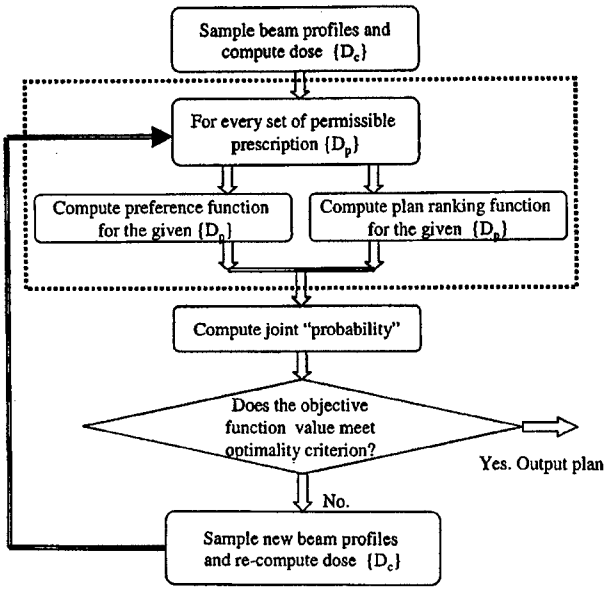

FIG. 2. A flow chart of the optimization process with the inclusion of predesigned preference function information.

Note that the conventional quadratic objective function is a special case of the above general objective function when the prescription takes a rigid value for each structure, as described by Eq. (3).

The optimization process is schematically shown in a flow chart (Fig. 2). The beam profile is determined by minimizing the above objective function using a conjugate gradient optimization algorithm. The details of the algorithm have been discussed in a previous paper.[33] Briefly, the calculation consists of three major steps: (i) assume an initial intensity profile for each incident beam; (ii) compute the "joint probability" given by Eqs. (8) and (9). For this purpose, we need to sample all combinations of the prescription doses of different structures and compute the function given in Eqs. (5) and (7) for each of these combinations; and (iii) optimization of the multidimensional "joint probability" function. The second step is fairly computationally intensive because we must compute the two functions for every sampling of the prescription doses. In our calculation, we typically assign four to seven discrete possible prescription doses for each structure. A finer discretization of the prescription dose did not seem lead to further improvement but would greatly increase the computation time. All calculations presented here are performed on a Personal Computer (PC) with an Intel Pentium® III 1 GHz CPU (Intel Corporation, Sunnyvale, CA). The computation time needed to obtain an optimal solution for a given set of system parameters (including beam configuration, preference function, importance factors) is typically less than ten minutes.

III. RESULTS AND DISCUSSION

A. A synthetic phantom case with a C-shaped tumor

To systematically study the performance of the statistical analysis-based inverse planning algorithm, we applied the

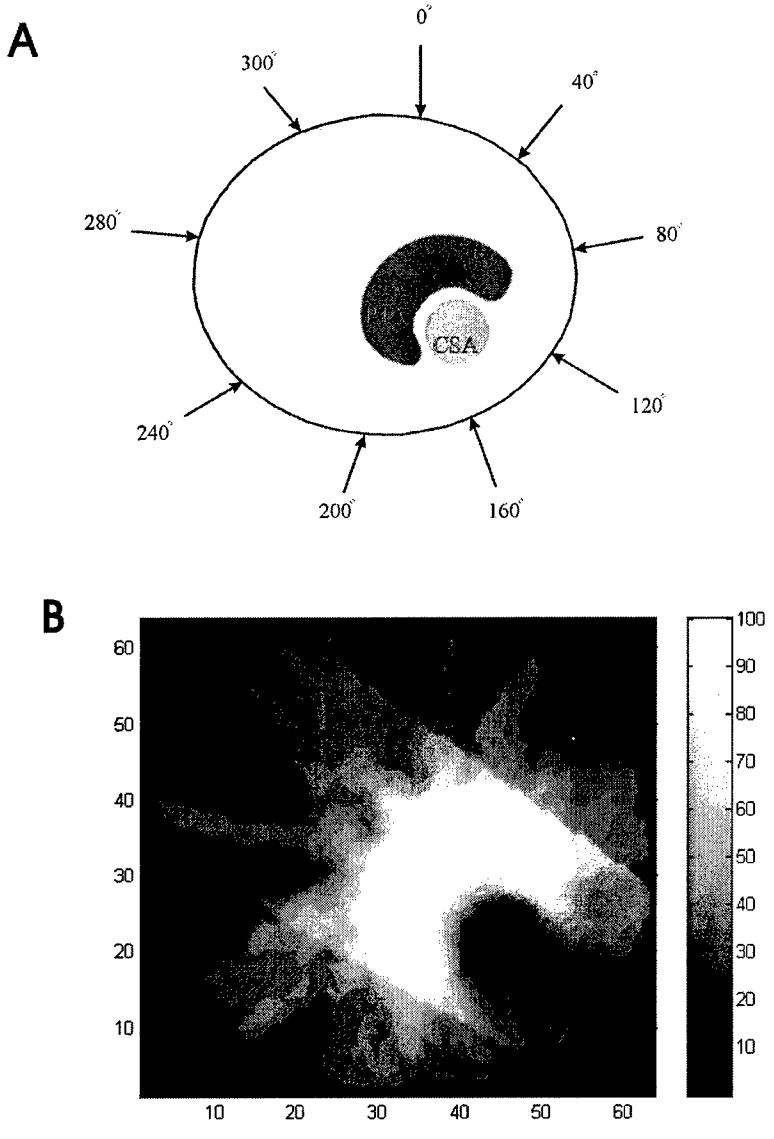

FIG. 3. (a) A sketch of a phantom case with a C-shaped tumor. The dose prescription is set 100 (arbitrary units) to the PTV and 0 to the circular OAR and normal tissue. (b) Dose distribution obtained using the "probabilistic" prescription shown in Fig. 4(a).

technique to a C-shaped tumor case [Fig. 3(a)] with a variety of preference functions and compared the results with that obtained using the conventional approach with a fixed dose prescription. Nine equally spaced 6 MV beams beginning at 0° (IEC) were used in this study. The prescription doses to the PTV and OAR in the conventional IMRT plans were 100 and 0 (the dose is in an arbitrary unit), respectively.

We first assigned three sets of symmetrical Gaussian distributions to the target while keeping the prescription to the sensitive structure at zero (Fig. 4). The Gaussian preference functions were represented by three sets of preference levels at seven discrete values (80, 87, 94, 100, 106, 113, and 120). The center of the Gaussian functions was set at 100. The preference levels for the seven doses are shown in Fig. 4 for each of the three situations studied here. The transverse dose distribution obtained using the statistical inverse planning formalism for the case shown in Fig. 4(a) is plotted in Fig. 3(b). As expected, target inhomogeneity increases as we loosen the constraint of the rigid dose prescription. This can be better demonstrated by using the differential DVH for each situation. As seen from the differential DVH plots (the right column of Fig. 4), the width of the differential function gradually increases, from 26.72, 28.59–30.39, as we gradually increase the acceptance levels for the doses different from the most desirable dose (100). This series of calculations provides us with preliminary evidence that the final dose distribution can be steered by varying the preference function.

Next, we constructed six sets of asymmetric preference functions for the target (Fig. 5 and Fig. 6). When higher preference levels were assigned to the doses higher than 100, we found that the target DVH is shifted to the high dose region. Interestingly, even when an extremely low preference (for instance, 1%) was assigned to the doses less than 100 [Fig. 5(b)], a noticeable underdosing relative to the conventional result was resulted. A similar phenomenon can also be

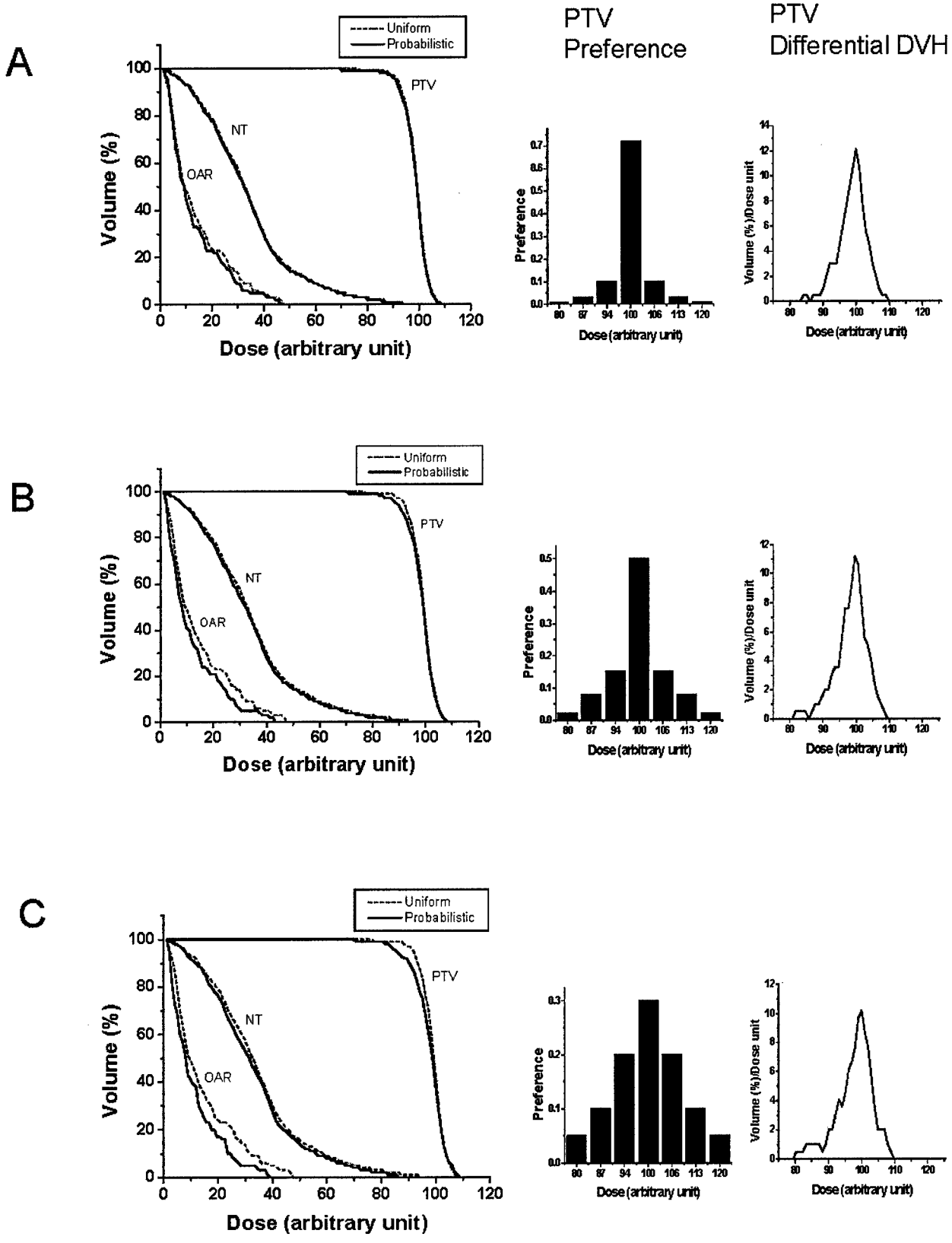

FIG. 4. DVHs of the PTV, OAR, and normal tissue (NT) obtained using the conventional rigid dose prescription (dotted line) and the "probabilistic" prescription (solid line). The Gaussian preference functions with different variances are shown in the middle panel. The right panel shows the differential DVHs for the target.

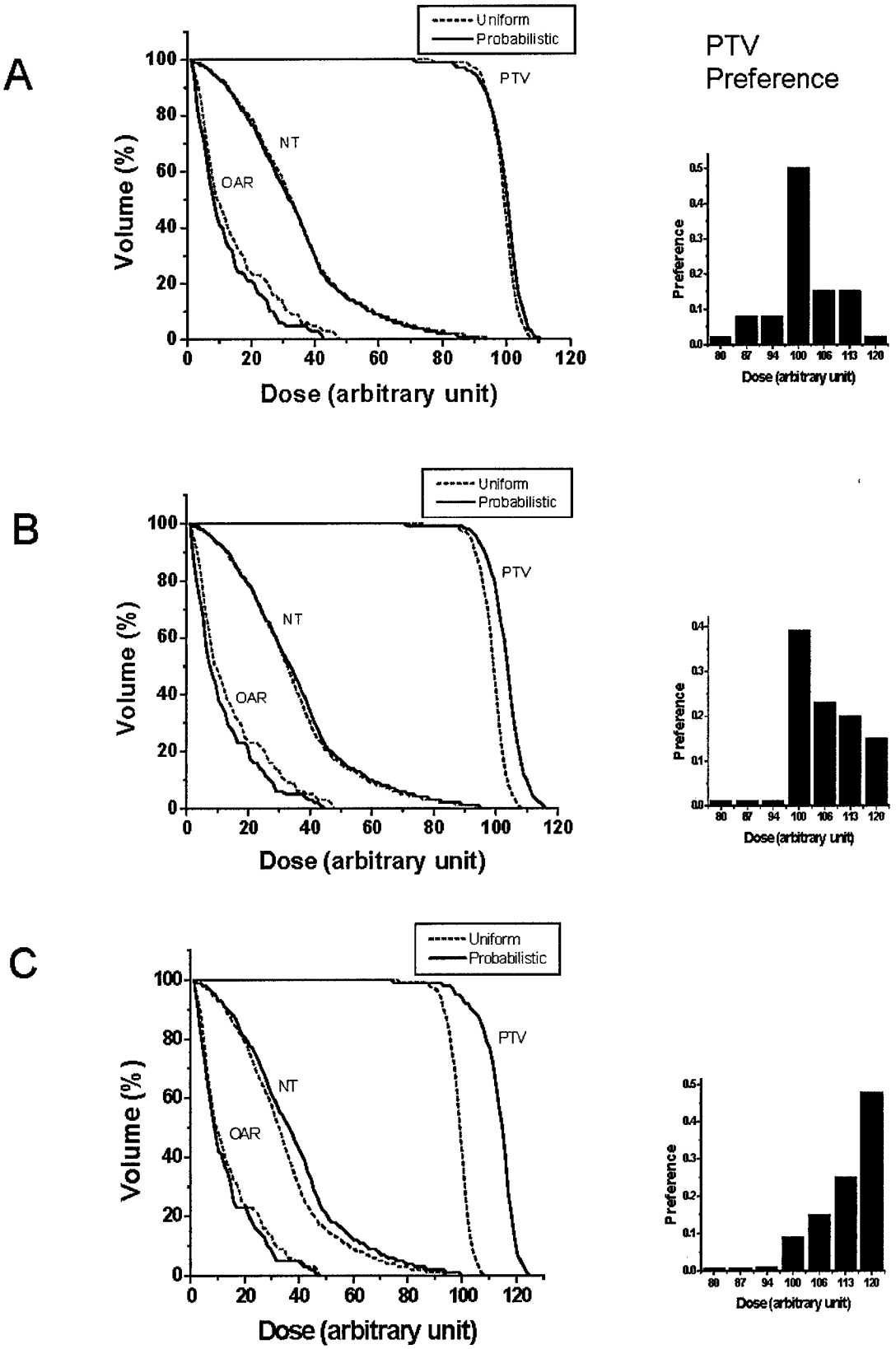

FIG. 5. DVHs of the PTV, OAR, and normal tissue (NT) obtained with the conventional rigid dose prescription (dotted line) and with the "probabilistic" prescription (solid line). The bar charts on right show the asymmetrical preference functions.

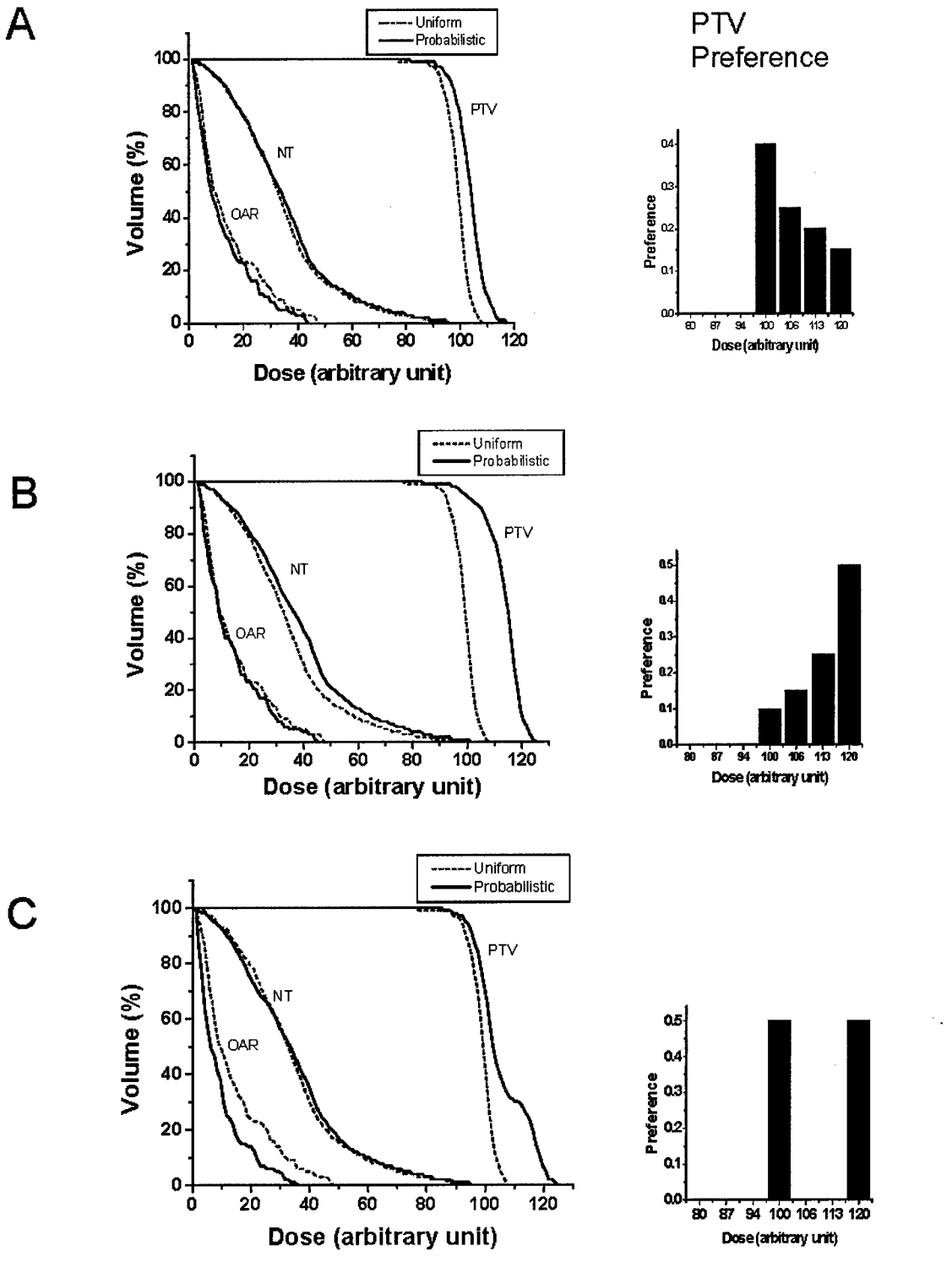

FIG. 6. DVHs of the PTV, OAR, and normal tissue (NT) obtained using the conventional rigid dose prescription (dotted line) and the new statistical inverse planning method for a variety of preference functions shown on the right panel (solid line).

seen from the result shown in Fig. 5(c), where only 0.5%, 0.7%, and 1% of preference levels were assigned to the dose values of 80, 87, and 94. This observation seems to indicate that the influence of the assigned preference level at a low dose plays an important role. In Fig. 6, we set the preference levels for the doses less than 100 to be 0 and only assign nonzero preference levels for the doses higher than 100. It is seen that in all these situations the minimum target dose is

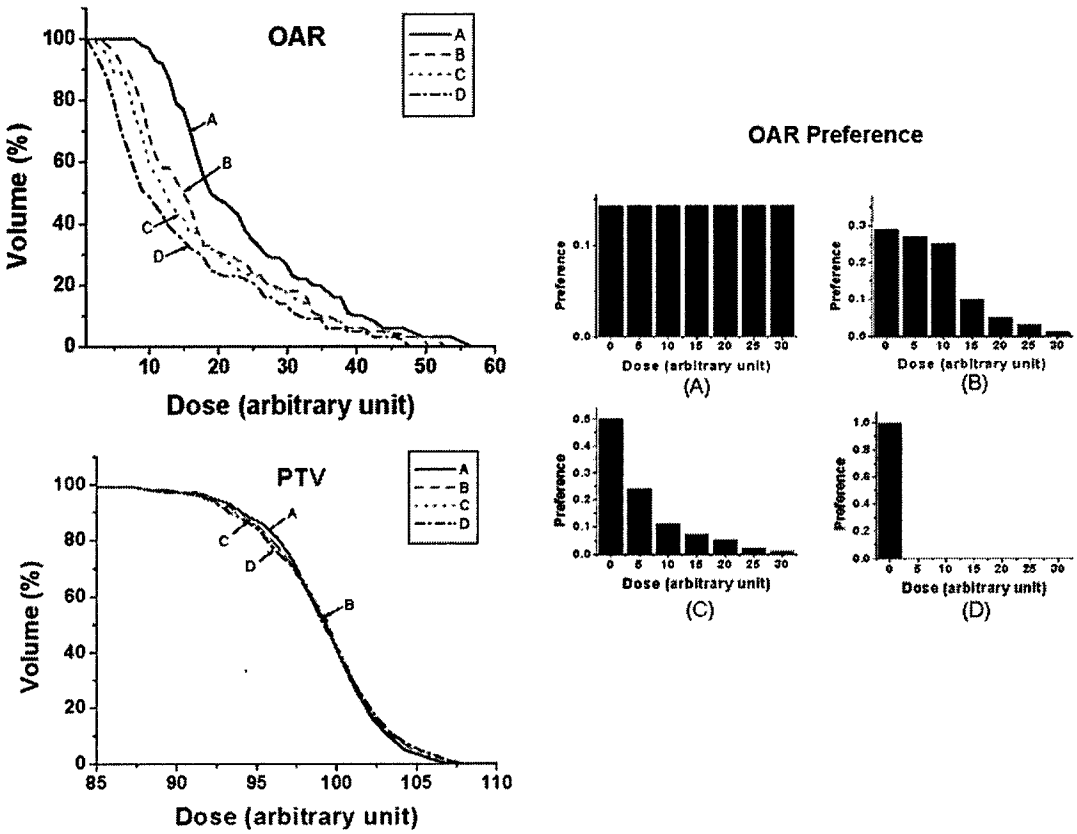

FIG. 7. DVHs of the OAR and PTV when the prescription dose to the OAR is modeled by (a) a uniform distribution, (b) a bell-shaped function, (c) an exponential decay function, and (d) a rigid value.

higher than that of the conventional plan. As a result of our preference over higher doses, the fractional volume at any dose less than 100 is improved in comparison to that of the conventional IMRT plan. In Fig. 6(c), we further exemplify the statistical analysis based inverse planning method by simplifying our preference to two doses (100 and 120), each with 50% preference levels. In this situation, in addition to that the doses in the target are shifted toward higher values, the target DVH exhibits a stepwise behavior: a plateau appears at around 110, which is in the middle of the two prescribed doses.

It is interesting to point out that the OAR sparing is improved as compared with the conventional IMRT plan in most cases studied in Figs. 5 and 6, even when the target dose is escalated. That is, the DVH of the OAR is not always shifted toward higher doses, as would occur if a higher dose is prescribed in a conventional inverse planning system. Instead, the dose to the OAR remained unchanged or even lowered in some cases. A reasonable explanation for the observed phenomenon is that, when a rigid dose prescription is replaced by a range of doses, the system is given more freedom for self-adjustment. As a benefit, a solution with a higher integral target dose and reduced OAR dose can be obtained from the expanded solution space.

We have also studied the behavior of the system when a range of doses is prescribed to the OAR. In this investigation, we kept the target prescription to 100 and allowed the OAR dose to take seven values: 0, 5, 10, 15, 20, 25, and 30 with the acceptance levels sampled from three different types of prescription distribution: uniform [Fig. 7(a)], bell-shaped [Fig. 7(b)], and exponential [Fig. 7(c)] functions. Figure 7(d) represents the conventional case with zero prescription to the OAR. The corresponding OAR and PTV DVHs are plotted in the left panel of Fig. 7. When the preference was uniformly sampled in the dose interval from 0 to 30, the resultant dose to the OAR was found to be the highest, as indicated by curve A in Fig. 7. The best target dose coverage was achieved in this situation. If the preference to a high dose was reduced, the DVH was gradually shifted to the low dose direction (curves B and C). It is not surprising that the best OAR sparing was achieved in the conventional case where a zero dose was prescribed to the OAR. The target dose homogeneity was slightly improved in all cases when a probabilistic prescription was given to the OAR. Similar to that described in the last paragraph, the results clearly demonstrate that the "probabilistic" prescription allows us to control the OAR dose distribution and indicate the usefulness of the statistic analysis approach.

B. The prostate case

The new inverse planning algorithm was also applied to study a six filed IMRT prostate treatment [Fig. 8(a)]. Four plans with different types of preference functions were gen-

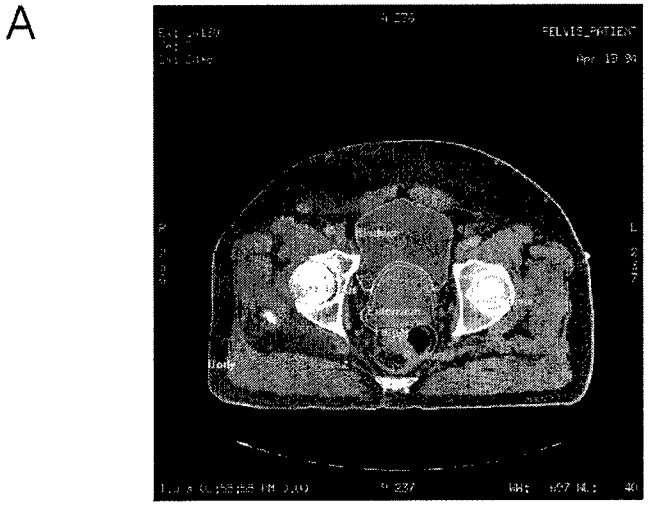

FIG. 8. A transverse slice showing the anatomical structures delineated for the prostate tumor (a) and (b) the dose distribution obtained using the "probabilistic" prescription shown in Fig. 9(a).

erated. In addition, a plan with rigid prescription (74 Gy on the target, 60 Gy on the bladder, and 40 Gy on the rectum) is also generated. The DVHs for this plan is plotted as dotted lines in Fig. 9 and is used as a reference for comparison. In all treatment plans, six beams were placed at the following angular positions: 0°, 55°, 135°, 180°, 225°, and 305°. The size of the pencil beam defined at the isocenter was 0.5 cm.

The DVH and preference functions for four different plans are schematically shown in Fig. 9. In the study shown in Figs. 9(a)–9(b), we kept the preference function of the sensitive structures unchanged and only varied the form of the preference function of the target. In Fig. 9(a), we assumed that target could take seven discrete values (74, 76, 78, 80, 82, 84, and 86 Gy) sampled from an exponential distribution. Compared with the dotted lines, the target DVH was shifted toward the high dose direction. The dose distribution corresponding to the preference function is shown in Fig. 8(b). The target DVH was shifted even further toward the high dose region [Fig. 9(b)] when a bell-shaped preference function was used with more emphasis on the target receiving doses at 74, 76, and 78 Gy. In both cases, doses to the rectum and bladder did not change significantly.

In Fig. 9(c) we show the DVHs when the preference function to the rectum deviates from the uniform distribution. As a result, the rectum dose was significantly lowered in all dose levels and the maximum dose was reduced from 66 to 57 Gy. Because of the proximity of the rectum to the prostate target, the maximum rectum dose was not restricted to 30 Gy, as specified in the preference function. We emphasize that the improvement in rectum and bladder sparing was achieved at cost of higher dose inhomogeneity in the prostate target. This reminds us that, in dose optimization, there is a dosimetric compromise. That is, the improvement in the dose to a structure is often accompanied by dosimetrically adverse effect(s) at other points in the same or different structures. The important point that one should note is that from the clinical point

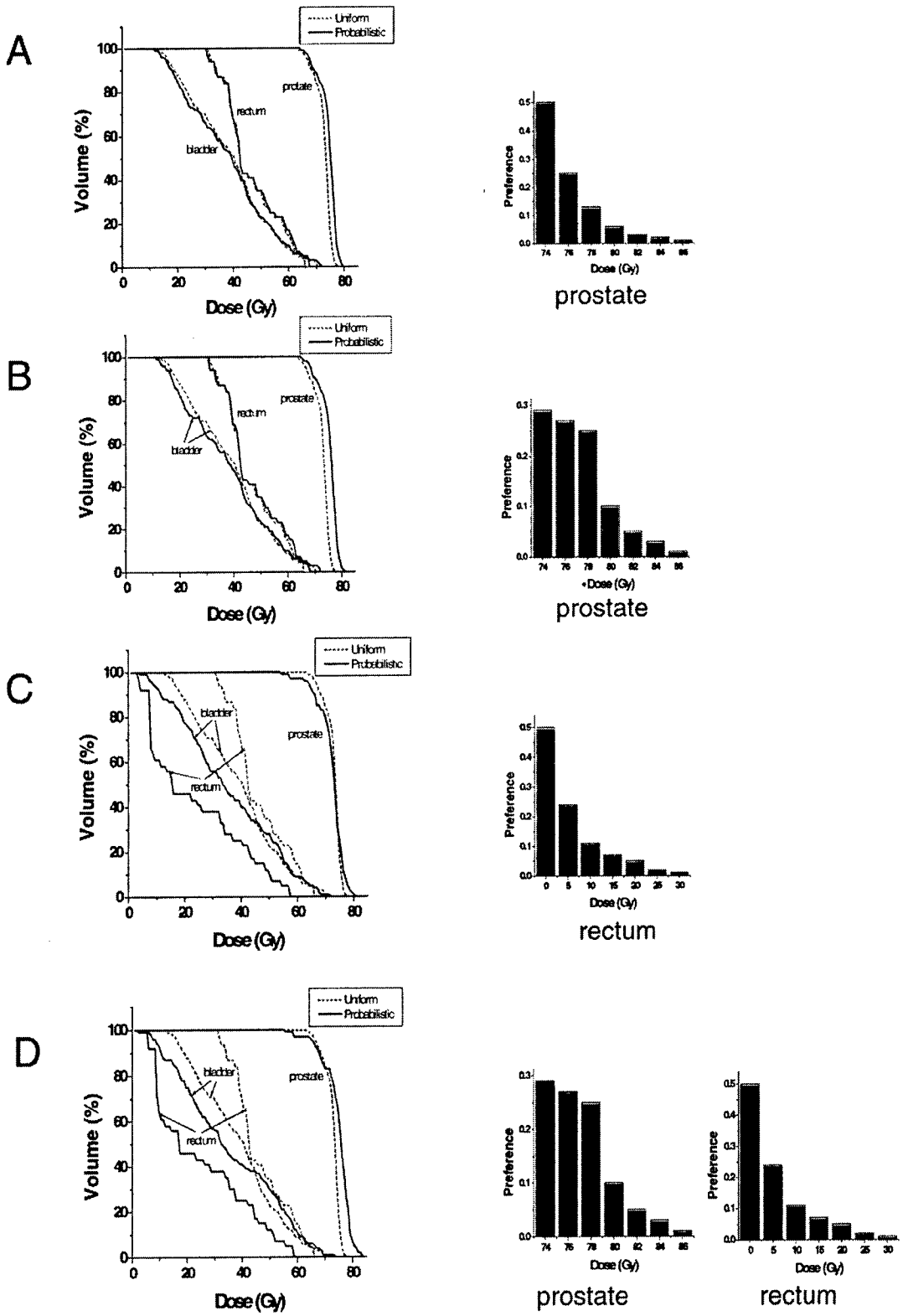

FIG. 9. A comparison of the DVHs obtained using the "probabilistic" prescription (solid line) and conventional rigid dose prescription (dotted line). The prostate and rectum prescriptions are represented on the right bar charts.

of view, some dose distributions are more acceptable than others and our goal is to find the solution that improves the plan to the largest possible extent, but with a clinically insignificant or acceptable sacrifice in OAR sparing. In order to achieve this, it is necessary to have a reasonable amount of controllability over the final dose distribution. In this sense we believe that the proposed formalism is valuable.

In addition, we varied the preference functions for both target and rectum [Fig. 9(d)]. The preference function for the rectum was the same as that in Fig. 9(c). Compared to the results shown in Fig. 9(c), we found that the target dose inhomogeneity was slightly improved.

IV. CONCLUSIONS

The formalism we derived here provides a general starting point for the study of a system with a probability density-based dose prescription. The inclusion of the partial information into the plan selection process represents a significant change from the conventional approaches. The proposed technique can be categorized into the general Bayesian decision-making theory,[31] which is a useful tool to deal with a system with "statistical" inference. In image analysis and many other fields of science and engineering, it has proven extremely useful to include the prior knowledge of the system variables into the estimation process.[31] The preference function proposed for radiotherapy optimization here serves as *a priori* probability density function in standard Bayesian statistics. The role of the preference function is to indicate our "bias" on the values of the system variables. By utilizing the partial information of the system variables, one can more effectively search the solution space and eliminate some unnecessary uncertainties in the optimization process.

In conclusion, we have developed a statistical analysis-based inverse planning algorithm to include preference and expert knowledge into the dose optimization process. Instead of a rigid dose prescription, the new approach allows us to prescribe a range of doses with predesigned preference levels. The technique represents a novel application of the general Bayesian decision-making theory[31] for dealing with statistical inference and is valuable for deriving a statistically optimal solution in the presence of uncertainties in system parameters. The method was demonstrated for a system with modulating prescriptions but can be easily extended to solve many other related problems (e.g., in biologically based dose optimization, one can incorporate the uncertainties of various radiobiology parameters into the inverse planning process using the frameset developed in this work[35]). The ill conditioning of the problem was improved because of the use of a less restrictive prescription and, as a result, new solutions that are otherwise inaccessible can be obtained naturally. It is demonstrated that the obtained solutions using the new approach strongly correlate with the preference function, suggesting that the planning process is controllable and predictable by the proposed method.

ACKNOWLEDGMENTS

We wish to thank Dr. A. Pugachev, Dr. J. G. Li, Dr. S. M. Crooks, Dr. Y. Yang, and Dr. A. L. Boyer for useful discussions. This work was partly supported by a Research Scholar Award from the American Cancer Society (RSG-01-022-01-CCE) and a research grant from the Department of Defense (BC996645). This work was presented in the 44th Annual AAPM Meeting, Montreal, 2002 and in the 44th Annual ASTRO Meeting, New Orleans, 2002.

[a]Author to whom correspondence should be addressed. Stanford University School of Medicine, Department of Radiation Oncology, 300 Pasteur Drive, Stanford, California 94305-5304. Electronic mail: lei@reyes.stanford.edu; phone: (650) 498 7896; fax: (650) 498 4015.

[1] T. Bortfeld, W. Schlegel, C. Dykstra, S. Levegrun, and K. Preiser, "Physical vs. biological objectives for treatment plan optimization," Radiother. Oncol. **40**, 185–187 (1996).

[2] T. Bortfeld, J. Stein, and K. Preiser. "Clinically relevant intensity modulation optimization using physical criteria," in *Proceedings of the XII International Conference on the Use of Computers in Radiation Therapy*, Salt Lake City, UT, 1997.

[3] L. Xing and G. T. Chen, "Iterative methods for inverse treatment planning," Phys. Med. Biol. **41**, 2107–2123 (1996).

[4] P. S. Cho, S. Lee, R. J. Marks II, S. Oh, S. G. Sutlief, and M. H. Phillips, "Optimization of intensity modulated beams with volume constraints using two methods: cost function minimization and projections onto convex sets," Med. Phys. **25**, 435–443 (1998).

[5] B. S. Teh, S. Y. Woo, and E. B. Butler, "Intensity modulated radiation therapy (IMRT): a new promising technology in radiation oncology," Oncologist **4**, 433–442 (1999).

[6] Y. Xiao, J. Galvin, M. Hossain, and R. Valicenti, "An optimized forward-planning technique for intensity modulated radiation therapy," Med. Phys. **27**, 2093–2099 (2000).

[7] S. M. Crooks and L. Xing, "Linear algebraic methods applied to intensity modulated radiation therapy," Phys. Med. Biol. **46**, 2587–2606 (2001).

[8] G. Starkschall, A. Pollack, and C. W. Stevens, "Treatment planning using a dose-volume feasibility search algorithm," Int. J. Radiat. Oncol., Biol., Phys. **49**, 1419–1427 (2001).

[9] A. Brahme, "Optimized radiation therapy based on radiobiological objectives," Semin Radiat. Oncol. **9**, 35–47 (1999).

[10] M. Langer, "Application of coloring theory to reduce intensity modulated radiotherapy dose calculations," Med. Phys. **27**, 2077–2083 (2000).

[11] I. C. W. Group, "Intensity-modulated radiotherapy: current status and issues of interest," Int. J. Radiat. Oncol., Biol., Phys. **51**, 880–914 (2001).

[12] G. A. Ezzell, "Genetic and geometric optimization of three-dimensional radiation therapy treatment planning," Med. Phys. **23**, 293–305 (1996).

[13] G. Starkschall, "A constrained least-squares optimization method for external beam radiation therapy treatment planning," Med. Phys. **11**, 659–665 (1984).

[14] D. H. Hristov and B. G. Fallone, "An active set algorithm for treatment planning optimization," Med. Phys. **24**, 1455–1464 (1997).

[15] C. B. Saw, K. M. Ayyangar, W. Zhen, M. Yoe-Sein, S. Pillai, and C. A. Enke, "Clinical implementation of intensity-modulated radiation therapy," Med. Dosim **27**, 161–169 (2002).

[16] K. S. Chao, F. J. Wippold, G. Ozyigit, B. N. Tran, and J. F. Dempsey, "Determination and delineation of nodal target volumes for head-and-neck cancer based on patterns of failure in patients receiving definitive and postoperative IMRT," Int. J. Radiat. Oncol., Biol., Phys. **53**, 1174–1184 (2002).

[17] S. Webb, "Optimisation of conformal radiotherapy dose distributions by simulated annealing," Phys. Med. Biol. **34**, 1349–1370 (1989).

[18] G. S. Mageras and R. Mohan, "Application of fast simulated annealing to optimization of conformal radiation treatments," Med. Phys. **20**, 639–647 (1993).

[19] X. H. Wang, R. Mohan, A. Jackson, S. A. Leibel, Z. Fuks, and C. C. Ling, "Optimization of intensity-modulated 3D conformal treatment plans based on biological indices," Radiother. Oncol. **37**, 140–152 (1995).

[20] L. Jones and P. Hoban, "A method for physically based radiotherapy

optimization with intelligent tissue weight determination," Med. Phys. **29**, 26–37 (2002).
[21] R. P. Li and F. F. Yin, "Optimization of inverse treatment planning using a fuzzy weight function," Med. Phys. **27**, 691–700 (2000).
[22] Y. Chen, D. Michalski, C. Houser, and J. M. Galvin, "A deterministic iterative least-squares algorithm for beam weight optimization in conformal radiotherapy," Phys. Med. Biol. **47**, 1647–1658 (2002).
[23] L. Xing, J. G. Li, S. Donaldson, Q. T. Le, and A. L. Boyer, "Optimization of importance factors in inverse planning," Phys. Med. Biol. **44**, 2525–2536 (1999).
[24] X. Wu and Y. Zhu, "An optimization method for importance factors and beam weights based on genetic algorithms for radiotherapy treatment planning," Phys. Med. Biol. **46**, 1085–1099 (2001).
[25] C. Cotrutz and L. Xing, "Using voxel-dependent importance factors for interactive DVH-based dose optimization," Phys. Med. Biol. **47**, 1659–1669 (2002).
[26] S. V. Spirou and C. S. Chui, "A gradient inverse planning algorithm with dose-volume constraints," Med. Phys. **25**, 321–333 (1998).
[27] A. Niemierko, M. Urie, and M. Goitein, "Optimization of 3D radiation therapy with both physical and biological end points and constraints," Int. J. Radiat. Oncol., Biol., Phys. **23**, 99–108 (1992).
[28] C. De Wagter, C. O. Colle, L. G. Fortan, B. B. Van Duyse, D. L. Van den Berge, and W. J. De Neve, "3D conformal intensity-modulated radiotherapy planning: interactive optimization by constrained matrix inversion," Radiother. Oncol. **47**, 69–76 (1998).
[29] S. M. Morrill, R. G. Lane, J. A. Wong, and I. I. Rosen, "Dose-volume considerations with linear programming optimization." Med. Phys. **18**, 1201–10 (1991).
[30] S. M. Morrill, K. S. Lam, R. G. Lane, M. Langer, and I. I. Rosen, "Very fast simulated reannealing in radiation therapy treatment plan optimization," Int. J. Radiat. Oncol., Biol., Phys. **31**, 179–188 (1995).
[31] L. Xing, J. G. Li, A. Pugachev, Q. T. Le, and A. L. Boyer, "Estimation theory and model parameter selection for therapeutic treatment plan optimization," Med. Phys. **26**, 2348–2358 (1999).
[32] Q. Wu and R. Mohan, "Algorithms and functionality of an intensity modulated radiotherapy optimization system," Med. Phys. **27**, 701–711 (2000).
[33] C. Cotrutz, M. Lahanas, C. Kappas, and D. Baltas, "A multiobjective gradient-based dose optimization algorithm for external beam conformal radiotherapy," Phys. Med. Biol. **46**, 2161–2175 (2001).
[34] J. Llacer, "Inverse radiation treatment planning using the Dynamically Penalized Likelihood method," Med. Phys. **24**, 1751–1764 (1997).
[35] L. Xing, J. Lian, and C. Cotrutz, "Inverse treatment planning with inclusion of model parameter uncertainty," in the 44th Annual AAPM Meeting, Montreal, 2002.
[36] R. B. Altman and R. Tombropoulos, "Probabilistic constraint satisfaction: application to radiosurgery," in the 18th Annual Symposium on Computer Applications in Medical Care, Washington, DC, 1994.